



universität  
wien

# MASTERARBEIT

„1,3-Dioxindan-2-carboxamide als selective O,O-  
Chelatliganden für die Entwicklung neuer  
organometallischer Ruthenium- und Rhodiumkomplexe  
in der Krebstherapie“

Stephan Mokesch, B.Sc.

angestrebter akademischer Grad

Master of Science (M.Sc.)

Wien, 29.01.2013

Studienkennzahl lt. Studienblatt: A 066 862

Studienrichtung lt. Studienblatt: Masterstudium Chemie

Betreuer: O. Univ.-Prof. Dr. Dr. Bernhard K. Keppler





universität  
wien

## MASTER THESIS

„1,3-Dioxoindan-2-carboxamides as selective O,O-  
chelating ligands for the development of novel  
organometallic anticancer drugs“

Stephan Mokesch, B.Sc.

Submitted in partial fulfillment of the requirements for the degree

Master of Science (M.Sc.)

Vienna, 29.01.2013

Supervisor:

O. Univ.-Prof. Dr. Dr. Bernhard K. Keppler



Es stellt sich heraus, daß das Fundament, auf dem alle unsere Erkenntnis ruht, nicht einfach ist, sondern daß zwei gänzlich voneinander verschiedene Prinzipien die Erkenntnis möglich machen, Anschauung *und* Denken. Nicht die Anschauung allein, aber auch nicht das Denken allein führt mich zu einer Erkenntnis. Beide müssen zusammen wirken, um eine Erkenntnis zustande zu bringen.

[Immanuel Kant, 1724-1804 – „die Kritik der reinen Vernunft“]

*Dedicated to my parents,  
who are, always have been, and always will be  
a great inspiration.*

## Acknowledgements

I would like to thank

O. Univ.-Prof. Dr. Dr. Bernhard K. Keppler for the opportunity to work in his group.

My supervisor Dr. Wolfgang Kandioller for the amazing support throughout the course of my entire thesis.

The NMR service team (Dr. Sergey Abramkin, Dipl.-Chem. Paul-Steffen Kuhn, Mag. Verena Pichler, Mag. Michael Primik, DI Melanie Schmidlehner, and Ao. Univ.-Prof. Dr. Markus Galanski) for the measurement of almost 250 spectra.

Prof. Vladimir Arion and Ing. Alexander Roller for x-ray data collection and structure refinement.

My laboratory colleagues Evelyn Balsano, B.Sc., Masha Babak, M.Sc., Dipl.-Chem. Britta Fischer, DI Melanie Schmidlehner, and Filip Groznica for the pleasant work atmosphere.

Our apprentice Filip Groznica for his help with my syntheses.

Mag. Elfriede Limberger and Mihai Odoleanu for enabling smooth work by dealing with administrative problems.

All members of the working group, especially Wolfgang, Evelyn, Melanie, Claudia, Paul, Filip, Alex, Elfi, and all the others, for inspiring and fun coffee breaks.

My friends for helping to preserve my sanity over the course of my master lectures and exams, especially Petra and Sonja.

Special thanks go to Sonja Schaller for her help with graphical problems of this thesis.

And last but not least, my entire family for supporting me emotionally and financially all these years.

For financial support:



## Abstract

Coordination compounds of transition metals are amongst the most important chemotherapeutics in cancer treatment. The prevalent metal-based anticancer drugs in clinical use are platinum complexes, such as cisplatin, carboplatin, and oxaliplatin. However, due to insufficient selectivity towards cancer cells, these drugs exhibit a number of severe side effects and another major disadvantage is the observation of acquired or intrinsic resistances. In order to circumvent these drawbacks, the scientific focus has shifted towards complexes with different metal centers such as gallium(III) and ruthenium(III). There are currently two ruthenium(III) complexes (NAMI-A and KP1019) in clinical trials, showing very promising results. In both cases the mode of action is thought to be initiated by *in vivo* reduction to the corresponding ruthenium(II) species in the hypoxic environment of the tumor tissue ("*activation by reduction*"). This hypothesis prompted the study of compounds, where the oxidation state +II of ruthenium is stabilized by coordination of an aromatic moiety, yielding so-called "piano-stool" complexes. Variations of the arene, the chelating ligand and the leaving group allow fine-tuning of chemical and biological properties, such as lipophilicity, water solubility and reactivity towards biomolecules. However, the biological properties of rhodium(III) complexes are nearly unexplored.

It has been reported that 1,3-dioxindan-2-carboxamides, due to structural similarities to known topoisomerase I/II inhibitors, exhibit very promising anticancer activity.

In the course of this master thesis a series of "piano-stool" configured ruthenium(II) and rhodium(III) complexes were synthesized with different *N*-alkylated 1,3-indandion-2-carboxamides as *O,O*-chelating ligands. These novel coordination compounds were characterized *via* 1D and 2D NMR spectroscopy, elemental analysis, and x-ray diffraction in two cases. Additionally, their solubility in PBS / 1 % DMSO was determined. By the use of ESI mass spectrometry the complexes were investigated towards their behavior in aqueous systems and their binding preferences towards biomolecules.

## Zusammenfassung

Übergangsmetallkomplexe zählen zu den wichtigsten Chemotherapeutika in der Behandlung von Krebs. Die dabei hauptsächlich Angewendeten sind Cisplatin, Carboplatin und Oxaliplatin. Durch unzulängliche Selektivität auf Tumorzellen weisen diese Wirkstoffe jedoch ein breites Spektrum an Nebenwirkungen, inklusive Resistenzen (angeeignet oder inhärent) auf. Um diese Nachteile zu umgehen, hat sich der Forschungsschwerpunkt auf Gallium(III)- und Ruthenium(III)-Komplexe verschoben. Im Moment zeigen zwei Ruthenium(III)-Komplexe (NAMI-A und KP1019) vielversprechende Ergebnisse und befinden sich in der zweiten Phase von klinischen Studien. In beiden Fällen geht man davon aus, dass die Aktivität der Wirkstoffe dadurch zustande kommt, dass das Zentralatom im hypoxischen Tumorgewebe zu Ruthenium(II) reduziert wird. Diese Hypothese veranlasste die Erforschung von Verbindungen, in denen das Rutheniumzentralatom schon in der Oxidationsstufe +II befindet. In diesen sogenannten „Pianostuhl“ Verbindungen, wird eben diese Oxidationsstufe durch einen facialen Arenliganden stabilisiert, der den Sitz des Pianostuhls bildet. Der Einsatz unterschiedlicher Arene, Chelatliganden und Abgangsgruppen machen ein breites Spektrum an Eigenschaften zugänglich. So lassen sich unter Anderem chemische und biologische Eigenschaften, wie zum Beispiel Lipophilie, Wasserlöslichkeit und die Reaktivität bezüglich Biomolekülen einstellen. Die biologischen Eigenschaften der analogen Rhodium(III)-Komplexen sind bislang größtenteils unerforscht.

Es ist erwiesen, dass 1,3-Dioxindan-2-carboxamide, wegen struktureller Ähnlichkeit zu bekannten Topoisomerase I/II-Inhibitoren, potentielle Zytostatika sind.

Im Rahmen dieser Masterarbeit wurde eine Reihe von „Pianostuhl“-konfigurierten Ruthenium(II)- und Rhodium(III)-Komplexen synthetisiert, mit unterschiedlich *N*-alkylierten 1,3-Indandion-2-carboxamiden als *O,O*-Chelatliganden. Diese neuartigen Koordinationsverbindungen wurden mit 1D und 2D NMR-Spektroskopie, Elementaranalyse und Röntgenstrukturanalyse charakterisiert. Zusätzlich wurde ihre Löslichkeit in PBS / 1 % DMSO bestimmt. Mittels ESI-Massenspektrometrie wurden besagte Komplexe auf ihr Verhalten in wässrigen Medien und ihr Bindungsverhalten mit Biomolekülen untersucht.



## Contents

<b>Abbreviations.....</b>	<b>1</b>
<b>1 Introduction.....</b>	<b>3</b>
1.1 Motivation for cancer research .....	3
1.2 Carcinogenesis.....	3
1.3 Cancer treatment.....	6
1.4 Classes of chemotherapeutics .....	7
1.5 Cytotoxic metal complexes.....	8
1.6 1,4-Naphthoquinones .....	20
1.7 1,3-Indandionecarboxamides .....	22
<b>2 Results and Discussion .....</b>	<b>24</b>
2.1 Synthesis and characterization of the ligands.....	24
2.2 Synthesis and characterization of complexes .....	31
<b>3 Experimental .....</b>	<b>45</b>
3.1 Equipment and Methods .....	45
3.2 Materials .....	47
3.3 General procedures.....	48
3.4 Synthesis of the ligand precursor 2-oxido-3-phenyliodonio-1,4-naphthoquinone .....	50
3.5 Syntheses of Ligands .....	51
3.6 Syntheses of ( $\eta^6$ -cymene)-ruthenium(II) complexes .....	60
3.7 Syntheses of ( $\eta^5$ -Cp*)-rhodium(III) complexes.....	70
<b>4 Conclusion .....</b>	<b>79</b>



## Abbreviations

1D/2D NMR	one- and/or two-dimensional NMR spectroscopy
Å	angstrom ( $10^{-10}$ m)
acac	acetylacetonato ligand
°C	degree Centigrade
bip	biphenyl
br	broad (NMR)
BRCA-gene	breast cancer gene
CDC	cell division cycle
CDK	cyclin dependent kinase
$\text{CDCl}_3$	deuterated chloroform
$\text{Cp}^*$	1,2,3,4,5-pentamethylcyclopentadienyl ligand
COSY	correlated spectroscopy (NMR)
cym	<i>p</i> -cymene
cyt	cytochrome C
$\delta$	chemical shift (NMR)
d	doublet (NMR)
5'-dAT(D)P	5'-desoxyadenosinetri(di)phosphate
DCM	dichloromethane
dha	dihydroanthracene
$\text{DMSO}(d_6)$	(deuterated) dimethyl sulfoxide
DNA	desoxyribonucleic acid
<i>e.g.</i>	<i>exempli gratia</i> (for example)
en	ethylenediamine
EPR	enhanced permeability and retention effect
eq	equivalent
ESI-MS	electrospray ionization mass spectrometry
<i>et al.</i>	<i>et alii</i> (and others)
EtOH	ethanol
5'-dGT(D)P	5'-desoxyguanosinetri(di)phosphate
h	hour
HIV	human immunodeficiency virus
HMBC	heteronuclear multiple bond correlation
HSA	human serum albumin

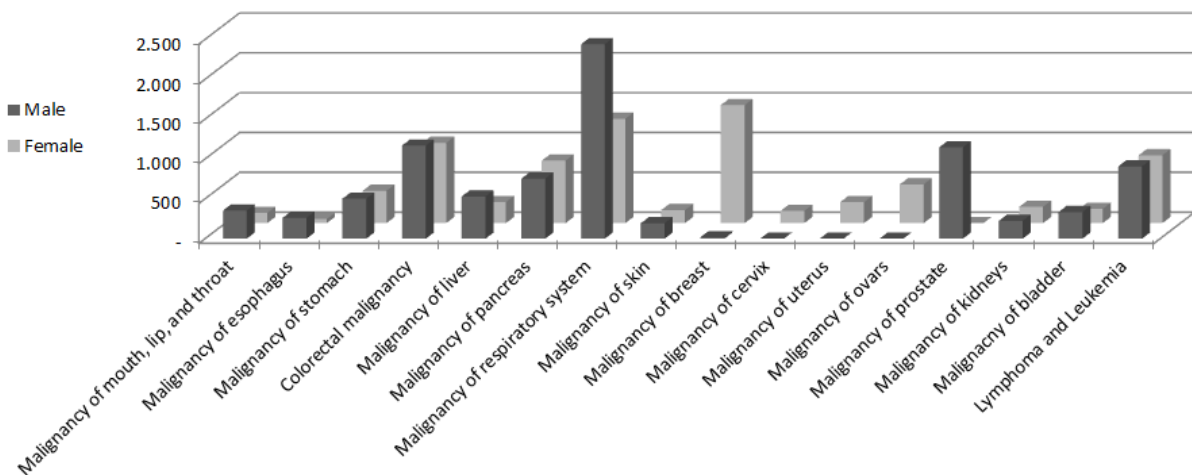
HSAB..... hard and soft acid and base principle  
 HSQC ..... heteronuclear single quantum coherence  
 (M)Hz ..... (mega)hertz ( $s^{-1}$ )  
 IC<sub>50</sub> ..... drug concentration that causes 50% cell growth inhibition  
 J ..... coupling constant (NMR)  
 (m/ $\mu$ /n)M ..... (milli/micro/nano)molar (mol / L; mmol / L;  $\mu$ mol / L; nmol / L)  
 m ..... multiplet (NMR)  
 min..... minute  
 MeOH ..... methanol  
 MMR..... mismatch repair  
 NMR ..... nuclear magnetic resonance spectroscopy  
 PBS ..... phosphate buffered saline  
 PDT ..... photodynamic therapy  
 pH..... pondus Hydrogenii (power of hydrogen)  
 pKa ..... log K<sub>a</sub> (acid dissociation constant)  
 ppm..... parts per million  
 RNA ..... ribonucleic acid  
 ROS..... reactive oxygen species  
 s ..... singlet (NMR)  
 tha ..... tetrahydroanthracene  
 Tf ..... transferrin  
 Ub..... ubiquitin

# 1 Introduction

## 1.1 Motivation for cancer research

Cancer is the second leading cause of death worldwide, after cardiovascular diseases. In 2011, 19,992 people died due to this disease in Austria where 52.9 % were males and 47.1% females<sup>1</sup>.

As cancer is a summarizing term, describing over 100 different diseases, it makes sense to analyze the mortality rates of the different types.



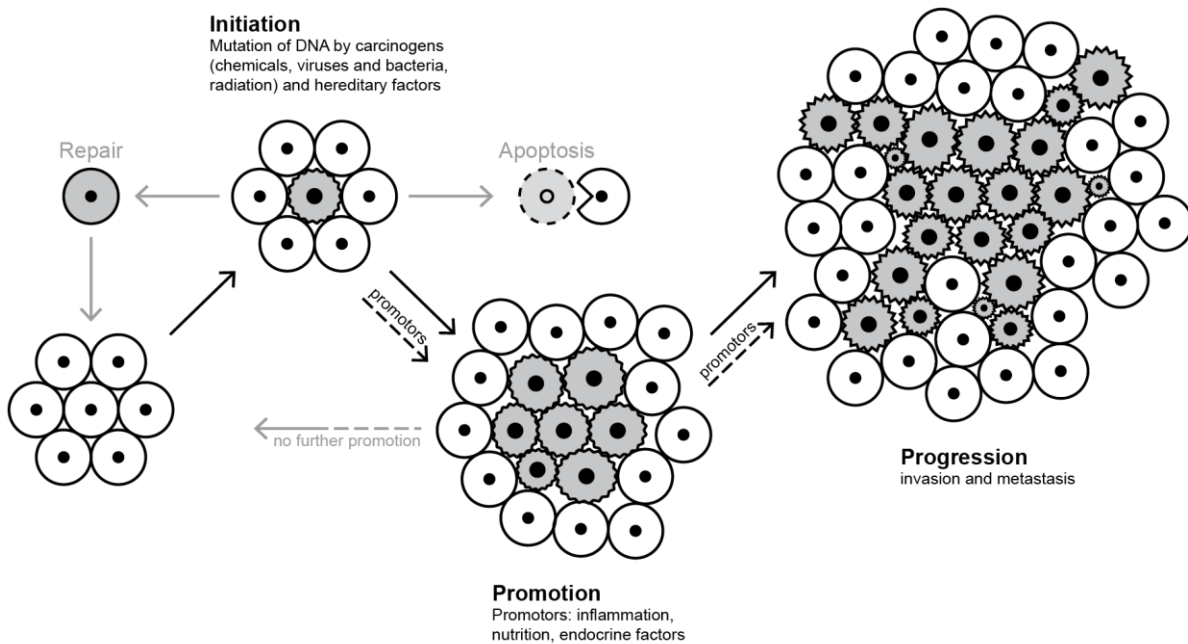
**Fig. 1** Cancer mortality in Austria divided into malignant origins

Fig. 1 shows that the highest incidences of malignancy caused deaths among men is attributed to lung cancer (23 %), followed by colorectal carcinoma (11 %), and prostate cancer (10%). Among women, the leading cancer related death cause is breast cancer (15 %), followed by lung cancer (14 %), and colorectal carcinoma (11 %).

## 1.2 Carcinogenesis

Cancer is an affliction, where cells start growing abnormally, invade the surrounding tissue, and spread to other parts of the body. Even though, there are over a hundred different cancerous diseases classified, they can be divided into three categories. Carcinomas are malignancies derived from epithelial cells (e.g. lung, breast, prostate, colorectal, and pancreatic tumors), sarcomas derive from mesenchymal cells (e.g. bone, cartilage, vascular, fat, and muscle), and finally, non-solid tumors derived from hematopoietic cells (e.g. leukemia and lymphoma).

<sup>1</sup> [http://www.statistik.at/web\\_de/statistiken/gesundheit/todesursachen](http://www.statistik.at/web_de/statistiken/gesundheit/todesursachen) visited 19/12/2012



**Fig. 2** Stages of carcinogenesis

The development of cancer from a single normal cell is called carcinogenesis and is generally divided into three stages: initiation, promotion, and progression (Fig. 2).

A cell is initiated by mutations of its DNA by different kinds of carcinogens, which can be divided into three subclasses: chemicals (N-nitrosamines, polycyclic aromatic hydrocarbons, heterocyclic aromatic amines, mycotoxins, heavy metals, hormones, and compounds mimicking hormones), biological, namely viruses (e.g. human papilloma virus, hepatitis B, HIV) or bacteria (*Helicobacter pylori*), and physical (radiation, including radioactivity). However, 5 – 10 % of cancers derive from hereditary factors (e.g. BRCA1 and BRCA2 are genes on the 17<sup>th</sup> and 13<sup>th</sup> chromosome, respectively<sup>2</sup>). People with defective BRCA genes have higher incidences of breast-, ovarian-, colorectal-, and prostate carcinomas). These mutations are generally removed; otherwise the programmed cell death (*i.e.* apoptosis) is initiated. In the case of relevant genes mutation, *i.e.* encoding DNA repair-, apoptosis-, or cell division cycle-behavior, these damages are irreversible. During the next step initiated cells are promoted, *i.e.* they are stimulated to form benign tumors *via* endogenous (e.g. hormones) and exogenous (e.g. tobacco and alcohol) factors. These preneoplastic (non-invasive) masses are dependent on constant stimulation by promoters, as their formation is completely reversible. Further exposition to carcinogens leads to fast and uncontrollable cell growth and division while progression.

<sup>2</sup> Calderon-Margalit, R., and Paltiel, O., *Int. J. Cancer*, **2004**, 112, 357-64.

Throughout carcinogenesis, cells acquire capabilities that distinguish them from normal cells<sup>3</sup>.

- ~ Self-sufficiency in growth signals: Chronic proliferation is accomplished by inherent production of growth factors, stimulating surrounding cells to provide growth factors for the cancer cell, or elevation of receptor proteins on the cell surface (*i.e.* hyperresponsiveness to growth factors).
- ~ Insensitivity to anti-growth signals or general inactivity of tumor suppressor genes
- ~ Evading apoptosis: If *e.g.* p53-function (a tumor suppressor protein) is lost, antiapoptotic regulators are expressed increasingly, and proapoptotic factors are downregulated.
- ~ Limitless replicative potential: Unlimited replication and evasion of cell senescence is achieved by extension of telomeric DNA.
- ~ Induction of angiogenesis: Tumors require nutrients and a way for evacuation of metabolic waste. Both needs are met *via* angiogenesis (*i.e.* formation of blood vessels). Shortage of oxygen (*i.e.* hypoxia) upregulates vascular endothelial growth factor-gene expression. The mixture of proangiogenic signals is usually unbalanced, leading to convoluted growth of vessels. This results in distorted and enlarged vessels, erratic blood flow, and leakiness (enhanced permeability and retention; 'EPR-effect')
- ~ Tissue invasion and metastasis: Altered expression of adhesion molecules weakens cell-cell association, leading to the so-called 'invasion-metastasis cascade'. After local invasion, the tumor invades blood and lymphatic vessels and cancer cells disseminate to other organs. There, they first form micrometastases (*i.e.* micronodules of cancer cells) of foreign tissue which then colonize and start invading this tissue as well.
- ~ Promoting inflammation of neoplasias: Inflammatory cells release actively carcinogenic chemicals (reactive oxygen species; 'ROS'), which lead to further mutations.
- ~ Reprogramming of energy metabolism: Due to the erratic growth of blood vessels and consecutive anaerobic areas, larger tumors often rely exceedingly on glycolysis, leading to lactate as waste (not carbon dioxide). This in turn, lowers the pH, the redox potential and increases the glutathione concentration in the tumor tissue<sup>4</sup>.

---

<sup>3</sup> Hanahan, D., and Weinberg, R.A., *Cell*, **2011**, 144, 646-74.

<sup>4</sup> Clarke, M.J., *Coord. Chem. Rev.*, **2003**, 236, 209-33.

### 1.3 Cancer treatment

Depending on location, type, and stage of development different methods of therapy are employed nowadays. They are surgical removal of tumors, radiation therapy, and the ever expanding field of chemotherapy. In most cases combinations of different therapy approaches are utilized. Three classes of treatment are distinguished: neoadjuvant (reducing the tumor mass before surgery or radiation), adjuvant (treatment of micrometastases and tumor remnants after surgery or radiation), and palliative (not meant to cure, but delay death), in case of non-treatable cancers)

Surgery: Benign, localized tumors are non-invasive and can usually be completely removed *via* surgery. Invasive primary tumors are sometimes minimized. However, in the case of (micro-) metastases and invasive tumors it usually isn't possible to remove the entire tumor.

Radiation: Radiation therapy utilizes highly energetic x-rays,  $\gamma$ -rays, or ionizing radiation in order to damage tumor cells. Only localized tumors and metastases are treatable *via* radiation. However, radiation harms both cancer and normal cells, and leads to considerable side effects, such as swelling of tissue, mucosal inflammation, and infertility due to gonadal damages. Due to the increased glutathione concentration in hypoxic tissue, DNA-radicals (caused by radiation) are oftentimes repaired through hydrogen donation leading to decreased sensitivity to radiation. The disorganized structure of tumors leaves them less efficient in dissipating heat. Applying a heat source to the tumor tissue weakens the cells and makes them more sensitive to chemotherapy<sup>5</sup>.

Chemotherapy: Knowledge of the inherent capabilities of cancer cells, inspired many different strategies to target cancer cells. These specially designed chemicals enter the cells *via* passive diffusion, transport proteins or by receptor-mediated endocytosis. Once inside these cells, they are aimed to cause damage to DNA or to proteins (e.g. in the cell division cycle CDC). Most anticancer drugs target fast dividing cells unselectively, causing severe side effects, as many different kinds of tissues have high replication rates as well (e.g. epithelial cells of oral mucosa, bones, gastrointestinal tract, and hair follicles). Others are designed to inhibit hormone production, due to the fact that hormones feed many types of cancer (e.g. breast cancer). Other strategies include immunotherapy and monoclonal antibody therapy. More sophisticated drug designs utilize chemicals that aren't cytotoxic, but are activated *in vivo* because of different properties of the tumor (e.g. reductive environment of the tumor; see section 1.2). These drugs are so-called 'prodrugs' and show far less side effects<sup>6</sup>.

---

<sup>5</sup> Ang, W.H., Casini, A., Sava, G., and Dyson, P.J., *J. Orgmet. Chem.*, **2011**, 696, 989-98.

<sup>6</sup> Sinhababu, A.K., and Thakker, D.R., *Advanced Drug Delivery Reviews*, **1996**, 19, 241-73.



#### 1.4 Classes of chemotherapeutics

- ~ Alkylating agents (e.g. Cyclophosphamide and Busulfan) are able to alkylate DNA, RNA and important proteins and therefore inhibit the cell replication.
- ~ Anti-metabolites (e.g. 5-fluoruracil and 6-thioguanin) are structurally similar to DNA nucleobases and are therefore integrated in the DNA double helix, inhibiting DNA replication, triggering CDC arrest and apoptosis *via* the mismatch repair (MMR) pathway. However, ca. 15% of solid tumors exhibit signs of MMR deficiency and are therefore resistant to treatment with anti-metabolites<sup>7</sup>.
- ~ Cytotoxic metal complexes: see section 0
- ~ Mitosis inhibitors: are compounds that interfere with the CDC. They inhibit the microtubule function and do not allow the cell to enter mitosis (e.g. taxol).<sup>8</sup>
- ~ Photodynamic Therapy (PDT): PDT uses non-toxic chemicals, which produce ROS upon irradiation, causing damage to DNA and proteins. PDT-drugs need to accumulate preferentially in cancer cells, have to produce high quantum yields of free radical intermediates, and have to absorb strongly at wavelengths which aren't absorbed by biological tissues (640 – 850 nm)<sup>9</sup>. PDT is usually employed in the case of easily accessible tumors of skin, neck, and bladder.
- ~ Topoisomerase inhibitors: Topoisomerase is an enzyme that regulates the DNA topology during protein synthesis. Two classes are found in mammalian cells: topoisomerase I (inducing controlled single strand breaks) and topoisomerase II (inducing double strand breaks). Representatives of these inhibitors are etoposide and doxorubicin), which are in clinical use.

Other strategies utilize other singularities of tumor cells. The EPR-effect, mentioned in section 1.2, inspired scientists to research nanoparticles as carriers of anticancer agents (e.g. liposomal- and micelle formulation<sup>10</sup>). Cancer cells depending on hormones have higher receptor-concentrations on their surfaces. Receptor-specific targeting drugs are therefore conjugates of hormones (e.g. osteosarcomas, estrogen-receptor positive breast cancer).

---

<sup>7</sup> Ernst, R.J., Song, H., and Barton, J.K., *J. Am. Chem. Soc.*, **2009**, 131, 2359-66.

<sup>8</sup> Qian, S., Chen, K., Morris-Natschke, S.L., and Lee, K.-H., *Curr. Pharm. Design*, **1998**, 4, 219-48.

<sup>9</sup> Levina, A., Mitra, A., and Lay, P.A., *Metallomics*, **2009**, 1, 458-70.

<sup>10</sup> Galanski, M., and Keppler, B.K., *Anti-Cancer Agents in Medicinal Chemistry*, **2007**, 7, 55-73.

## 1.5 Cytotoxic metal complexes

Metal ions are essential for life. Bulk metals have structural functions (e.g. Ca, Mg, Zn), others are charge carriers for ion pumps or signal transductions (e.g. Na, K, Ca). Redox-active metal ions transport electrons through the body (e.g. Fe, Cu, Mn) and others are present in the active site of enzymes; catalyzing vital reactions in eukaryotic organisms (e.g. Zn, Mg).

The earliest Chinese and Arabian records of metals used in medicine are dated back 3,500 years ago. Nowadays more and more coordination compounds are found in clinical use, as “*metal complexes, with their wide spectrum of coordination numbers, coordination geometries, thermodynamic and kinetic preferences (which cover enormous scales of magnitude) for ligand atoms, and in some cases redox activity, offer novel mechanisms of action which are unavailable to organic compounds*”<sup>11</sup>.

Metals are currently employed as direct reaction partners for biomolecules, carriers for *in vivo* delivered biologically active ligands, and as catalysts for *in vivo* generation of ROS.

### 1.5.1 Platinum complexes

The use of metal complexes for cancer treatment was inspired by Barnett Rosenberg. He investigated the effects of an electric field on *E. coli* growth in chloride rich medium employing platinum electrodes. The bacteria grew filamentously, a result of cell division inhibition. After careful investigation of his experimental set-up, he figured out that *cis*-diamminedichloridoplatinum(II) (cisplatin, Fig. 3) was formed<sup>12</sup>. Cisplatin is a square planar complex, first mentioned by Michael Peyrone in 1844<sup>13</sup>.

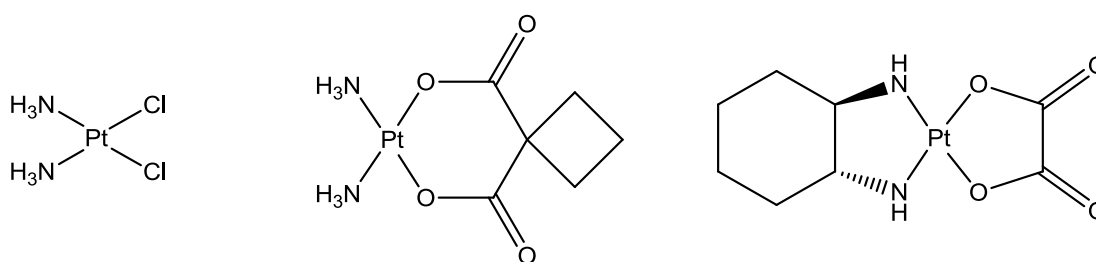


**Fig. 3** Structures of cisplatin, carboplatin, and oxaliplatin (left to right)

Said complex was then investigated *in vitro* and *in vivo*, passed the clinical trials and approved for cancer treatment (1978). Cisplatin exhibits efficacy against testicular-, ovarian-, head-, neck-, bronchial-, and bladder cancer<sup>14</sup>.

<sup>11</sup> Yan, Y.K., Melchart, M., Habtemariam, A., and Sadler, P.J., *Chem. Commun.*, **2005**, 4764-76.

<sup>12</sup> Rosenberg, B., *Platinum Metals Rev.*, **1971**, 15, 42-51.

<sup>13</sup> Peyrone, M., *Ann. Chem. Pharm. LI*, **1844**, 1-29.

<sup>14</sup> Reisner, E., Arion, V.B., Keppler, B.K., and Pombeiro, A.J.L., *Inorg. Chim. Acta*, **2008**, 361, 1569-83.

Cisplatin enters fast dividing cells *via* passive diffusion or actively by employing copper-transport proteins. Due to the fact that the intracellular chloride concentration decreases about two orders of magnitude (extracellular: 100mM, cell nucleus 4mM), one or both chlorido leaving groups are exchanged against water molecules. The activated positively charged complex is an attractive target for biological nucleophiles. About 1 % of the administered cisplatin reaches and interacts with DNA. In the case of mono-functional adducts, the DNA is distorted by about 6° and in the case of bi-functional adducts, about 13°. The adduct formed in 60 – 65 % of these cases are intrastrand G-G adducts, followed by intrastrand A-G adducts (20 – 25 %). Since cisplatin does not attack DNA specifically, it was proposed that apoptosis is not only initiated by the formation of DNA adducts but protein adducts as well<sup>15</sup>.

However, cisplatin shows severe side effects. Apart from high nephro-, neuro-, and ototoxicity, its administration results in hair loss and nausea, or even in intrinsic or acquired resistance. These adverse effects prompted the search for complexes, similar to cisplatin with leaving groups exhibiting lower exchange rates. This led to the development of carboplatin (Fig. 3). It shows efficacy against the same cancers as cisplatin but exhibits less toxic behavior, especially nephrotoxicity. Another complex, typically used for the treatment of metastatic colorectal cancer is oxaliplatin (Fig. 3). Its non-leaving group (*trans*-(R,R)-diaminocyclohexane), was introduced to reduce the exchange rate of leaving group.

While there is still considerable progress made in the research of novel platinum complex for cancer treatment (including octahedral Pt(IV) compounds), more and more effort is made to find active compounds with different metal centers.

---

<sup>15</sup> Sava, G., Jaouen, G., Hillard, E.A., and Bergamo, A., *J. Chem. Soc., Dalton Trans.*, **2012**, 41, 8226-34.

### 1.5.2 Ruthenium Complexes

Ruthenium was discovered in 1844 by the Russian chemist Karl Ernst Claus, who named the metal after his country (*lat.* Ruthenia). It is considered to be the most seldom and lightest of the platinum metals. According to the hard and soft acid and base (HSAB) principle Ru(II) is a soft acid, preferring soft ligands.

Ruthenium compounds have been investigated as immunosuppressants, nitric oxide scavengers, antimicrobials (e.g. malaria, Chagas disease), anticancer, and dental alloys<sup>11,16</sup>. In 1976, the first ruthenium compound with anticancer abilities (*fac*-[RuCl<sub>3</sub>(NH<sub>3</sub>)<sub>3</sub>]) was mentioned<sup>17</sup>. Due to solubility problems, this compound was not further investigated.

Ruthenium complexes have a number of specific characteristics and advantages to platinum compounds:

- ~ Rate of ligand exchange: Ru(II) and Ru(III) complexes show exchange kinetics, very similar to those of Pt(II) compounds. The ruthenium-ligand exchange kinetics can vary over several orders of magnitude upon ligand variation.
- ~ Accessible oxidation states: Ru(II), Ru(III), and Ru(IV) are accessible under physiological conditions and prefer octahedral geometry. This hexavalency leaves the possible ligand spheres of ruthenium compounds more versatile than Pt(II) complexes.
- ~ Lower general toxicity: Due to the fact that ruthenium is the heavier congener of iron, it can bind to biomolecules that usually transport iron. Amongst others like human serum albumin (HSA), it binds to transferrin (Tf), a glycoprotein (80 kDa) composed of a single polypeptide chain, arranged in two similar lobes. Each lobe binds one Fe<sup>3+</sup> ion through two tyrosine-, one histidine-, one aspartate residue, and one bidentate carbonate ion<sup>4</sup>. As mentioned in section 1.2, cancer cells exhibit a high nutrient requirement, leading to a higher expression of transferrin receptors on the cell surfaces. This fact enables a different and more selective mode of action for ruthenium.

The possibility of this new mode of action prompted the research of Ru(III)-compounds. Alessio *et al.* synthesized the first ruthenium compound to enter and complete phase I clinical trials: imidazolium[*trans*-tetrachlorido(S-dimethyl sulfoxide) imidazole ruthenate(III)] (NAMI-A, Fig. 4). This complex shows low *in vitro* cytotoxicity but remarkable efficacy against metastases *in vivo*<sup>18</sup>. It was proposed that rather proangiogenic proteins than DNA are the main targets of NAMI-A, leading to reduced cell invasiveness and migration<sup>19</sup>.

<sup>16</sup> Allardyce, C.S., and Dyson, P.J., *Platinum Metals Rev.*, **2001**, 45, 62-69.

<sup>17</sup> Bruijninx, P.C.A., and Sadler, P.J., *Advances in Inorganic Chemistry*, **2009**, 61, 1-62.

<sup>18</sup> Bruijninx, P.C.A., and Sadler, P.J., *Current Opinion in Chemical Biology*, **2008**, 12, 197-206.

<sup>19</sup> Bharti, S.K., and Singh, S.K., *Int. J. PharmTech Res.*, **2009**, 1, 1405 - 20.

The ruthenium(III) compound to follow NAMI-A through phase I clinical trial was synthesized by Keppler *et al.*, namely imidazolium[*trans*-tetrachloridobis(1H-indazole) ruthenate(III)] (KP1019, Fig. 4). This complex shows remarkable efficacy against colorectal carcinoma cell lines SW707 and SW948. A 70 – 90 % reduction of tumor size and even complete remission were observed *in vivo*, at concentrations well below the first signs of toxicity<sup>20</sup>.

The complex passively diffuses or is actively transported *via* transferrin receptor mediated endocytosis into the cell<sup>4</sup>. In both cases, Ru(III) is thought to be not the active species. According to the “activation by reduction” hypothesis, Ru(III) is supposed to be reduced to Ru(II) in the hypoxic environment of the tumor<sup>14</sup> (see section 1.2). This reduction leads to a labilization of the Ru(II)-Cl bond which in turn makes the central ion a more attractive target for biomolecule-nucleophiles. Formation of ROS is another possible way for the substance to harm the cancer cells<sup>21</sup>.

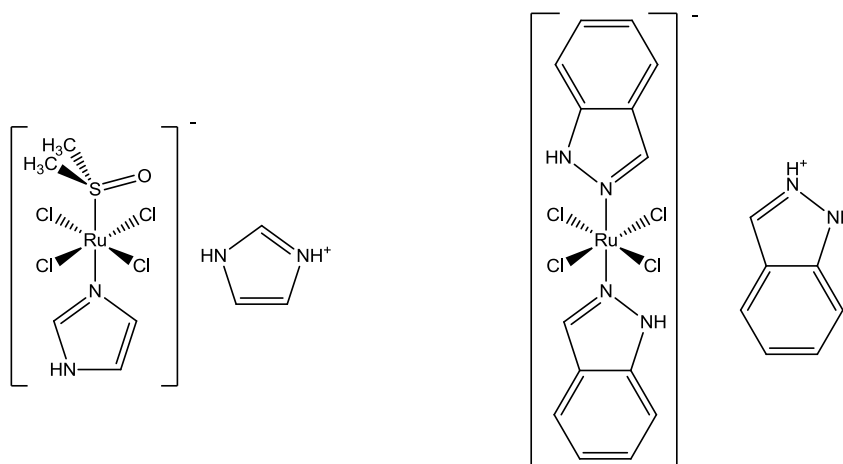


**Fig. 4** Structures of NAMI-A (left) and KP1019 (right)

This hypothesis led scientists to research anticancer drugs with ruthenium(II) as metal center.  $\eta^6$ -Coordinated arenes are known to stabilize this oxidation state and at the same time provide a lipophilic “face”, facilitating passive diffusion into cells. Additionally, these compounds exhibit good water solubility. These pseudo-octahedral half-sandwich [Ru<sup>II</sup>( $\eta^6$ -arene)(X)(Y)(Z)] complexes have so-called ‘piano-stool’ configuration (see Fig. 5) where the arene is the seat and the ligands X, Y, and Z are the chair legs. This scaffold is among the best studied ruthenium complexes with respect to catalysis<sup>22,23,24</sup>. Their biological properties, however, have only started to be investigated a few years ago.

<sup>20</sup> Galanski, M., Arion, V.B., Jakupec, M.A., and Keppler, B.K., *Current Pharmaceutical Design*, **2003**, 9, 2078-89.

<sup>21</sup> Kapitza, S., Jakupec, M.A., Uhl, M., Keppler, B.K., and Marian, B., *Cancer Lett.*, **2005**, 226, 115-21.

<sup>22</sup> Dixneuf, P.H., *Pure and Applied Chemistry*, **1989**, 61, 1763-70.

<sup>23</sup> Demonceau, A., Simal, F., and Noels, A.F., *NATO Science Series, II: Mathematics, Physics and Chemistry*, **2002**, 56, 227-45.

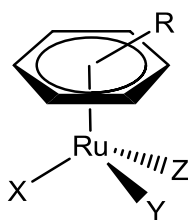


**Fig. 5** 'piano-stool' configured Ru(II) complex

The arene ligand not only enables passive diffusion through the lipid bilayer of biological membranes but also lowers the leaving group displacement probability. Depending on the structural ligands, there can be more than 89 % halogenated species found in blood plasma. Due to the lower chloride concentration in the nucleus, however, 45 – 65 % highly reactive aquo-species is found. Fig. 6 depicts this aquation behavior and shows the possible pathways of these compounds into the nucleus.

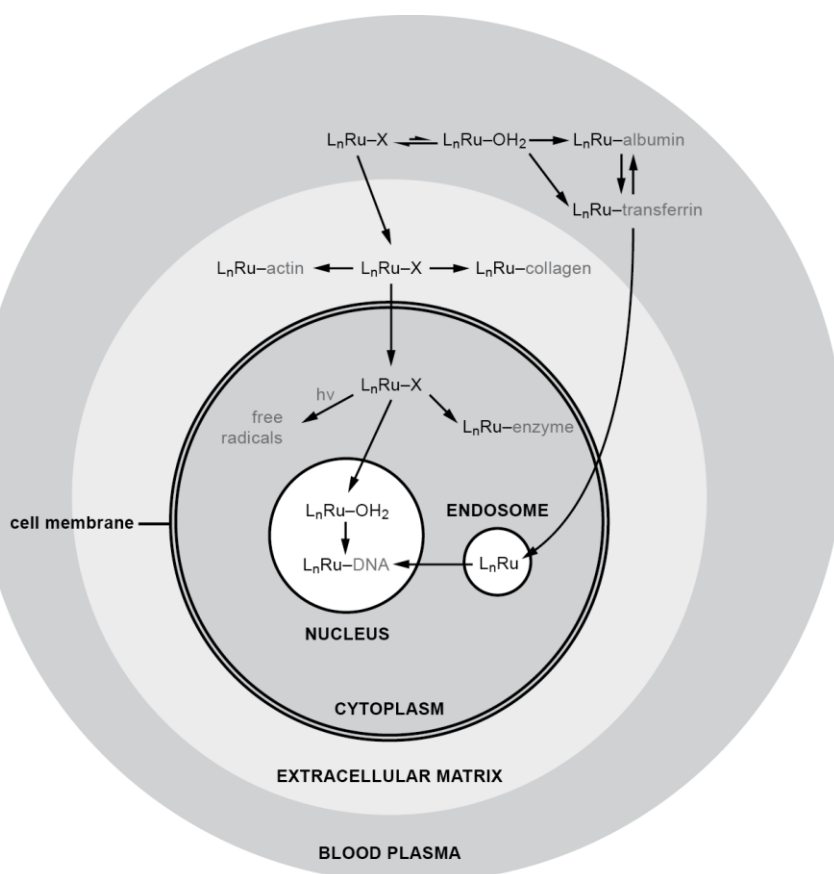


**Fig. 6** Mode of action of Ru(II)-arene complexes<sup>9</sup>. ( $L_n$  are tightly bound ligands)

As mentioned in section 1.5.1, the positively charged aqua-species is highly reactive and is able to interact with biological targets.

<sup>24</sup> Simal, F., Jan, D., Démonceau, A., and Noels, A.F., *ACS Symposium Series*, **2000**, 768, 223-33.

## Effects of ligand substitution of 'piano-stool' complexes<sup>17,28</sup>

The enormous number of possible ligand spheres makes the attainable properties incredibly versatile and easily fine-tunable.

~ 'piano-stool' complexes with three monodentate ligands

Complexes with three monodentate ligands, such as halides, acetonitrile, and isonicotinamide did not show noteworthy cytotoxicity. The proposed theory, explaining this fact, is that the leaving groups of complexes are too labile. This would mean that the complexes react with matrix components before reaching relevant biological targets.

One well known scaffold with three monodentate ligands is  $[\text{Ru}^{\text{II}}(\eta^6\text{-cym})\text{Cl}_2(\text{pta})]$  (pta = 1,3,5-triaza-7-phosphaadamantane, Fig. 7) and derivatives thereof. These ruthenium arene pta-complexes (RAPTA) are weakly cytotoxic *in vitro*, but show antimetastatic activity *in vivo* via induction of G<sub>2</sub>/M phase arrest<sup>5</sup>. It shows promising efficacy by reducing lung metastases of breast carcinoma. These complexes show similar aquation chemistry as other half-sandwich complexes.

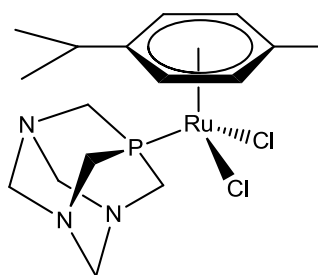


**Fig. 7** RAPTA-C complex

~ Effects of bidentate ligand systems (*N,N*-, *N,O*-, *O,O*-, and *S,O*-chelates)

The variation of chelating ligands has the most dramatic effect on the cytotoxicity. The resulting ring size (5 or 6), however, does only seem to effect the stability of the resulting complexes<sup>17</sup>.

- ~ *N,N*-chelates: Bidentately coordinated aliphatic diamines show good cytotoxicities.  $[(\eta^6\text{-arene})\text{Ru}^{\text{II}}(\text{en})(\text{Z})]$  (en = ethylenediamine) exhibit antiproliferative activity in the range of cisplatin and carboplatin, depending on the arene. Guanine-N7 is the electron densest site on DNA, making it the favored site for ruthenium coordination, apart from the phosphate groups of the DNA-backbone<sup>25</sup>. Another reason for the guanine affinity is the possibility of a stabilizing hydrogen bond to the G-O6 (Fig. 8). Generally, the following preference is observed: G-N7 > T-N3 > C-N3 > A-N7 ~ A-N1<sup>29,26</sup>. Ruthenium coordination to nucleobases results in DNA-unwinding up to 7 - 14 %<sup>27</sup>. It binds to the terminal carboxylic and amino groups and amino acid residues in the following order: L-cys > L-met > L-his<sup>11</sup>. Coordinated bipyridine and phenanthroline ligands are inactive *in vitro*, suggesting importance of the hydrogen bonds of the amine groups. This theory was affirmed by coordination to *N*<sup>1</sup>,*N*<sup>1</sup>,*N*<sup>2</sup>,*N*<sup>2</sup>-tetramethylethylenediamine. The resulting complex did not show noteworthy cytotoxicity<sup>28</sup>.

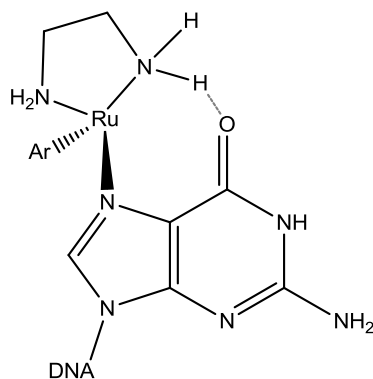


**Fig. 8** Hydrogen bond between en-ligand and G-O6

The reactive aqua-complex is known to dissociate with a  $\text{pK}_a$  of 7.71 – 8.01<sup>29</sup>, leaving the complex more inert to substitution of the hydroxo ligand.

<sup>25</sup> Kljun, J., Bytcek, A.K., Kandioller, W., Bartel, C., Jakupec, M.A., Hartinger, C.G., Keppler, B.K., and Turel, I., *Organometallics*, **2011**, 30, 2506-12.

<sup>26</sup> Pizarro, A.M., and Sadler, P.J., *Biochimie*, **2009**, 91, 1198-211.

<sup>27</sup> Liu, H.-K., and Sadler, P.J., *Acc. Chem. Res.*, **2011**, 44, 349-59.

<sup>28</sup> Habtemariam, A., Melchart, M., Fernandez, R., Parsons, S., Oswald, I.D.H., Parkin, A., Fabbiani, F.P.A., Davidson, J.E., Dawson, A., Aird, R.E., Jodrell, D.I., and Sadler, P.J., *J. Med. Chem.*, **2006**, 49, 6858-68.

<sup>29</sup> Ronconi, L., and Sadler, P.J., *Coord. Chem. Rev.*, **2007**, 251, 1633-48.



- ~ N,O-chelates: usual ligands providing a N,O-chelating scaffold are amino acids. The resulting complexes, however, did not show significant cytotoxicities.
- ~ O,O-chelates: despite the lack of the possibility for hydrogen bonding, these complexes show good to moderate cytotoxicities. Substitution of (en) with (acac = acetylacetonato) yielding  $[\text{Ru}^{\text{II}}(\eta^6\text{-arene})(\text{acac})(\text{Z})]$  (Fig. 9) results in vastly different selectivity towards nucleobases. Competitive binding of G and A revealed a somewhat higher affinity for A (A-N7 > A-N1), due to repulsive interactions between the carbonyl oxygen of acac and G-O6. More sophisticated O,O-chelating ligands, such as 3-hydroxy-4-pyrone ligands (Fig. 9) are very versatile synthetic platforms and can be utilized for fine-tuning of chemical and biological properties.  $\text{IC}_{50}$  values as low as 40  $\mu\text{M}$  in colon carcinoma cell line CH1 were observed<sup>30</sup>.

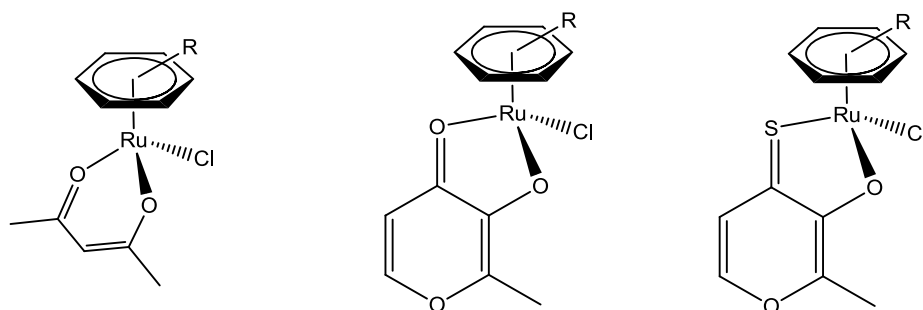


**Fig. 9**  $[(\eta^6\text{-arene})\text{Ru}^{\text{II}}(\text{acac})(\text{Cl})]$ ,  $[(\eta^6\text{-arene})\text{Ru}^{\text{II}}(\text{maltolato})(\text{Cl})]$ , and  $[(\eta^6\text{-arene})\text{Ru}^{\text{II}}(\text{thiomaltolato})(\text{Cl})]$   
(from left to right)

- ~ S,O-chelates: Substitution of the keto oxygen by sulfur (Fig. 9) leads to increased cytotoxicity towards ovarian cancer cell line CH1 (maltolato-complex:  $\text{IC}_{50} = 81 \pm 14 \mu\text{M}$ , thiomaltolato-complex:  $\text{IC}_{50} = 13 \pm 4 \mu\text{M}$ ) and colon carcinoma cell line SW480 (maltolato-complex:  $\text{IC}_{50} = 159 \pm 41 \mu\text{M}$ , thiomaltolato-complex:  $\text{IC}_{50} = 5.1 \pm 0.5 \mu\text{M}$ ).<sup>30</sup> The activity was explained by the increased stability of the complexes under physiological conditions.

<sup>30</sup> Kandjoller, W., Kurzwehnhart, A., Hanif, M., Meier, S.M., Henke, H., Keppler, B.K., and Hartinger, C.G., *J. Organomet. Chem.*, **2011**, 696, 999-1010.

~ Effects of different facial arene ligands:

Sadler *et al.* studied the effects of different arenes on the cytotoxicity of these complexes<sup>17,29,27,28</sup>.

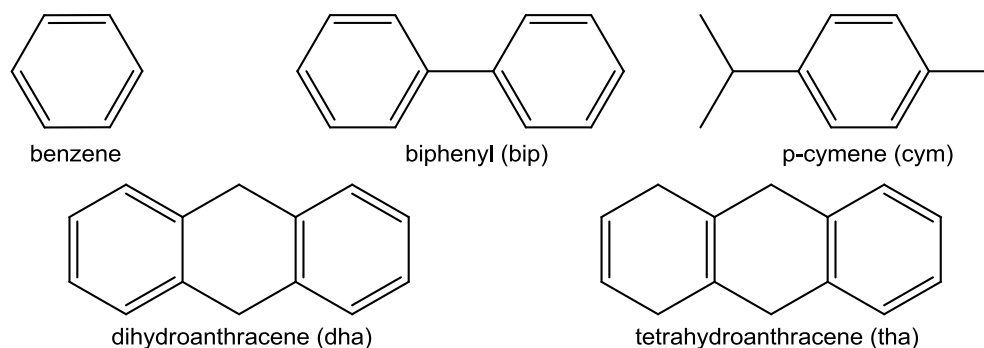


**Fig. 10** commonly used arene ligands for 'piano-stool' configured complexes

Generally, it can be stated that the cytotoxicity increases with the lipophilicity of the ligand and the following trend in the human ovarian carcinoma (A2780) cell line was observed:  $[\text{Ru}^{\text{II}}(\eta^6\text{-benzene})(\text{en})(\text{Cl})]$  ( $\text{IC}_{50} = 17 \mu\text{M}$ ) <  $[\text{Ru}^{\text{II}}(\eta^6\text{-cym})(\text{en})(\text{Cl})]$  ( $\text{IC}_{50} = 10 \mu\text{M}$ ) <  $[\text{Ru}^{\text{II}}(\eta^6\text{-bip})(\text{en})(\text{Cl})]$  ( $\text{IC}_{50} = 5 \mu\text{M}$ ) <  $[\text{Ru}^{\text{II}}(\eta^6\text{-dha})(\text{en})(\text{Cl})]$  ( $\text{IC}_{50} = 2 \mu\text{M}$ ) <  $[\text{Ru}^{\text{II}}(\eta^6\text{-tha})(\text{en})(\text{Cl})]$  ( $\text{IC}_{50} = 0.5 \mu\text{M}$ ) ~ Cisplatin. It was found that dha, tha, and bip complexes bind 50 % of calf thymus DNA within 10 – 15 minutes in cell free media whereas on the other hand, cymene complexes took up to three hours. Circular dichroism data revealed that bip and anthracene DNA-adducts cause bending without denaturation *via* minor groove binding or intercalation, much like cisplatin adducts. However, cym adducts seem to distort DNA more severely than cisplatin *via* stiffening. This stiffening can be felt over a range of at least seven basepairs in both directions, resulting in thermal destabilization of DNA and even denaturation<sup>26,31</sup>. Alkyl groups on the arene increase the electron density of the ruthenium center through  $\pi$ -electron donation, leading to stronger ruthenium – arene bonds.

However, no impact on the cytotoxicity was observed for O,O- or S,O chelates by variation of the arene ligand.

In the case of strong  $\pi$ -accepting chelate ligands (*e.g.* azopyridine ligands), the weaker  $\pi$ -accepting arene (*e.g.* bip) can be displaced under mild conditions in aqueous solution. This phenomenon is known as arene loss.

<sup>31</sup> Brabec, V., and Novakova, O., *Drug Resistance Updates*, **2006**, 9, 111-22.

~ Effect of leaving group substitution

Leaving group substitution has the weakest influence on the reactivity of ruthenium half-sandwich complexes. Higher electronegativity of the ligand results in lower electron density of the central atom and a more polarized metal – (pseudo-)halido bond. The observed trend is:  $\text{Cl}^- \sim \text{Br}^- > \text{I}^- > \text{N}_3^-$ <sup>32</sup>.

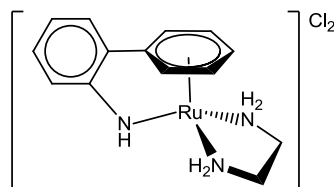


**Fig. 11** tethered sandwich-complex

Some efforts have been made to design tethered complexes (Fig. 11). Due to easily fine-tunable ring strain and pH, the tether dissociates offering a vacant site for biomolecule interaction<sup>33</sup>. More rigid tether scaffold, however, decreased the stability of the ruthenium arene bond, leading to arene loss.

### 1.5.3 Rhodium Complexes

Rhodium was discovered in 1803 by William Hyde Wollaston. Due to the deep red coloration of aqueous solutions of its salts, he named the element after the rose (*gr.* Rhodon). According to the HSAB principle it is a borderline acid, preferring carboxyl oxygen, amino nitrogen, and coordinates to DMSO *via* oxygen not sulfur, like ruthenium.

Rhodium compounds have been investigated<sup>16</sup> as dental alloys, antimicrobials (*e.g.* malaria, Leishmaniasis), antibiotics, and anticancer compounds, including radiosensitizers. 12 years before Rosenberg's serendipitous discovery of cisplatin, Taylor et al. mentioned anticancer activity of rhodium(III) chloride trihydrate<sup>34</sup>. However, rhodium complexes were considered unlikely candidates for anticancer agents, due to their general toxicity and low solubility. Additionally,  $[\text{Rh}(\text{H}_2\text{O})_6]^{3+}$  has exchange rates of four orders of magnitude lower than its square planar Pt analog  $[\text{Pt}(\text{H}_2\text{O})_4]^{2+}$ .

In 2003, the first Rh(III) complexes with interesting biological activity were mentioned<sup>35</sup>. As mentioned in section 0, mismatch repair (MMR) deficient cells are resistant to chemotherapy employing antimetabolites. MMR corrects single base errors arising during DNA synthesis. If

<sup>32</sup> Bugarcic, T., Habtemariam, A., Deeth, R.J., Fabbiani, F.P.A., Parsons, S., and Sadler, P.J., *Inorg. Chem.*, **2009**, 48, 9444-53.

<sup>33</sup> Pizarro, A.M., Melchart, M., Habtemariam, A., Salassa, L., Fabbiani, F.P.A., Parsons, S., and Sadler, P.J., *Inorg. Chem.*, **2010**, 49, 3310-319.

<sup>34</sup> Taylor, A., and Carmichael, N., *Cancer Studies* 2, **1953**, 5314, 36-79.

<sup>35</sup> Junicke, H., Hart, J.R., Kisko, J., Glebov, O., Kirsch, I.R., and Barton, J.K., *PNAS*, **2003**, 100, 3737-42.

these faults go uncorrected, they are converted to mutations in subsequent DNA replications, e.g.:  $[\text{Rh}(\text{chrysi})(\text{bpy})_2]^{3+}$  (chrysi = 5,6-chrysenequinone diimine) and  $[\text{Rh}(\text{phzi})(\text{bpy})_2]^{3+}$  (phzi = benzo[a]phenazine-5,6-quinone diimine) (Fig. 12) .

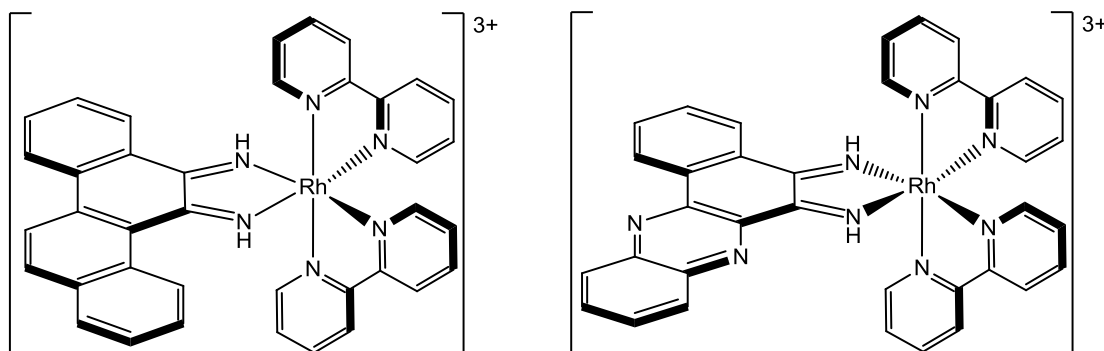


**Fig. 12**  $[(\text{chrysi})(\text{bpy})_2\text{Rh}]^{3+}$  (left) and  $[(\text{phzi})(\text{bpy})_2\text{Rh}]^{3+}$  (right)

Both of these complexes have remarkable affinity for base-pair mismatches.  $[(\text{chrysi})(\text{bpy})_2\text{Rh}]^{3+}$  binds 80 % of DNA mismatches, its specificity going so far as to bind one mismatch in a 2,725 base-pair linearized plasmid duplex. This recognition is thought to be associated with local helix instability due to base mispairings. Binding to mismatched sites involves insertion of the ligand into the DNA double strand from the minor groove and expulsion of both mismatched nucleobases<sup>36</sup>. The affinity was revealed by DNA photocleavage after intercalation. In mismatch repair proficient cell line SW620, no significant photocleavage was observed after incubation with the  $[\text{Rh}(\text{chrysi})(\text{bpy})_2]^{3+}$ .  $[\text{Rh}(\text{phzi})(\text{bpy})_2]^{3+}$  has a higher stabilization of the resulting DNA adduct due to better  $\pi$ - $\pi$ -stacking between the aromatic heterocycle (phzi) and the nucleobases. Both complexes show promising in vitro activity on colorectal carcinoma cell line HCT116.

Half-sandwich complexes of Rh have been subject to investigation as well<sup>37</sup>. The exchange rate of  $[\text{Rh}(\text{H}_2\text{O})_6]^{3+}$  increases by 14 orders of magnitude upon introduction of a facial 1,2,3,4,5-pentamethylcyclopentadienyl ( $\text{Cp}^*$ ) ligand ( $[\text{Rh}(\eta^5\text{-Cp}^*)(\text{H}_2\text{O})_3]^{3+}$ ). This labilizing effect is less prominent with neutral arene ligands, *i.e.* cym or benzene. As with 'piano-stool' configured ruthenium complexes, the effects of different chelate scaffolds have been studied.

<sup>36</sup> Cordier, C., Pierre, V.C., and Barton, J.K., *J. Am. Chem. Soc.*, **2007**, 129, 12287-95.

<sup>37</sup> Geldmacher, Y., Oleszak, M., and Sheldrick, W.S., *Inorg. Chim. Acta*, **2012**, 393, 84-102.

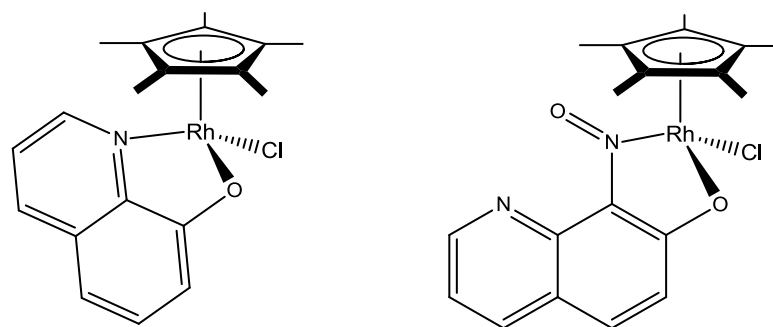


**Fig. 13**  $[\text{Cl}(\eta^5\text{-Cp}^*)(\text{qno})\text{Rh}]$  (left) and  $[\text{Cl}(\eta^5\text{-Cp}^*)(\text{npox})\text{Rh}]$  (right)

$\text{Rh(III)}(\eta^5\text{-Cp}^*)$  complexes with *N,O*-chelating ligands (Fig. 13) show remarkable efficacy:  $\text{IC}_{50}$ -values as low as 0.8  $\mu\text{M}$ , 0.9  $\mu\text{M}$ , and 5.0  $\mu\text{M}$  were observed for  $[\text{Rh}(\eta^5\text{-Cp}^*)(\text{qno})\text{Cl}]$  towards human melanoma SK-Mel, C-32, and human glioblastoma SNB-19 cells, respectively.<sup>37</sup>

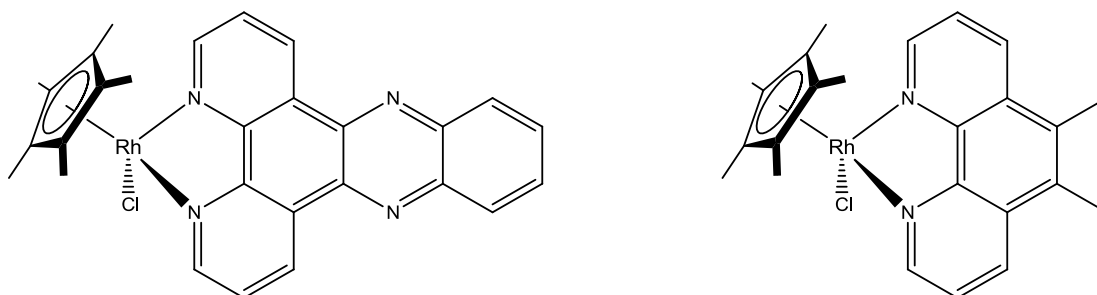


**Fig. 14**  $[\text{Cl}(\eta^5\text{-Cp}^*)(\text{dppz})\text{Rh}]$  (left) and  $[\text{Cl}(\eta^5\text{-Cp}^*)(5,6\text{-Me}_2\text{phen})\text{Rh}]$  (right)

$\text{Rh(III)}(\eta^5\text{-Cp}^*)$  complexes with *N,N*-chelating ligands (Fig. 14) exhibited immediate effects on isolated mouse liver mitochondria, inducing cytochrome C release, leading to apoptosis.<sup>37</sup>

Apart from the discussed platinum-, ruthenium-, and rhodium anticancer compounds, there is considerable research going on in the fields of gallium, osmium, iridium, titanium, germanium, and arsenic anticancer compounds.

## 1.6 1,4-Naphthoquinones

Naphthoquinones are secondary metabolites of many different life forms (including fungi, algae, and plants). There are 1,2-naphthoquinones and 1,4-naphthoquinones, depending on the keto group positions on the naphthalene scaffold. Mammals depend on vitamin K (Fig. 15) as a cofactor in different carboxylases, vital for the synthesis of blood clotting factors and other proteins. Menadione, however, is a synthetic 'vitamin K', which proved to be cytotoxic.

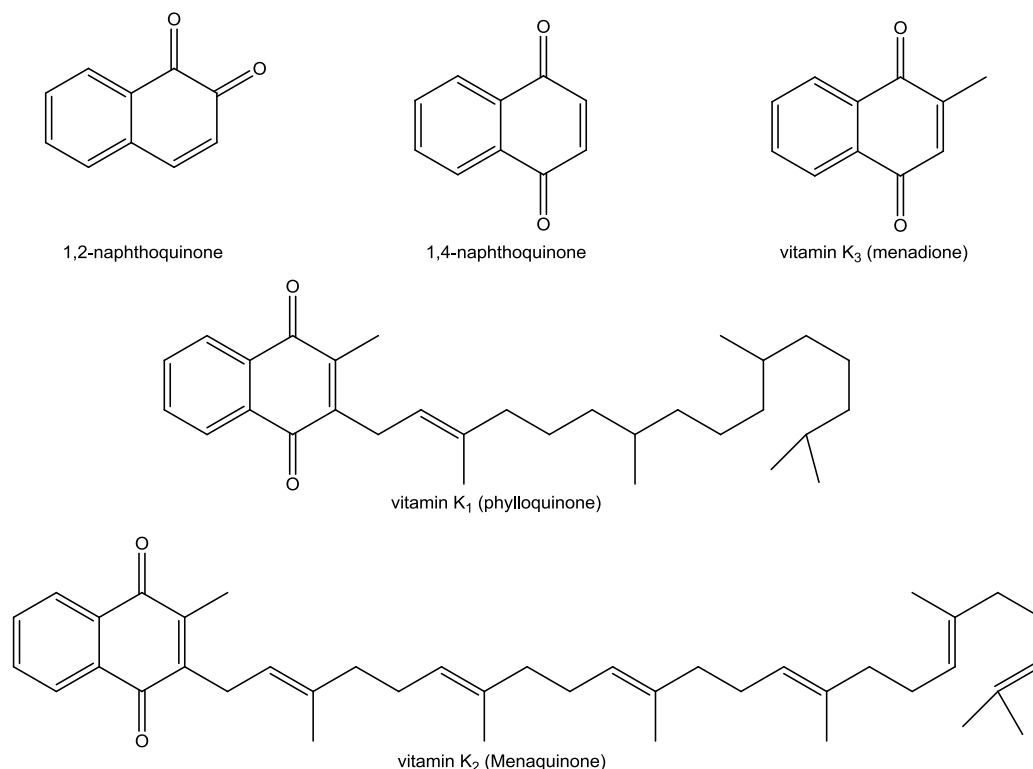


**Fig. 15** different naphthoquinone scaffolds and vitamin K

Naphthoquinones exhibit an enormous variety of different biological effects, such as antibiotic<sup>38</sup>, anti-tuberculosis<sup>39</sup>, anti-malaria<sup>40</sup>, anti-larvae<sup>38</sup>, anti-mollusk<sup>38</sup>, herbicidal<sup>38</sup>, fungicidal<sup>38</sup>, pesticidal<sup>40</sup>, anti-platelet<sup>41</sup>, and certain trimers even show anti-HIV potential<sup>40</sup>.

Naphthoquinones are redox active and are able to generate ROS *in vivo*.<sup>42</sup> These reactive oxygen species induce apoptosis via the intrinsic or extrinsic mitochondrial pathways<sup>43</sup>. Furthermore, the naphthoquinone scaffold is found in a number of topoisomerase II inhibitors<sup>44</sup>. Fig. 16 shows the structure of doxorubicin and mitoxantrone. Additionally,

<sup>38</sup> Tsukatani, T., Higuchi, T., Suenaga, H., Akao, T., Ishiyama, M., Ezoe, T., and Matsumoto, K., *Anal. Biochem.*, **2009**, 393, 117-25.

<sup>39</sup> Clark, N.G., *Pestic. Sci.*, **1985**, 16, 23-32.

<sup>40</sup> Spyroudis, S., *Molecules*, **2000**, 5, 1291-330.

<sup>41</sup> Lee, J.-J., Zhang, W.-Y., Yi, H., Kim, Y., Kim, I.-S., Shen, G.-N., Song, G.-Y., and Myung, C.-S., *Biochem. Biophys. Res. Comm.*, **2011**, 411, 213-18.

<sup>42</sup> Watanabe, N., and Forman, H.J., *Arch. Biochem. Biophys.*, **2003**, 411, 145-57.

<sup>43</sup> McKallip, R.J., Lombard, C., and Sun, J., *Toxicol. Appl. Pharmacol.*, **2010**, 247, 41-52.

<sup>44</sup> Wang, B., Miao, Z.W., and Wang, J., *Amino Acids*, **2008**, 35, 463-68.

naphthoquinones are known to inhibit cdc25 phosphatases. Cdc25 and its homologues are known to activate cyclin dependent kinases (CDK) via dephosphorylation. This activation, among other factors, guides the cell through all checkpoints of the CDC. In later-stage and more aggressive tumors, enhanced expression of cdc25A, cdc25B, and cdc25C is found<sup>45</sup>. When inhibited, the cell goes into CDC arrest and apoptosis, consecutively<sup>46,47</sup>. Fig. 16 shows the structure of compound 5 and NSC 95397.

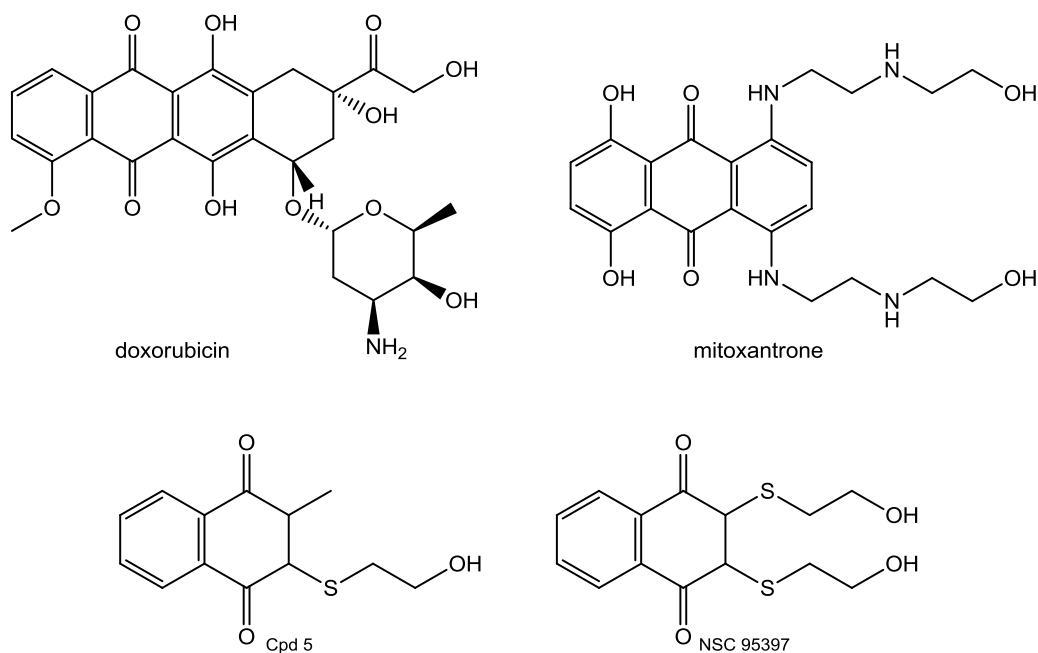


**Fig. 16** biologically active naphthoquinone derivatives

<sup>45</sup> Lavecchia, A., Di Giovanni, C., Pesapane, A., Montuori, N., Ragno, P., Martucci, N.M., Masullo, M., De Vendittis, E., and Novellino, E., *J. Med. Chem.*, **2012**, 55, 4142-58.

<sup>46</sup> Brun, M.-P., Braud, E., Angotty, D., Mondésert, O., Quaranta, M., Montes, M., Miteva, M., Gresh, N., Ducommun, B., and Garbay, C., *Bioorg. Med. Chem.*, **2005**, 13, 4871-79.

<sup>47</sup> Braud, E., Goddard, M.-L., Kolb, S., Brun, M.-P., Mondésert, O., Quaranta, M., Gresh, N., Ducommun, B., and Garbay, C., *Bioorg. Med. Chem.*, **2008**, 16, 9040-49.

## 1.7 1,3-Indandionecarboxamides

1,3-Indandiones are versatile and readily available starting materials for the synthesis of complex derivatives thereof. Reactions with amines<sup>48</sup> give rise to quinolones, structurally interesting diazo compounds, and in the case of 1,3-indandione-2-carboxylic acid ethyl ester, 1,3-indandione-2-carboxamides<sup>49</sup>. They constitute a class of compounds that is relatively unexplored for biological activity. Fig. 17 shows the general structure of these compounds. Due to the fact that the amide is substituted with two  $\beta$ -carbonyl groups, theoretically three enolic tautomers are possible. The enolization was found to occur on the amide side rather than on the C-carbonyl groups. Crystal picking revealed that both different constitutional isomers gave rise to differently colored crystals in solid form<sup>50</sup>.

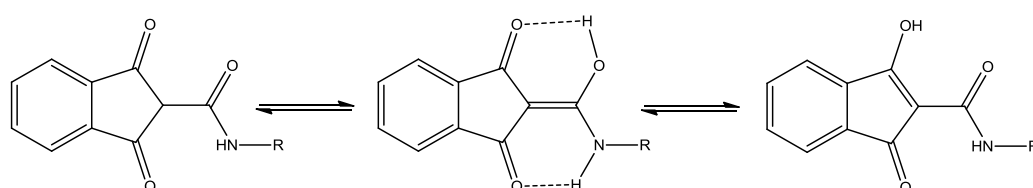


**Fig. 17** General structure of an 1,3-indandione-2-carboxamide (left) and tautomeric enols

However, in solvents with low polarity they exist solely as enols of the amide<sup>51</sup>. Compared to other amide enolates, 1,3-indandione-2-carboxamides were not found to exhibit notable acidity.

One mixed topoisomerase I/II inhibitor, currently in clinical trials is TAS-103 (6-[[2-(dimethylamino)-ethyl]amino]-3-hydroxy-7*H*-indeno[2,1-*c*]quinolin-7-one dihydrochloride, see Fig. 18).

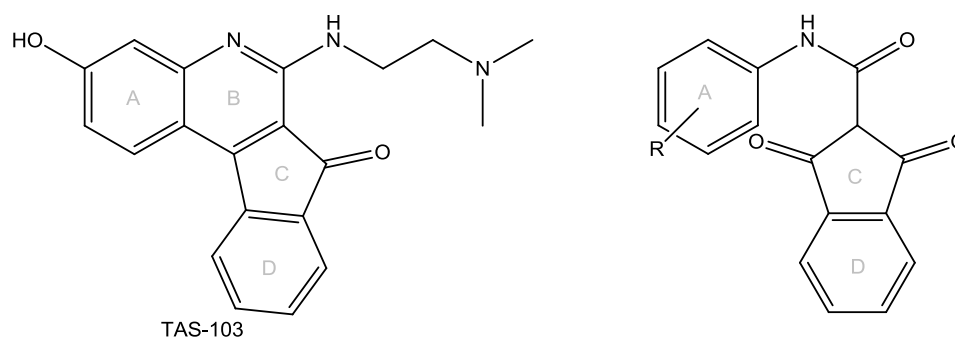


**Fig. 18** mixed isomerase I/II inhibitors

<sup>48</sup> Afsah, E.-S., and Zimaity, T., *Bull. Chem. Soc. Jpn.*, **1979**, 52, 3092-95.

<sup>49</sup> Malamidou-Xenikaki, E., Spyroudou, S., and Tsanakopoulou, M., *J. Org. Chem.*, **2003**, 68, 5627-31.

<sup>50</sup> Song, J., Mishima, M., and Rappoport, Z., *Org. Lett.*, **2007**, 9, 4307-10.

<sup>51</sup> Lei, Y.X., and Rappoport, Z., *J. Org. Chem.*, **2002**, 67, 6971-78.



Based on this compound 1,3-indanedione-2-carboxamide derivatives (see Fig. 18) were synthesized and tested on human colon carcinoma cell line HCT-15, ovarian carcinoma cell line SK-OV3, breast adenocarcinoma cell line MD-MB-468, and breast ductal carcinoma cell line T-47D<sup>52</sup>. Tab. 1 compares the excellent IC<sub>50</sub>-values of these indandiones to the already established doxorubicin.

**Tab. 1** Comparison of IC<sub>50</sub>-values of known topoisomerase II inhibitor and newly synthesized 1,3-indandione-2-carboxamide derivatives

Compound	IC <sub>50</sub> [μM]			
	HCT15	SK-OV-3	MD-MB-468	T-47D
2-methoxy	1.6	6	3.1	5.3
4-methyl	1.7	1.2	4.1	4
3,5-dichloro	1.4	20	5	3
doxorubicin	0.022	0.012	0.002	0.005

<sup>52</sup> Jung, J.-K., Ryu, J., Yang, S.-I., Cho, J., and Lee, H., *Arch. Pharm. Res.*, **2004**, 27, 997-1000.

## 2 Results and Discussion

The original goal of this thesis was the design of a synthetic route, yielding 3-hydroxy-1,4-naphthoquinones derivatives and 'piano-stool' configured ( $\eta^6\text{-cym}$ )Ru<sup>II</sup> and ( $\eta^5\text{-Cp}^*$ )Rh<sup>III</sup> complexes of these chelating ligands (Fig. 19). In order to increase their solubility, amino substituents were supposed to be introduced in the 2-position of the naphthoquinone scaffold. These complexes were characterized via <sup>1</sup>H-NMR, <sup>13</sup>C-NMR, different two dimensional NMR-techniques, x-ray diffraction analysis, and elemental analysis. Additionally, their melting point, solubility, stability and metabolism in cell free media were determined.

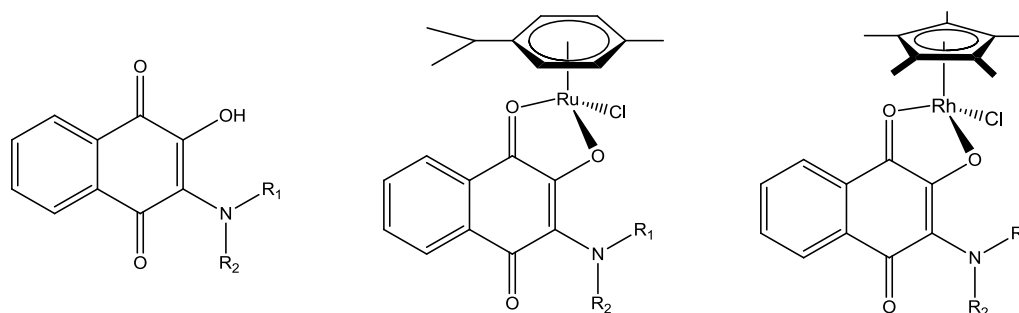


Fig. 19 Desired compounds in the course of this thesis

### 2.1 Synthesis and characterization of the ligands

#### 2.1.1 Synthesis of the ligands

Many different nucleophilic substitution strategies were carried out. Some of which using 2-hydroxy-1,4-naphthoquinone (lawsone) as starting material, others 2,3-dichloro-1,4-naphthoquinone or 2-halido-3-hydroxy-1,4-naphthoquinone. No approach, however yielded the desired 2-amino-3-hydroxy-1,4-naphthoquinone.

The strategy reported by Francisco *et al.*<sup>53</sup>, included the derivatization of lawsone with a 3-((3-nitrophenyl)diazenyl) substituent and subsequent reduction in order to yield the free 2-amino-3-hydroxy-1,4-naphthoquinone (**L0**). 2-Hydroxy-3-((3-nitrophenyl)diazenyl)naphthalene-1,4-dione (**L0p**) was synthesized with 96 % yield (Fig. 20).

<sup>53</sup> Francisco, A.I., Casellato, A., and Vargas, M.D., *Org. Prep. Proced. Int.*, **2009**, 41, 323-26.

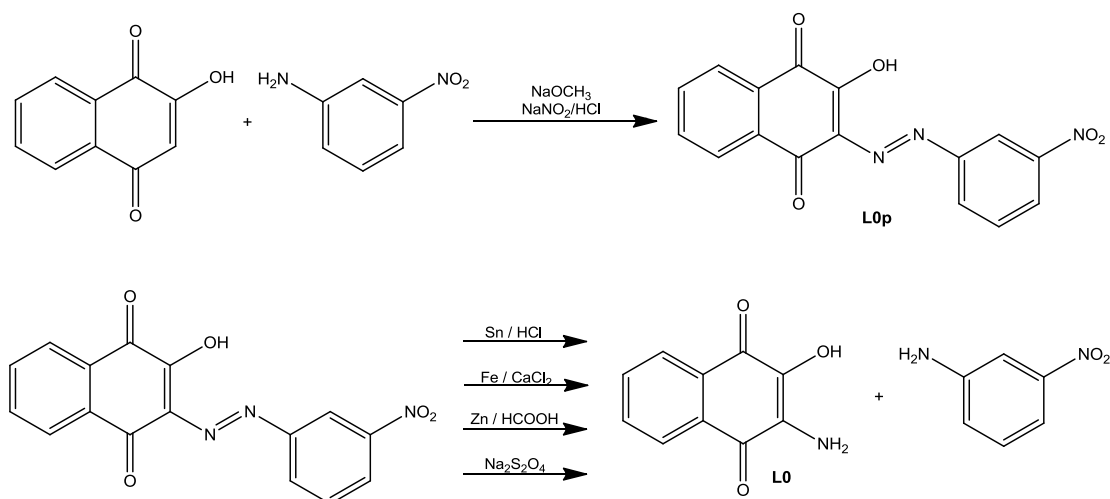


**Fig. 20** Reaction scheme to yield **L0p** and **L0**

The subsequent reductive cleavage was performed in four different conditions leading to either no desired product, or unsatisfactory yields (Tab. 2). Of the three metals used, only the main group element tin did yield **L0**. In the case of iron and zinc, removal of the metal powder resulted in depletion of the educt/product. The assumption of complexation of educt/product with these transition metals, inspired the reduction with sodium dithionite. This reduction, however, reduced the naphthoquinone moiety as well. The usual route of oxidation of the resulting 1,4-dihydroxynaphthalene, employing atmospheric oxygen, didn't yield the desired product either. Therefore, another synthetic approach was utilized.

**Tab. 2** Reduction conditions in order to yield **L0**

Reducing agent	Solvent	Temperature; Reaction time	Equivalents Reducing agent	yield
Sn / HCl <sup>53</sup>	conc. HCl / EtOH		6.7 eq. Sn	10%
Fe / CaCl <sub>2</sub> <sup>54</sup>	EtOH	60 °C; 5 h	3 eq. Fe- powder 12 eq. CaCl <sub>2</sub>	-
Zn / HCOOH <sup>55</sup>	MeOH	rf.; 2 h	2 eq. Zn-powder 5 eq. HCOOH	-
Na <sub>2</sub> S <sub>2</sub> O <sub>4</sub> <sup>56</sup>	EtOH	rf.; 3 h	4 eq. Na <sub>2</sub> S <sub>2</sub> O <sub>4</sub>	-

<sup>54</sup> Chandrappa, S., Vinaya, K., Ramakrishnappa, T., and Rangappa, K.S., *Synlett*, **2010**, 20, 3019-22.

<sup>55</sup> Serwa, R., Nam, T.-g., Valgimigli, L., Culbertson, S., Rector, C.L., Jeong, B.-S., Pratt, D.A., and Porter, N.A., *Chem. Eur. J.*, **2010**, 16, 14106-14.

<sup>56</sup> Hassan, G.S., and Soliman, G.A., *Eur. J. Med. Chem.*, **2010**, 45, 4104-12.

First a zwitter ionic precursor (2-oxido-3-phenyliodonio-1,4-naphthoquinone) was synthesized by reaction of lawsone with (diacetoxyiodo)benzene overnight in chloroform. The yields were excellent; usually around 91%. In acidic medium, the dipole is an electrophile, supposed to be attacked by nucleophiles, like amines. After many unsuccessful attempts, the reaction of 2-oxido-3-phenyliodonio-1,4-naphthoquinone with benzylamine in chloroform (dried over molecular sieves) did yield product.

**Tab. 3** Generated 1,3-dioxindanes

Amine	Reaction time	Yield	Product
Methylamine	30 h	85 %	L1
Ethylamine	30 h	83 %	L2
Propylamine	72 h	74 %	L3
Benzylamine	8 h	96 %	L4

NMR characterization (section 2.1.2) of the synthesized products, however, revealed that the naphthoquinone scaffold had rearranged to the corresponding 1,3-dioxindanes. The mechanism of the Wolff-type rearrangement is mapped out in Fig. 21. Elimination of iodobenzene leads to the ketocarbene, which subsequently rearranges to a ketene *via* ring-contraction. This highly reactive intermediate then reacts with the amine, yielding an 1,3-indandione-2-carboxamide. If water was present, 1,3-indandione-2-carboxylic acid would be formed, which would then decarboxylate and 1,3-indandione would be the product<sup>57</sup>. Due to the afore mentioned biological activity of this scaffold (section 1.7) and the lack of complexes thereof in literature, 1,3-indandione-2-carboxamides became the new focus of this master thesis.

<sup>57</sup> Papoutsis, I., Spyroudis, S., and Varvoglis, A., *Tet. Lett.*, **1994**, 35, 8449-52.

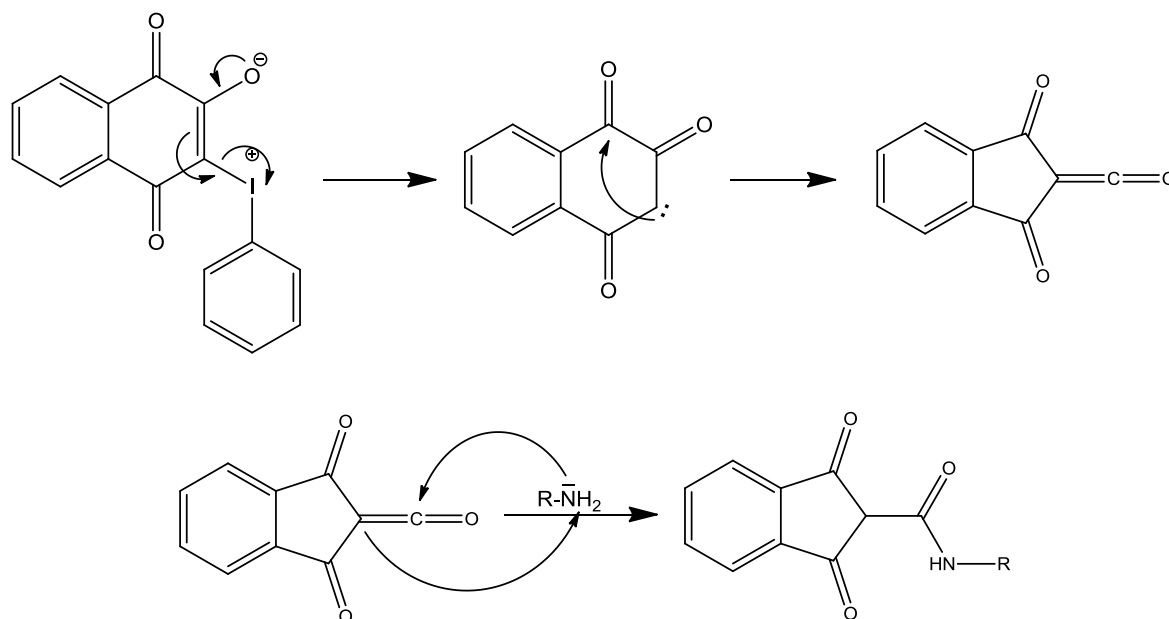


**Fig. 21** Wolff Rearrangement and subsequent reaction with an amine

2-Oxido-3-phenyliodonio-1,4-naphthoquinone reacts with an amine in chloroform (dried over molecular sieves) under argon atmosphere for varying amounts of time, depending on the amine (Fig. 22) and after aqueous work up the desired ligand were isolated in good to excellent yields (74 – 96 %).

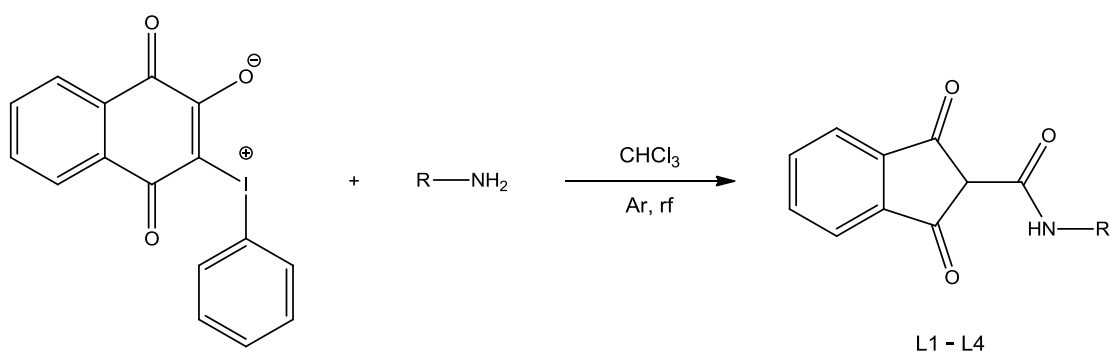


**Fig. 22** Synthesis of ligands **L1 – L4**

The synthesized 1,3-indandione-2-carboxamides are shown in Fig. 23. Apart from the primary amines methylamine, ethylamine, propylamine, and benzylamine, the reaction was also carried out with secondary amines (dimethylamine, diethylamine, diisopropylamine, pyrrolidine, and piperidine), and with functionalized amines (morpholine, *N*-methylpiperazine, 2-morpholinopropylamine, ethylenediamine, 1,4-diaminobutane, ethanolamine, 3-aminopropanol, 2-aminobutan-1-ol, glycine, 4-aminobutanoic acid, and 6-aminocaproic acid). However, in every case, the reaction mixture was refluxed for days, and TLC analysis showed no conversion in any case. In the case of propargylamine, the reaction yielded the

desired *N*-propargyl-1,3-indancarboxamide with good yield (73 %). This compound was not used for complexation because the triple bond is capable of forming  $\eta^2$ -coordination compounds with transition metals, but can be used as precursor for further modifications.

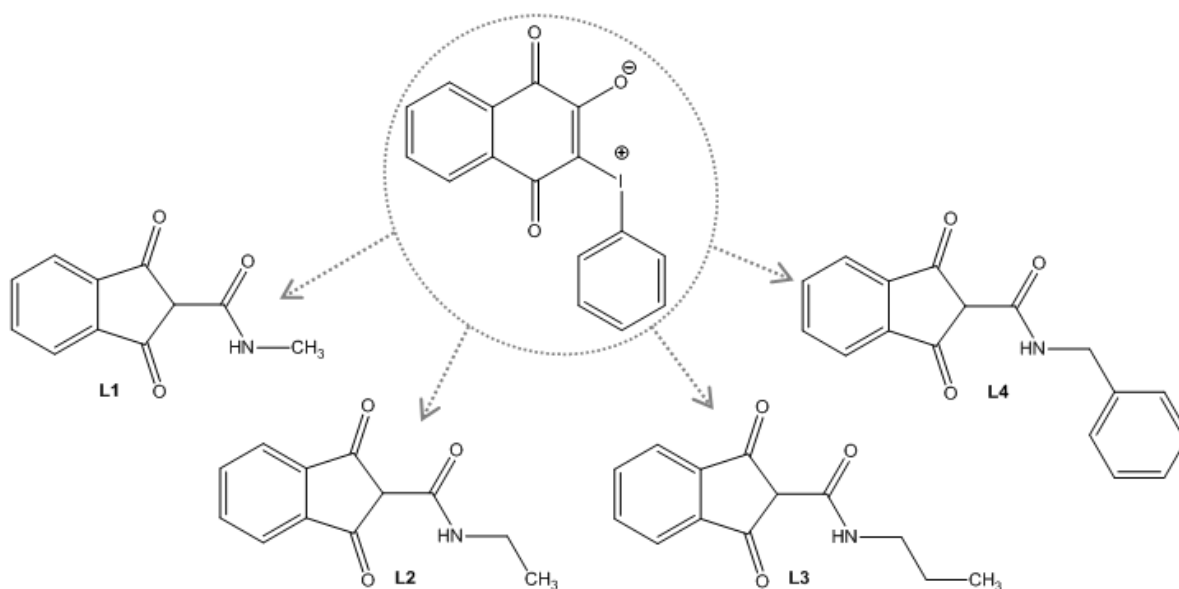


**Fig. 23** Synthesized ligands

### 2.1.2 Characterization of the ligands

The ligands **L1** - **L4** were characterized with elemental analysis, and  $^1\text{H-NMR}$  and  $^{13}\text{C-NMR}$  in deuterated dimethyl sulfoxide ( $\text{DMSO-d}_6$ ). Furthermore the melting point and solubility were determined.

#### $^1\text{H-NMR}$

The indane-scaffold protons were typically found at 7.55 – 7.67 ppm. The arising multiplet is highly symmetric, which is a clear indication of the scaffold, not being an unsymmetrically substituted naphthoquinone.

The amino protons were found around 8.7 ppm, evidence of this signal not arising from a hydroxyl-proton, which would be shifted further down-field. In the case of **L4** this signal is shifted to 9.2 ppm due to the additional deshielding effect of the benzyl substituent.

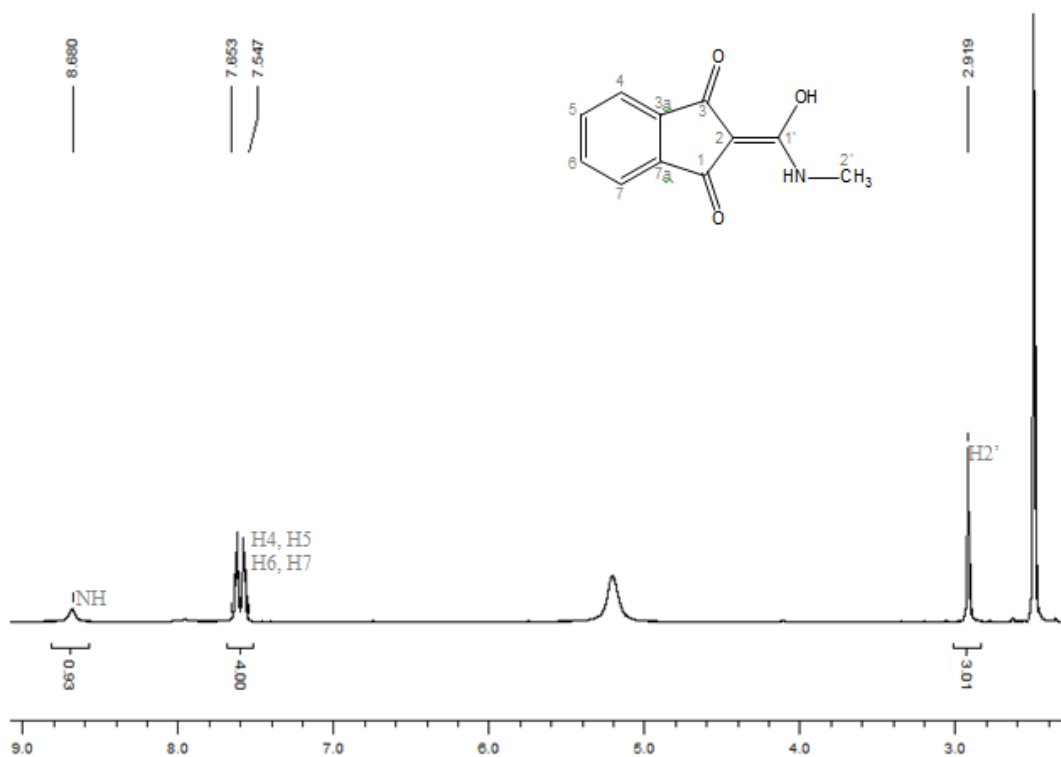
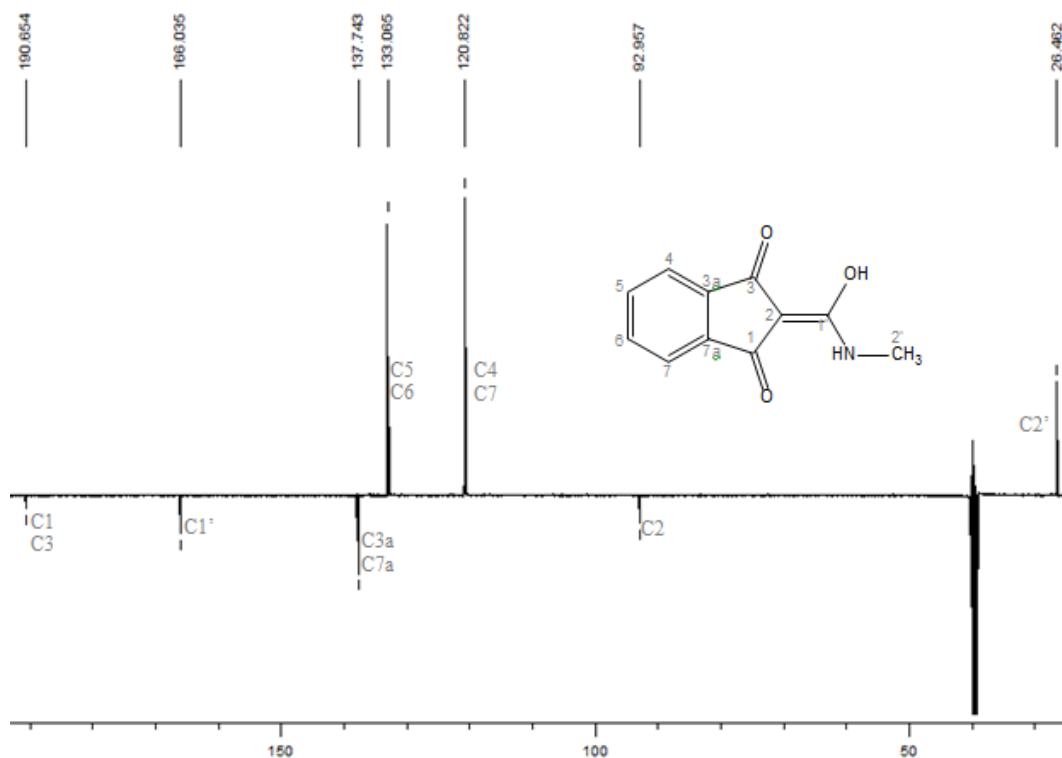


Fig. 24  $^1\text{H-NMR}$  of **L1**

## <sup>13</sup>C-NMR

The keto-carbon signals were found at around 191 ppm, as expected. The amide carbon signals were found typically at 166 ppm.

Another clear indication of the indandione scaffold formed, is the symmetry found with the aromatic carbons. The annealed carbons showed one signal found around 138 ppm, C4/C7 at around 121 ppm, and C5/C6 at 133 ppm, respectively.



**Fig. 25** <sup>13</sup>C-NMR of L1

Theoretically, there are four tautomers possible (Fig. 26). The symmetry found in the <sup>1</sup>H-NMR and <sup>13</sup>C-NMR spectra, proves the statement from section 1.7. The amide carbon is enolized.

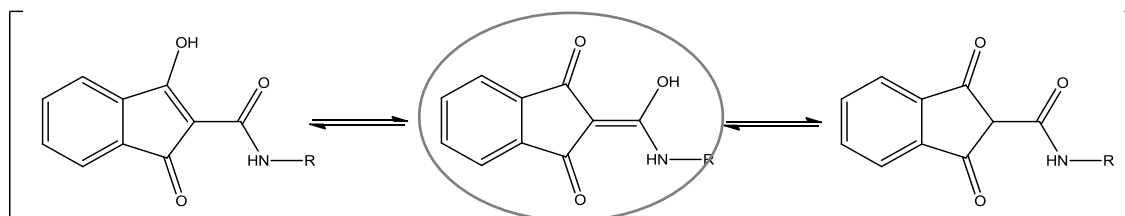


**Fig. 26** possible tautomers



## 2.2 Synthesis and characterization of complexes

### 2.2.1 Synthesis of $Ru^{II}(\eta^6\text{-cym})$ complexes<sup>58</sup>

The ligand was deprotonated with sodium methoxide in methanol under argon atmosphere. A solution of the precursor dimer bis[dichlorido( $\eta^6$ -p-cymene)ruthenium(II)] in dichloromethane was added and the reaction mixture was stirred for 30-35 hours under argon atmosphere. The solvent was evaporated, and the byproduct, sodium chloride, was separated by dissolving the residue in dichloromethane and subsequent filtration. The complex was precipitated by addition of *n*-hexane to a concentrated solution of the complex in dichloromethane.

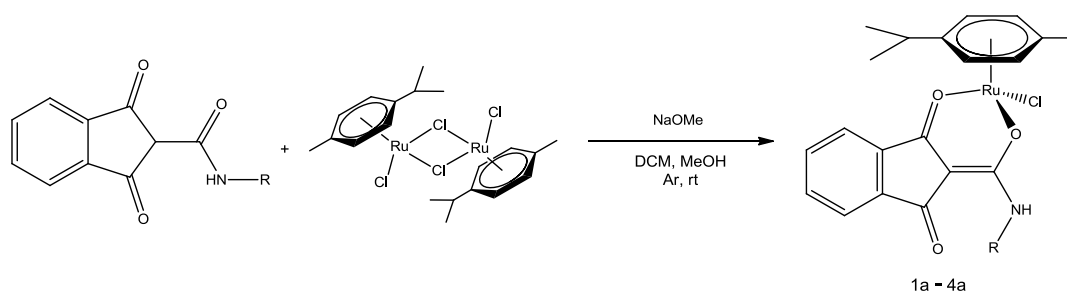


Fig. 27 Synthesis of  $Ru^{II}(\eta^6\text{-cym})$  complexes

### 2.2.2 Synthesis of $Rh^{III}(\eta^5\text{-Cp}^*)$ complexes

The ligand was deprotonated with sodium methoxide in methanol under argon atmosphere. A solution of the precursor dimer bis[dichlorido( $\eta^5$ -1,2,3,4,5-pentamethylcyclopentadiene)rhodium(III)] in dichloromethane was added and the reaction mixture was stirred for 30-35 hours under argon atmosphere. The solvent was evaporated, and the byproduct, sodium chloride, was separated by dissolving the residue in dichloromethane and subsequent filtration. The complex was precipitated by addition of *n*-hexane to a concentrated solution of the complex in dichloromethane. For further purification, all ( $\eta^5\text{-Cp}^*$ ) $Rh^{III}$  complexes had to be reprecipitated from DCM / *n*-hexane.

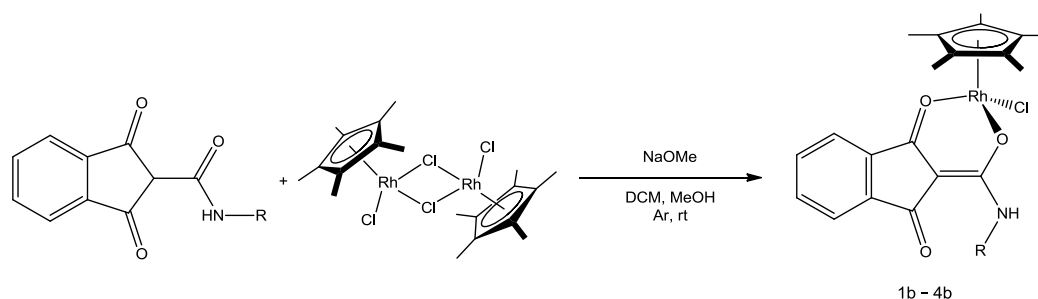
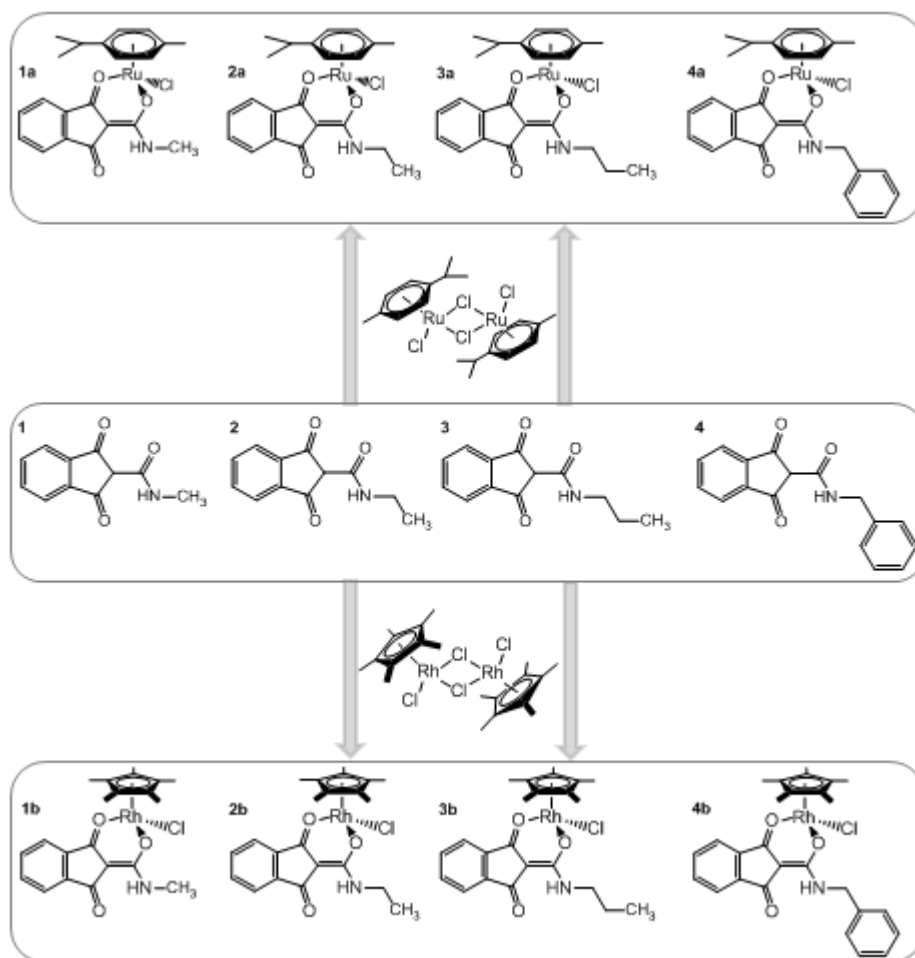


Fig. 28 Synthesis of  $Rh^{III}(\eta^5\text{-Cp}^*)$  complexes

<sup>58</sup> Bennett, M.A., and Smith, A.K., *J. Chem. Soc., Dalton Trans.*, **1974**, 233-41.



**Fig. 29** Overview of synthesized complexes

### 2.2.3 Characterization of $Ru^{II}(\eta^6\text{-cym})$ complexes via NMR spectroscopy

In general, the  $^1\text{H-NMR}$ ,  $^{13}\text{C-NMR}$ , and 2D spectra of the organoruthenium compounds were measured in  $\text{CDCl}_3$ , due to the limited stability in  $\text{DMSO-d}_6$ .

#### $^1\text{H-NMR}$

The electron withdrawing effect of ruthenium causes the 1,3-indandione signals to be shifted upfield, while the cymene-signals are shifted downfield and all detected signals were assigned *via* 2D-NMR analysis.

The four indan-scaffold protons were split up into two multiplets, where H5, H6, and H7 (7.4 ppm) were found to be shifted further upfield than H4 (7.52 ppm). The NH signals were shifted upfield as well, and were typically found at 8.5 ppm. Again, the NH signal of **4a** was found further downfield (8.9 ppm). In  $\text{CDCl}_3$  the coupling of NH with the respective H2' is visible, as opposed to the ligand-NH signals found in  $\text{DMSO-d}_6$ . In the case of **1a**, a quartet is found, and the spectra of **2a**, **3a**, and **4a** show a triplet.

Due to the ruthenium being an asymmetric center, the now diastereotopic H2' protons of **4b** were split up into two dd signals, found at 4.5 ppm and 4.7 ppm.

The signals of the facial cymene ligand, were shifted downfield, compared to the signals of the dimeric precursor. The cymene signal Hb did not shift and remained at 5.34 ppm, however the doublet was split into two symmetrical multiplets, whereas Hc shifted from 5.47 ppm to 5.61 ppm. He (m), Hf (m), and Hg (s) were all shifted upfield by approximately 0.1 ppm.

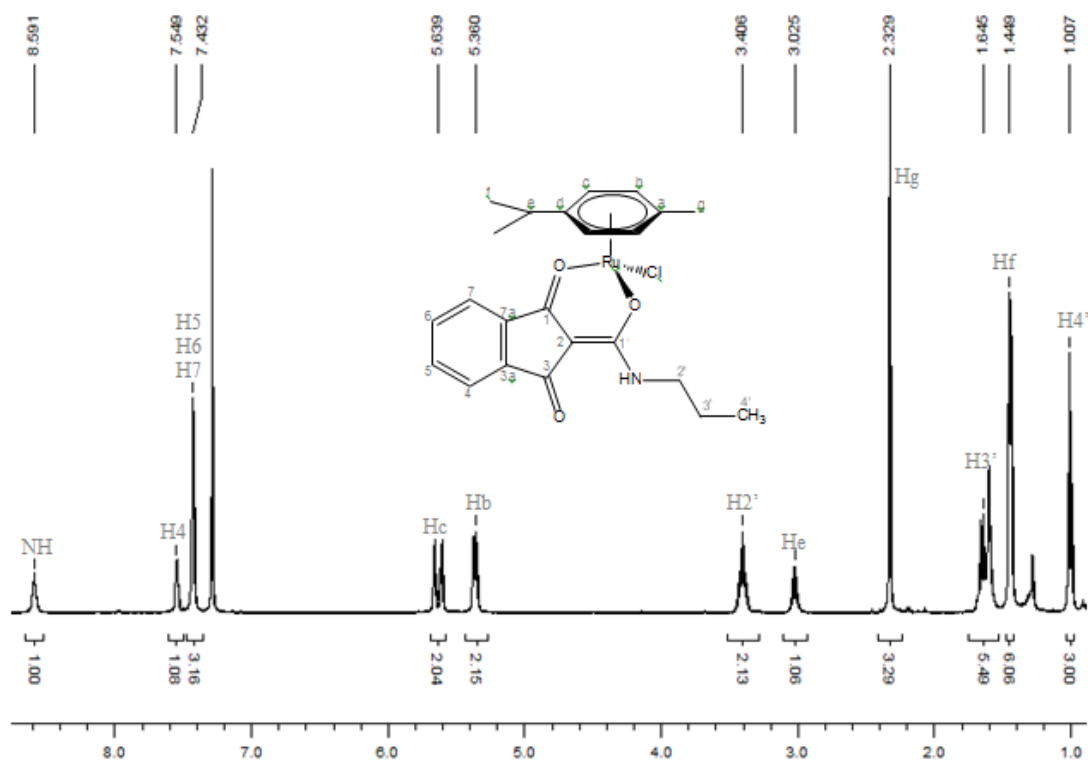


Fig. 30 <sup>1</sup>H-NMR of **3a**

## <sup>13</sup>C-NMR

Due to the fact that the coordinated ruthenium atom leaves the ligand unsymmetrical, all symmetry in the spectra is lost as well. As expected, the cymene signals were shifted upfield (leaving the protons more deshielded) on average by about 1 ppm. The signals of Cb, Cc, and Cf were split into two separate signals because of the generation of an asymmetric center.

The ligand signals were found more or less at the same chemical shift as in the ligand spectra, even if every carbon gave a separate signal. The coordination shifted the carbonyl carbons, and the C2 signal significantly. C2 was shifted from 93 ppm to 98 ppm in the respective coordination compound. The free carbonyl remained at the same chemical shift, but the coordinated C1 was shifted downfield by about 2.5 ppm (from 191 ppm to 192.5 ppm).

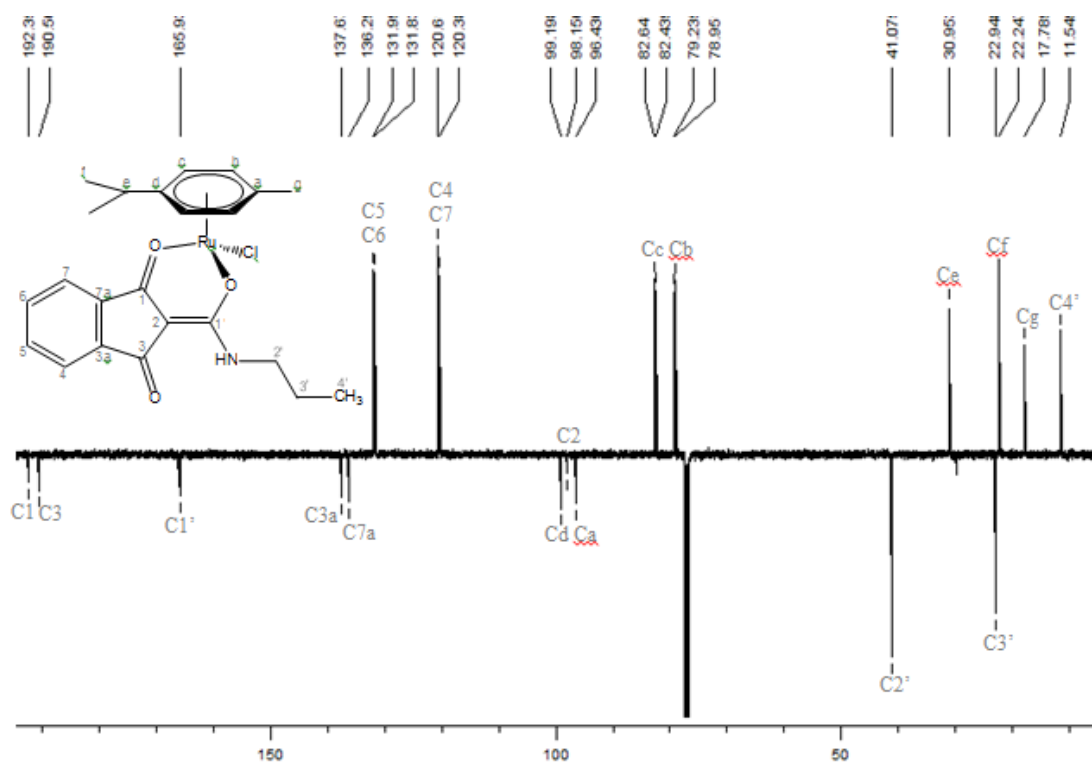
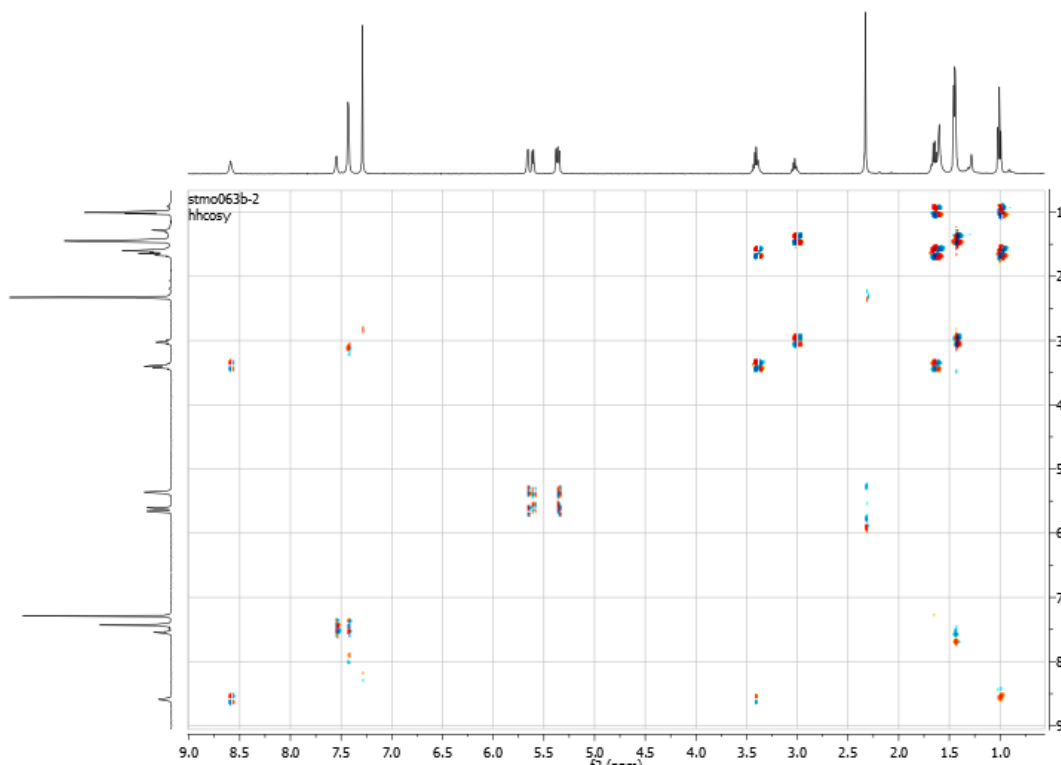


Fig. 31 <sup>13</sup>C-NMR of 3a

## 2D-NMR

Via  $^1\text{H}$ - $^1\text{H}$ -COSY,  $^1\text{H}$ - $^{13}\text{C}$ -HMBC, and  $^1\text{H}$ - $^{13}\text{C}$ -HSQC (Fig. 34), every carbon signal and the indane proton multiplets were assigned. In the  $^1\text{H}$ -NMR spectrum of **3a**, the residual water signal (1.57 ppm) overlays the H3'-signal (1.59 - 1.65 ppm) and obscures its integration.



**Fig. 32**  $^1\text{H}$ - $^1\text{H}$ -COSY of **3a**

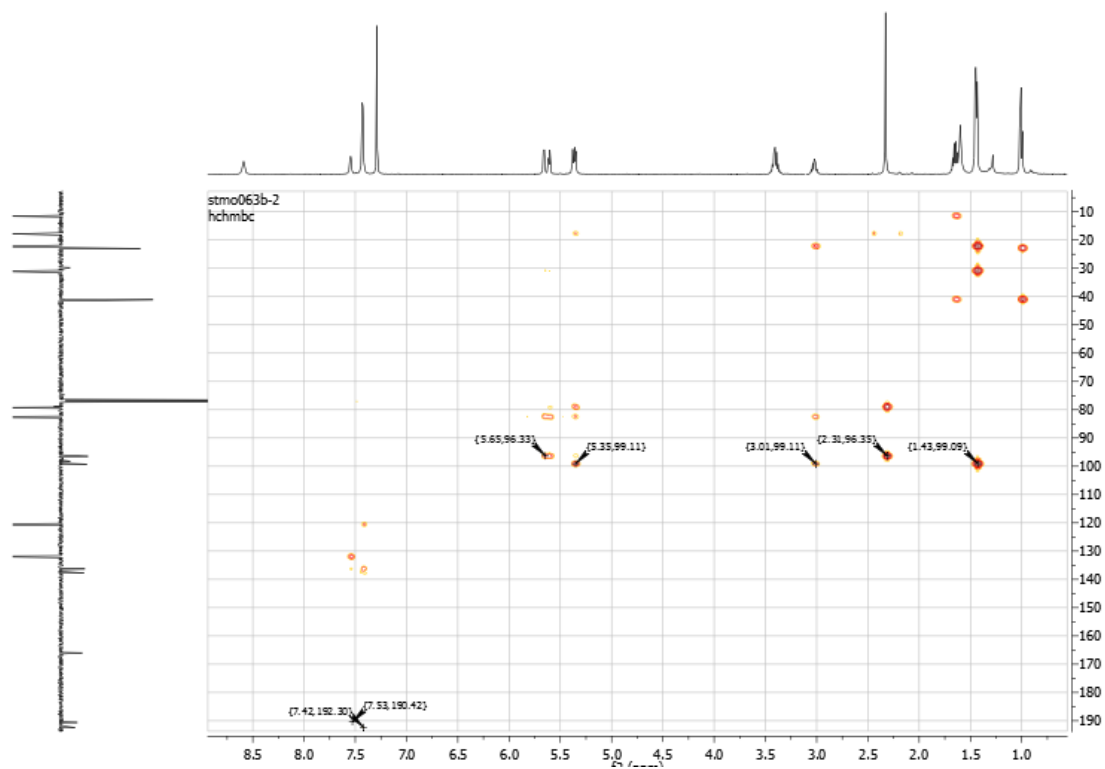


Fig. 33  $^1\text{H}$ - $^{13}\text{C}$ -HMBC of 3a

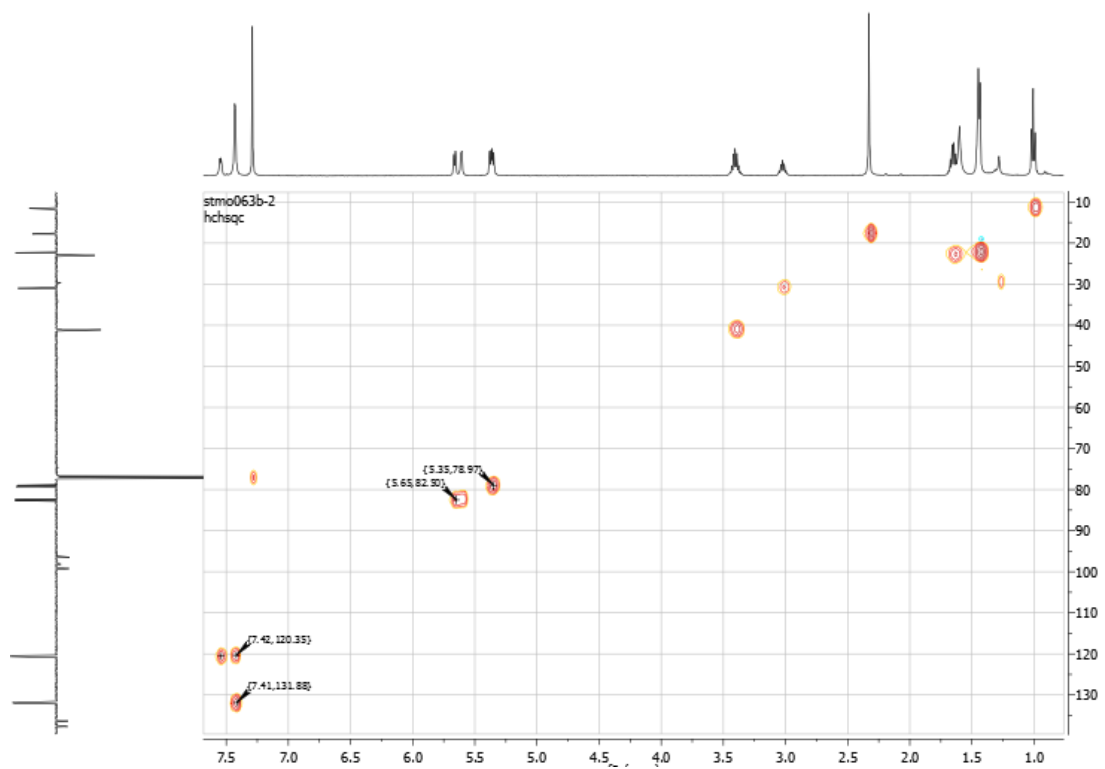


Fig. 34  $^1\text{H}$ - $^{13}\text{C}$ -HSQC of 3a

## 2.2.4 Characterization of $Rh^{III}(\eta^5-Cp^*)$ complexes via NMR spectroscopy

In general, the  $^1H$ -NMR,  $^{13}C$ -NMR, and 2D spectra of the organorhodium compounds were measured in  $CDCl_3$ .

### $^1H$ -NMR

The same general trends as found for the  $Ru(II)$  organometallics were observed for the rhodium complexes. The 1,3-indandione signals were shifted upfield by about the same magnitude as in the spectra, discussed in section 2.2.3. The splitting patterns are the same, as observed with the ruthenium complexes. The  $Cp^*$  signals were shifted downfield by 0.8 ppm (from 1.62 ppm to 1.70 ppm), but remained singlets, as expected.

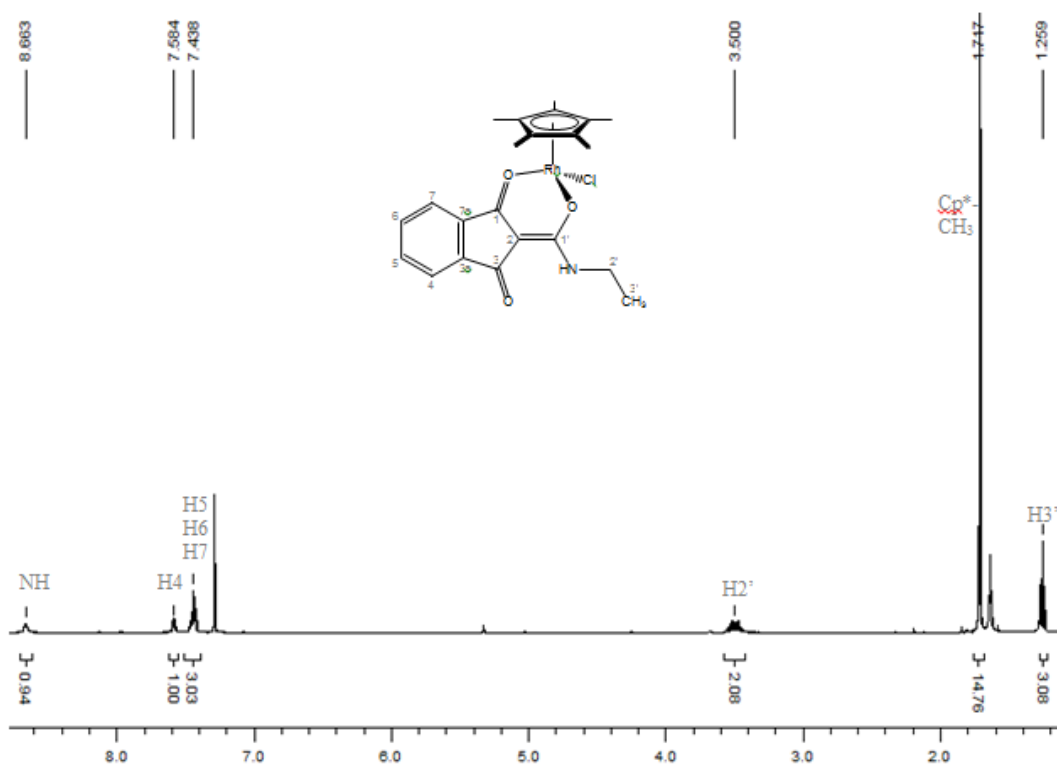


Fig. 35  $^1H$ -NMR of **3b**

## $^{13}\text{C}$ -NMR

The ligand signals were split up into individual signals, upon the introduction of an asymmetric center into the molecule. The same shift-values were found as with the ligand carbon signals in the analogous ruthenium complex spectra. The  $\text{Cp}^*$  carbon signals were shifted upfield. The ring carbons showed one signal at 92.4 ppm (dimeric precursor: 94.3 ppm) and the methyl groups showed a signal at 8.8 ppm (dimeric precursor: 9.5 ppm).

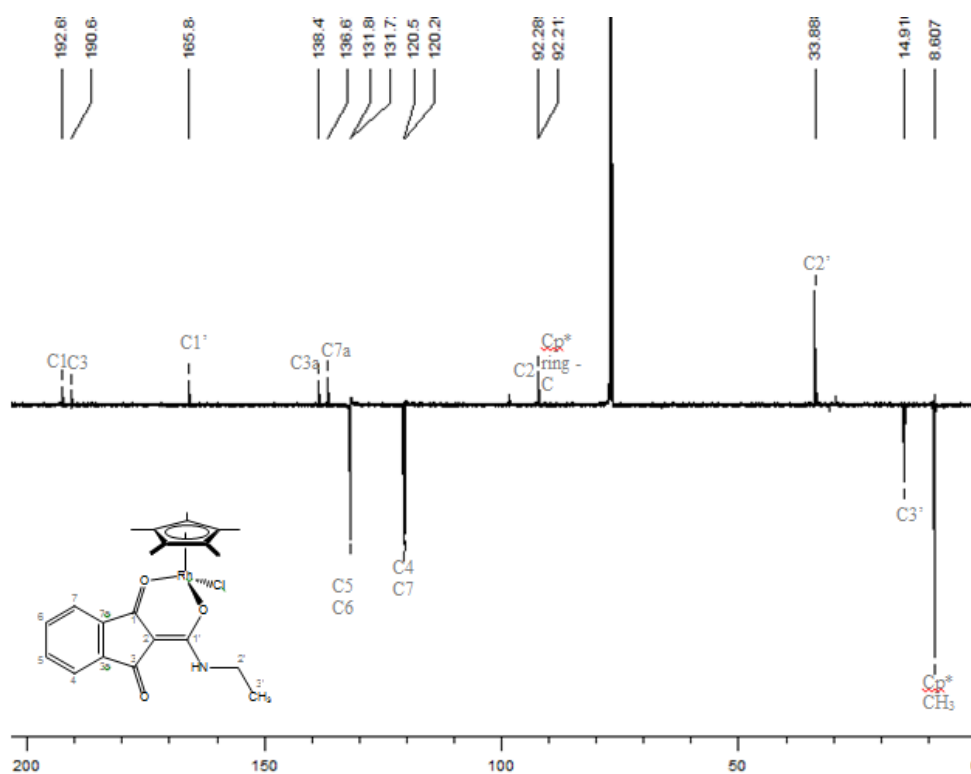


Fig. 36  $^{13}\text{C}$ -NMR of 3b

## 2D-NMR

Via  $^1\text{H}$ - $^1\text{H}$ -COSY,  $^1\text{H}$ - $^{13}\text{C}$ -HMBC, and  $^1\text{H}$ - $^{13}\text{C}$ -HSQC, every carbon signal and the indane proton multiplets were assigned. Every multiplet found in the  $^1\text{H}$ -NMR spectra of the rhodium complexes were caused by the same protons as in the ruthenium spectra.



### 2.2.5 Characterization of Ru<sup>II</sup>( $\eta^6$ -cym) complexes **3a** and **4a** via x-ray diffraction analysis

Single crystals were obtained via slow diffusion crystallization of **3a** and **4a** from pentane / chloroform. Both compounds showed the typical pseudo-octahedral ‘piano-stool’ configuration, with the facial  $\eta^6$ -p-cymene ligand being the seat, whereas the chlorido and the chelating ligands acting as the feet. The chelating deprotonated 1,3-indandionecarboxamide ligands bind bidentately to the ruthenium center, forming non-planar 6-membered rings (Fig. 37). Both compounds crystallized in triclinic single crystals in the centrosymmetric space group P-1.

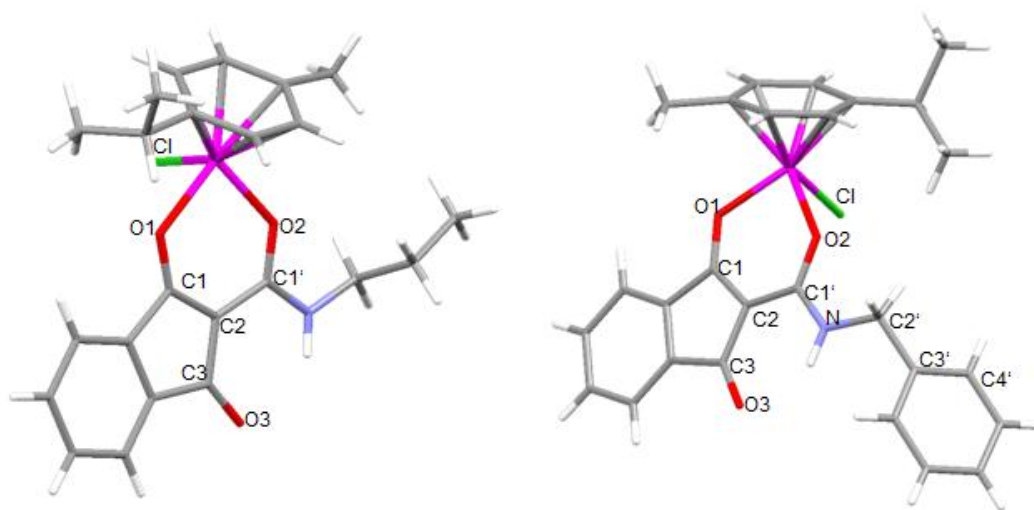


**Fig. 37** Crystal structures for compounds **3a** (left) and **4a** (right)

Tab. 4 lists the relevant bond lengths and angles. The first noteworthy fact is that in both compounds the coordination bonds of Ru to both oxygens are in the same range, namely in the case of **3a** [2.0922(25) and 2.0924(26) Å] and in the case of **4a** [2.1075(20) and 2.0798(20) Å]. The coordination bond of Ru to Cl is 2.4038(9) and 2.4191(8) Å in **3a** and **4a**, respectively.

The prevalent question to be answered is the bonding in the chelate ring. The bond length of the carbonyl C1-O1 [**3a**: 1.2658(45) Å; **4a**: 1.2671(34) Å] is slightly longer than C3-O3 [**3a**: 1.2327(48) Å; **4a**: 1.2217(34) Å]. However, due to the electron withdrawing effect of the transition metal center, both carbonyl bonds of **3a** are longer than they usually are (1.222 Å<sup>59</sup>). In the case of **4a**, the electron donating effect of the benzyl substituent counteracts the ruthenium's electron withdrawal, leading to a carbonyl bond length in the expected vicinity. The measured bond lengths for C1-C2 [**3a**: 1.3961(55) Å; **4a**: 1.4066(39) Å], C2-C1' [**3a**: 1.4383(53) Å; **4a**: 1.4401(38) Å], and the equal bond length of

<sup>59</sup> Carey, F. A. and Sundberg, R. J., *Advanced Organic Chemistry; Part A: Structure and Mechanisms*, fifth edition, Springer Publishing, USA, 2007

C1'-O1' [**3a**: 1.2646(43) Å; **4a**: 1.2663(34) Å] to C1=O1 suggests no distinct double bonds in the chelate ring system, but  $\pi$ -electron delocalization. Furthermore, the observed torsion angles of O1-Ru-O1'-C1' [**3a**: 6.61(30)°; **4a**: 9.81(24)°] clearly show that the chelate rings are non-planar, as mentioned before.

Hydrogen bonding was observed in both cases between NH and O3 (2.201 Å for **3a** and 2.096 Å for **4a**). The benzyl side chain is twisted out of the indandione plane with a torsion angle of 116.05(31)°.

Tab. 5 gives an overview of the relevant crystal data and details of the data collection.

**Tab. 4** Relevant bond lengths and angles

Compound	<b>3a</b>	<b>4a</b>
Ru-Cl [Å]	2.4038(9)	2.4191(8)
Ru-O2 [Å]	2.0922(25)	2.1075(20)
Ru-O1' [Å]	2.0924(26)	2.0798(20)
C1=O1 [Å]	1.2658(45)	1.2671(34)
C3=O3 [Å]	1.2327(48)	1.2217(34)
C1'-O1' [Å]	1.2646(43)	1.2663(34)
C2-C1' [Å]	1.4383(53)	1.4401(38)
C1-C2 [Å]	1.3961(55)	1.4066(39)
C2-C3 [Å]	1.4469(51)	1.4492(38)
NH-O3 [Å]	2.201	2.096
O1-Ru-O1' [°]	88.65(10)	90.00(8)
Cl-Ru-O1' [°]	84.60(8)	84.54(6)
Cl-Ru-O1 [°]	86.03(7)	84.27(6)
C1=O1-Ru [°]	123.34(25)	121.88(18)
C2-C1=O1 [°]	130.69(34)	130.33(26)
C1-C2-C1' [°]	124.90(33)	125.50(26)
C2-C1'-O1' [°]	123.08(35)	123.73(25)
C1'-O1'-Ru [°]	129.00(25)	127.66(18)
O3=C3-C2 [°]	128.40(37)	128.47(26)
O1-Ru-O1'-C1' [°]	6.61(30)	9.81(24)
N-C2'-C3'-C4' [°]	-	116.05(31)

**Tab. 5** Crystal data and details of data collection (where:  $R_{\sigma} = \sum |F_0| - |F_0| / \sum |F_0|$ ;  $wR_2 = \{\sum [w(F_0^2 - c^2)]^2\} / w \sum \{(F_0^2 - c^2)\}^{1/2}$ ;  $GOF = \sum [w(F_0^2 - c^2)] / (n-p)^{1/2}$ )

Compound	<b>3a</b>	<b>4a</b>
Chemical Formula	C <sub>23</sub> H <sub>26</sub> ClNO <sub>3</sub> Ru	C <sub>27</sub> H <sub>26</sub> ClNO <sub>3</sub> Ru
M [g/mol]	500.98	549.02
T [K]	100	100
Crystall size [mm]	0.05·0.05·0.13	0.07·0.13·0.22
Crystal color and shape	Orange, block	Orange, block
Crystal system	Triclinic	Triclinic
Space group	P-1	P-1
a [Å]	11.2925(3)	7.7476(11)
b [Å]	12.9510(4)	12.466(2)
c [Å]	15.5387(4)	12.598(2)
α [°]	90.3350(10)	93.589(9)
β [°]	110.2610(10)	101.776(7)
γ [°]	90.057(2)	102.005(7)
V [Å <sup>3</sup> ]	2131.86	1158.04
Z	4	2
ρ [g/cm <sup>3</sup> ]	1.561	1.574
<i>h</i> range	-13/13	-6/10
<i>k</i> range	-15/15	-17/17
<i>l</i> range	-16/18	-17/17
No. reflections	44318	35185
No. parameters	534	299
R <sub>int</sub>	0.0322	0.1178
R <sub>sigma</sub>	0.0284	0.0920
wR <sub>2</sub>	0.0894	0.1490
GOF	1.053	1.022

### 2.2.6 Stability investigation of complexes 1a and 1b via ESI-MS

The stability aqueous solution is a crucial parameter for anticancer drugs and was determined for compounds **1a** and **1b** at 37°C over a period of 48 h. The mass spectra were recorded after 1, 3, 6, 24, and 48 h according to the method, mapped out in section 3.1.

The rhodium complex proved to be stable over the entire 48 h period. **1a**, on the other hand, inexplicably shows an unidentifiable peak at  $m/z$   $552.99 \pm 0.02$  additionally to the characteristic  $[M-Cl]^+$  peak (**1a**:  $m/z$   $438.06 \pm 0.01$ ,  $m_{ex}$ : 438.06; **1b**:  $m/z$   $440.07 \pm 0.01$ ,  $m_{ex}$ : 440.07). This unidentifiable peak is only found in the first 6 h and vanishes afterwards. Additionally, the stability in a buffer ( $NH_4HCO_3$ ) solution was determined. The ruthenium complex did not show an  $[M-Cl]^+$  peak in any of the spectra, but a myriad of different solvent adducts, allowing the conclusion, that complex **1a** is not a likely candidate to reach intact the tumor cells *in vivo*.

The rhodium complex showed the same distribution of the  $[M-Cl]^+$  peak, the ligand peak, and the aquation species  $[Rh(\eta^5-Cp^*)(OH)O]$  in all of the spectra. This consistent distribution suggests these separate moieties to be formed during the spraying process, which also suggests sufficient stability in buffered solution.

### 2.2.7 Investigation of biomolecule interaction behavior of 1a and 1b via ESI-MS

To obtain further knowledge of possible cellular targets of the synthesized transition metal complexes, their reactivity towards nucleoside triphosphates (5'-dATP and 5'-dGTP), selected amino acids (L-histidine [His], L-cysteine [Cys], and glycine [Gly]), and proteins (ubiquitin [Ub] and cytochrome C [cyt]) was investigated by the method mapped out in section 3.1.

In the study of **1a**'s reactivity towards amino acids the following trends were observed. The kinetically favored products is  $[Ru_2L1(\eta^6-cym)_2(\mu-Cys)]^+$  ( $m/z$   $710.99 \pm 0.05$ ,  $m_{th}$ : 711.04). This dinuclear species is formed in the first hour of incubation and engrosses about 57 % of the adduct spectrum. The formation of this adduct is favored to a point, where no initial **1a** was found. Over the course of the following incubation its magnitude depletes drastically (after 48 h, only 5 % remain). The other kinetically favored adduct is  $[Ru(\eta^6-cym)(His)]^+$  ( $m/z$   $390.03 \pm 0.04$ ,  $m_{th}$ : 390.08), occupying almost 60 % of the adduct distribution after 24 h. Its amount depletes as well, giving rise to the thermodynamically stable product  $[Ru(\eta^6-cym)(Cys)]^+$  ( $m/z$   $355.97 \pm 0.04$ ,  $m_{th}$ : 356.03). This L-cysteine affinity becomes clear, when calling to mind the HSAB principle, stating that the soft character of ruthenium prefers the soft character of sulfur to nitrogen of L-histidine). No glycine adducts were detected.

The reactivity of the rhodium complex **1b** towards amino acids revealed similar trends as found for **1a**. The kinetically and thermodynamically favored adducts are with L-cysteine  $[\text{Rh}(\eta^5\text{-Cp}^*)(\text{Cys})]^+$  ( $m/z$   $357.99 \pm 0.04$ ,  $m_{\text{th}}$ : 358.03) and  $[\text{Rh}(\eta^5\text{-Cp}^*)(\text{Cys})]_2^+$  ( $m/z$   $715.00 \pm 0.04$ ,  $m_{\text{th}}$ : 715.06), respectively. Both species are formed within the first hour of incubation and remain the prevalent adducts (both species always occur with 30 – 60 % of all adducts formed). The L-histidine adduct  $[\text{Rh}(\eta^5\text{-Cp}^*)(\text{His})]^+$  ( $m/z$   $392.04 \pm 0.03$ ,  $m_{\text{th}}$ : 392.08) is less prominent with its highest occurrence found after 24 h of incubation with an extent of 19 %. Again, no glycine adducts were detected. During the entire incubation about 3 % of residual **1b** was found.

The reactivity of **1a** towards the selected nucleoside triphosphates reveals a clear selectivity of the  $\text{Ru}(\eta^6\text{-cym})$  moiety towards guanine:  $[\text{Ru}(\eta^6\text{-cym})(5'\text{-dATP})]^{2-}$  ( $m/z$   $738.93 \pm 0.01$ ,  $m_{\text{th}}$ : 738.97; < 10 %),  $[\text{Ru}(\eta^6\text{-cym})(5'\text{-dATP})]^-$  ( $m/z$   $742.00 \pm 0.02$ ,  $m_{\text{th}}$ : 742.00; ~ 15 %),  $[\text{Ru}(\eta^6\text{-cym})(5'\text{-dGTP})]^-$  including its sodium adduct ( $m/z$   $756.00 \pm 0.02$ ,  $m_{\text{th}}$ : 755.98; ~ 20 %), and the most prevalent  $[\text{Ru}(\eta^6\text{-cym})(5'\text{-dGTP})]^{2-}$  ( $m/z$   $754.94 \pm 0.01$ ,  $m_{\text{th}}$ : 754.97; > 50 %).

The reactivity of the rhodium complex **1b** towards said nucleoside triphosphates was elucidated with the same experimental setup for the ruthenium analogue. The following distribution was found:  $[\text{Rh}(\eta^5\text{-Cp}^*)(5'\text{-dGDP})]^-$  ( $m/z$   $678.03 \pm 0.02$ ,  $m_{\text{th}}$ : 678.02; ~ 5 %),  $[\text{Rh}(\eta^5\text{-Cp}^*)(5'\text{-dATP})]^{2-}$  ( $m/z$   $740.95 \pm 0.01$ ,  $m_{\text{th}}$ : 740.98; ~ 5 %),  $[\text{Rh}(\eta^5\text{-Cp}^*)(5'\text{-dGTP})]^{2-}$  ( $m/z$   $756.96 \pm 0.01$ ,  $m_{\text{th}}$ : 756.98; ~ 6 %),  $[\text{Rh}(\eta^5\text{-Cp}^*)(5'\text{-dADP})]^-$  ( $m/z$   $662.04 \pm 0.01$ ,  $m_{\text{th}}$ : 662.03; < 30 %), and the most prevalent adduct:  $[\text{Rh}(\eta^5\text{-Cp}^*)(5'\text{-dATP})]^-$  ( $m/z$   $742.01 \pm 0.01$ ,  $m_{\text{th}}$ : 741.99; > 52 %). The preferred nucleophile attacking the  $\text{Rh}(\eta^5\text{-Cp}^*)$  fragment seems to be 5'-dATP, as almost 90 % of the found adducts were containing the adenosine moiety. Furthermore, the occurrence of nucleoside diphosphates suggests binding to the phosphate chain, leading to elimination of the terminal phosphate. The fact that no diphosphate adducts were found in the analogue spectra of **1a**, rules out phosphate elimination due to the spraying process.

Both complexes were incubated with amino acids and nucleoside triphosphates in order to determine which kind of nucleophiles are able to interact with **1a** and **1b** *in vivo*. However, no significant amounts of nucleoside adducts and the same distribution of amino acid adducts was found. This finding suggests that possible biological activity can only be attributed protein interaction and not to interaction with DNA.

The reactivity of the complexes towards the proteins ubiquitin (Ub) and cytochrome C (cyt) were performed to further understand the *in vivo* behavior, where cyt represents a possible biological target and the model protein Ub was chosen to depict the complex' reactivity towards proteins in general. Ub has two possible binding sites (Met1 and His68), whereas cyt has three (His26, His33, and Met65). Due to the fact that these samples were diluted with formic acid (0.02 %(v/v)) in order to denature the present proteins, they occur in differently charged states (Ub: 7-14 and cyt: 11-19). This fact convolutes the mass spectra, making it necessary to deconvolute the spectra.

The reactivity of **1a** towards cyt is lower than the reactivity towards Ub. Over the duration of the incubation more and more cyt-adduct was observed, however, not more than 20 % of cyt was found in the form of  $[\text{Ru}(\eta^6\text{-cym})(\text{Cyt})]^+$  ( $m/z$  12,592.8  $\pm$  2.0,  $m_{\text{th}}$ : 12,593.4), and over 80 % as unreacted cytochrome C. On the other hand, ubiquitin shows more reactivity towards the ruthenium complex. At first the kinetic product  $[\text{Ru}_2(\eta^6\text{-cym})_2(\text{Ub})]^+$  ( $m/z$  9,030.6  $\pm$  2.1,  $m_{\text{th}}$ : 9,031.6) was observed, but after 24 h, this intermediate makes up only 5 % of the entire Ub-population. The adduct  $[\text{Ru}(\eta^6\text{-cym})(\text{Ub})]^+$  ( $m/z$  8,798.12  $\pm$  1.6,  $m_{\text{th}}$ : 8,798.6) is the most prevalent formed species. After one hour over 60 % of the present Ub occurs as the mono-Ru adduct and was nearly fully converted after 48 h (92%).

Rhodium complex **1b** showed about the same reactivity towards cyt. The adduct  $[\text{Rh}(\eta^5\text{-Cp}^*)(\text{cyt})]^+$  ( $m/z$  12,595.0  $\pm$  1.0,  $m_{\text{th}}$ : 12,595.4) never makes up more than 10 % of the cyt population. The other 90 % are unreacted cyt. In contrast to the **1a**, the rhodium analogue does not form an ub adduct containing two  $\text{Rh}(\eta^5\text{-Cp}^*)$  moieties. However, as already seen for **1a**, only 7 % of unreacted ubiquitin was detected. Even by reducing the incubation time to one hour, over 92 % of the Ub was converted yielding  $[\text{Rh}(\eta^6\text{-cym})(\text{Ub})]^+$  ( $m/z$  8,801.1  $\pm$  1.6,  $m_{\text{th}}$ : 8,800.6).

These results suggest that reaction with cytochrome C is not a likely pathway for possible biological activity.

### 3 Experimental

#### 3.1 Equipment and Methods

##### NMR spectra

The NMR spectra were recorded at 25 °C using a *Bruker FT-NMR spectrometer Avance III™ 500 MHz*. <sup>1</sup>H NMR spectra were measured at 500.10 MHz and <sup>13</sup>C-Spectra at 125.75 MHz in deuterated dimethyl sulfoxide (DMSO-d<sub>6</sub>) or chloroform (CDCl<sub>3</sub>). 2D NMR spectra were measured using a gradient-enhanced mode.

##### Elemental analyses

CHN – elemental analyses were carried out with a *Perkin Elmer 2400 CHNS/O Series II* elemental analyzer in the microanalytical laboratory of the University of Vienna. CHNS – elemental analyses were performed with a *Eurovector EA3000 Elemental Analyzer* in the same laboratory.

##### Melting points

Melting points were determined with a *Büchi Melting Point M-560*.

##### X-ray structures

Single crystals of **3a** and **4a** suitable for x-ray diffraction analysis were grown by slow diffusion chloroform/pentanes at 4 °C. The x-ray diffraction data was recorded on a *Bruker X8 APEX II CCD diffractometer* at 100 K.

##### Solubility

The solubility was determined by dissolving the compound in DMSO and dilution to a final concentration of 1 % DMSO/PBS. The highest concentrated dilution, where no precipitation of the compound occurred, was the determined solubility.

## ESI-MS

Electrospray ionization mass spectra were recorded on a *Bruker AmaZon SL ion trap mass spectrometer* (Bruker Daltonics GmbH). Data was acquired and processed using Compass 1.3 and Data Analysis 4.0 (Bruker Daltonics GmbH). Protein spectra were deconvoluted by applying the maximum entropy algorithm with a 0.2 *m/z* mass step and 0.5 *m/z* instrument peak width.

Mass spectra were recorded *via* direct infusion with a sample-concentration of 5  $\mu\text{M}$  and a flow rate of 240  $\mu\text{L/h}$ . Small molecules were measured with the following settings: dry temperature – 180 °C, nebulizer – 8.00 psi, dry gas – 6.00 L/min, and the high voltage capillary was set to -4500 V or +4500 V for positive and negative mode, respectively. The target mass was set to 600 *m/z*. Proteins were measured with the following settings: dry temperature – 180 °C, nebulizer – 6.00 psi, dry gas – 6.00 L/min, the high voltage capillary was set to -3500 V, and the target mass was set to 1,000 *m/z*.

Stability-measurement and small molecule samples were diluted with water : methanol (50 : 50), whereas protein samples were diluted with water : methanol : formic acid (49.9 : 49.9 : 0.2), where proteins have their highest possible positive charge. Stock solutions of complexes **1a** and **1b** were prepared in DMSO and diluted to a final concentration of 1 % DMSO/H<sub>2</sub>O. The molar ratios used for interaction studies were complex : L-histidine : L-cysteine : glycine (1 : 1 : 1 : 1), complex : 5'-dATP : 5'-dGTP (1 : 1 : 1), complex : amino acids : nucleoside triphosphates (1 : 1 : 1), and complex : ubiquitin : cytochrome C (1 : 1 : 1). Mass spectra were recorded after 1, 3, 6, 24, and 48 hours of incubation at 37 °C.

The relative intensities discussed in 2.2.6 and 2.2.7 refer to the percent peak area of all assignable rhodium or ruthenium adduct-areas in the respective spectrum.



## 3.2 Materials

### Solvents used for synthesis and mass spectrometric measurements

The used solvents were purchased from commercial sources and distilled prior use. Chloroform was dried over molecular sieves (3 Å) before use.

Methanol (HPLC grade; Fisher) and Millipore water (milliQ H<sub>2</sub>O; 18.2 MΩ; Synergy 185 UV Ultrapure Water System, Millipore) were used for mass spectrometric investigations.

### Chemicals used for the ligand synthesis

2-Hydroxy-1,4-naphthoquinone (99 %; Acros Organics), sodium nitrite (puriss., Riedel-de Haën), 3-nitroaniline (Riedel-de Haën), (diacetoxyiodo)benzene (Aldrich), methylamine (40 % solution in water; Merck), ethylamine (70 % solution in water; Merck), propylamine (≥ 99.0 %; Fluka), benzylamine (≥ 99.0 %; Fluka), sodium hydroxide (≥ 98 %; Sigma-Aldrich), hydrochloric acid (30 – 33 %; Donauchem), sodium sulfate (anhydrous; 99 %; Acros Organics)

Molecular sieves (3Å; beads; 4 – 8 mesh; Sigma-Aldrich)

### Chemicals used for the synthesis of rhodium and ruthenium complexes

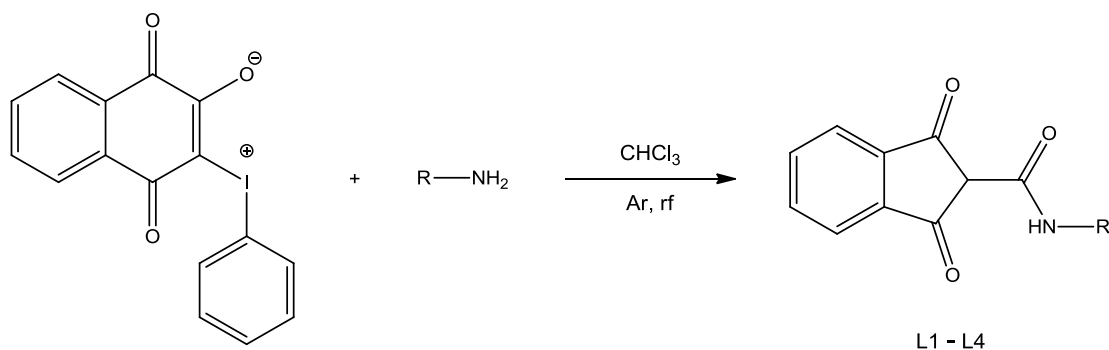
Ruthenium(III) chloride hydrate (Johnson Matthey), α-terpinene (90 %; Acros Organics), rhodium(III) chloride hydrate (Johnson Matthey), 1,2,3,4,5-pentamethylcyclopentadiene (95 %; Aldrich), sodium methoxide (~ 95 %; Fluka)

### Chemicals used for mass spectrometric analyses of complexes L1a and L1b

Glycine (Merck), L-cysteine (Fluka), L-histidine (Merck), guanosine 5'-triphosphate sodium salt hydrate (≥ 95 %; Sigma), adenosine 5'-triphosphate disodium salt (Calbiochem), ammonium bicarbonate (≥ 99.5 %; Fluka), ubiquitin (≥ 98%; bovine erythrocytes; Sigma), cytochrome C (99 %; horse heart; Sigma), formic acid (p.a.; Fluka)

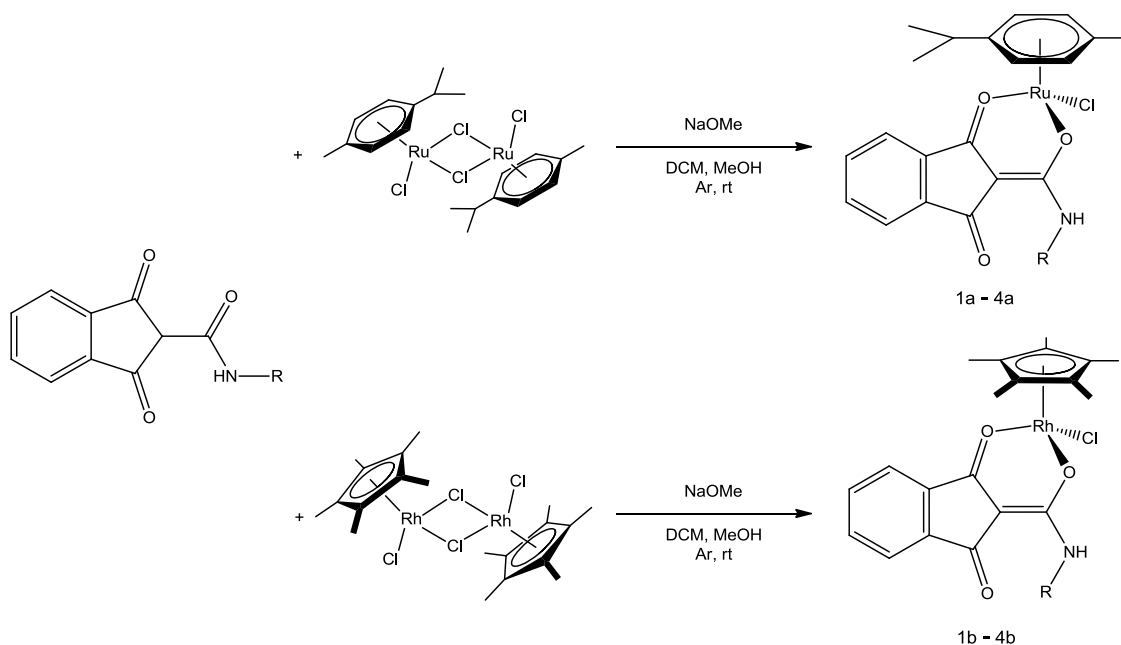
### 3.3 General procedures

#### 3.3.1 General procedure for the synthesis of 1,3-dioxo-2-indancarboxamide ligands



After suspending 2-oxido-3-phenyliodonio-1,4-naphthoquinone (1 eq) in chloroform (dried over molecular sieves), the amine (1 eq) was added. The mixture was refluxed under argon until TLC analysis (n-hexane: ethyl acetate = 1:1) showed full conversion of the educt (reaction times varied from eight hours to three days). The reaction mixture was then extracted with sodium hydroxide (1 M in water) until the aqueous phase became colorless. The alkaline extracts were combined and washed with chloroform. The aqueous layer was acidified with hydrochloric acid (30 % / 33 %) leading to precipitation of the product. The resulting suspension was extracted with dichloromethane and the combined organic layers were dried over anhydrous sodium sulfate, filtered, evaporated to dryness, and dried *in vacuo*. (yields varied from 74 % until 96 %)

### 3.3.2 General procedure of the synthesis of ( $\eta^5$ -Cp\*)-rhodium(III) and ( $\eta^6$ -cymene)-ruthenium(II) complexes

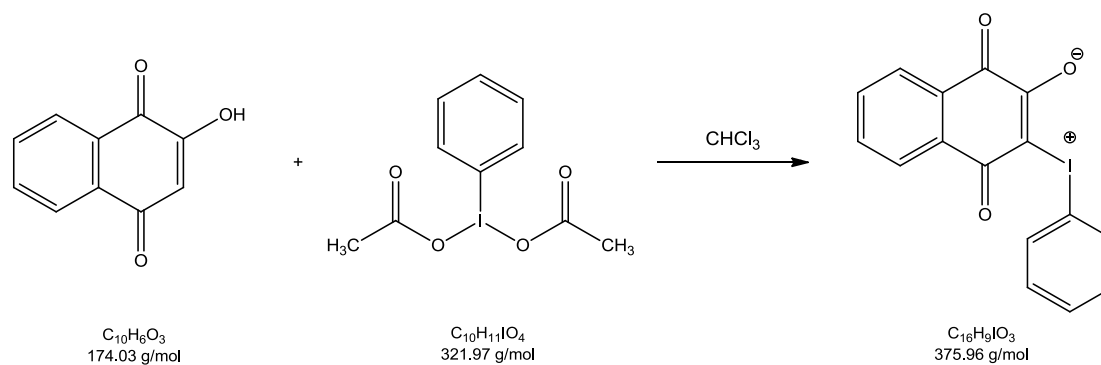


1,3-Dioxoindancarboxamide ligand (1 eq) and sodium methoxide (1.1 eq) were dissolved in methanol and stirred for ten minutes under argon atmosphere. Afterwards, a solution of the precursor dimer bis[dichlorido( $\eta^6$ -p-cymene)ruthenium(II)] or bis[dichlorido( $\eta^5$ -1,2,3,4,5-pentamethylcyclopentadiene)rhodium(III)] (0.9 eq) in DCM was added and the reaction mixture was stirred for 30 - 35 hours under argon atmosphere. The solvent was evaporated, the residue dissolved in DCM, filtrated, and concentrated under reduced pressure to a final volume of ca. 2 mL. The complex was then precipitated by addition of *n*-hexane and separated by filtration. The product was washed with cold *n*-hexane and dried *in vacuo*.

The yields of the ( $\eta^6$ -cymene)-ruthenium(II) complexes ranged from 57 % to 84 %.

The ( $\eta^5$ -Cp\*)-rhodium(III) complexes were precipitated twice from DCM - *n*-hexane for purification and their yields ranged from 76 % to 85 %.

### 3.4 Synthesis of the ligand precursor 2-oxido-3-phenyliodonio-1,4-naphthoquinone



#### Synthesis<sup>53</sup>:

A suspension of 2-hydroxy-1,4-naphthoquinone (2.00 g, 11.48 mmol, 1 eq) in chloroform (25 mL) was cooled to 0°C. (Diacetoxyiodo)benzene (3.7 g, 11.48 mmol, 1 eq) was added and after one hour of stirring at 0°C, the mixture was slowly warmed to room temperature and stirred overnight. The formed yellow precipitate was filtered off and washed with chloroform and dried *in vacuo*.

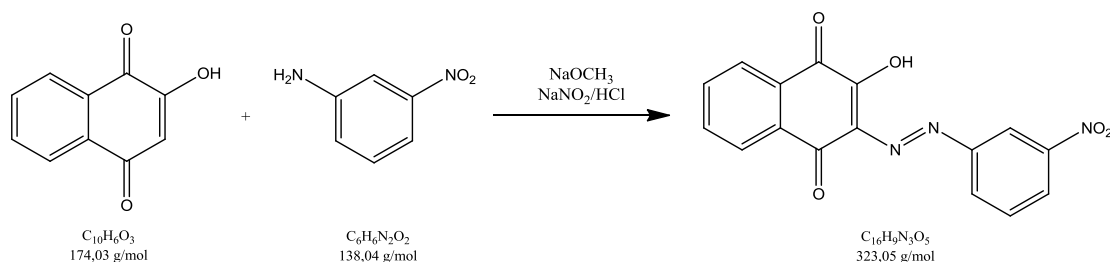
Yield: 3.93g (91%), yellow solid

Melting point: 126 – 127 °C

<sup>1</sup>H-NMR (500.10 MHz, DMSO-d<sub>6</sub>) δ: 7.37 – 8.09 (m, 9H, H<sub>Ar</sub>).

### 3.5 Syntheses of Ligands

#### 3.5.1 Synthesis of 2-hydroxy-3-((3-nitrophenyl)diazenyl)naphthalene-1,4-dione (L0p)



#### Synthesis<sup>53</sup>:

3-Nitroaniline (714 mg, 5.17 mmol, 1.8 eq) was suspended in water (distilled, 600  $\mu$ L) and hydrochloric acid (600  $\mu$ L). After addition of ice (~200 mg), the mixture was cooled to 0 °C and a solution of sodium nitrite (238 mg, 3.45 mmol, 1.2 eq) in water (distilled, 320  $\mu$ L) was added slowly. This mixture was stirred at 0 °C for ~ 30 minutes. A suspension of 2-hydroxy-1,4-naphthoquinone (499 mg, 2.87 mmol, 1 eq) and sodium methoxide (171 mg, 3.17 mmol, 1.1 eq) was cooled to 0 °C and the first mixture added dropwise. The resulting suspension was stirred for one hour, the formed precipitate was filtered off and washed with ice-cold water (distilled).

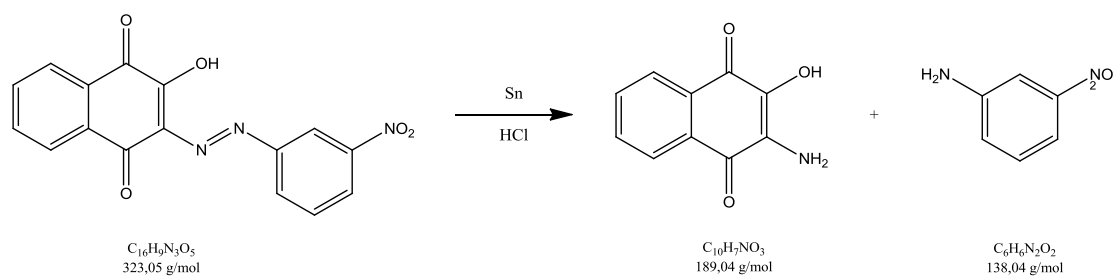
Yield: 890 mg (96 %), orange solid

Melting point: 156 – 158 °C

Solubility: 0.06 mg/mL  $\equiv$  0.19 mM

<sup>1</sup>H-NMR (500.10 MHz, DMSO-d<sub>6</sub>)  $\delta$ : 7.58 – 8.70 (m, 8H<sub>Ar</sub>), 13.18 (br s, 1H, OH).

### 3.5.2 Synthesis of 2-amino-3-hydroxy-1,4-naphthoquinone (L0)



#### Synthesis<sup>53</sup>:

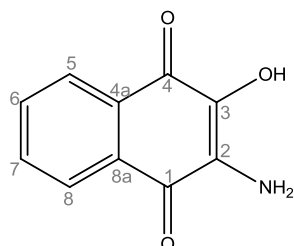
Compound **L0p** (1 g, 3.1 mmol, 1 eq) was suspended in ethanol (20 mL), tin (pellets, 2.27 g, 19.12 mmol, 6.45 eq), and hydrochloric acid (13 mL) was added. The reaction mixture was refluxed for 4.5 hours. After the solution was allowed to cool to room temperature, sodium hydroxide (pellets) was added to adjust the pH to 14. The tin precipitate was filtered through silica and after acidification with hydrochloric acid to pH = 1, the mixture was extracted with DCM. The organic phase was dried over anhydrous sodium sulfate and evaporated. The crude product was purified *via* column chromatography using *n*-hexane : ethyl acetate (5 : 1).

Yield: 57 mg (10 %), dark purple solid

Melting point: 179 – 183 °C

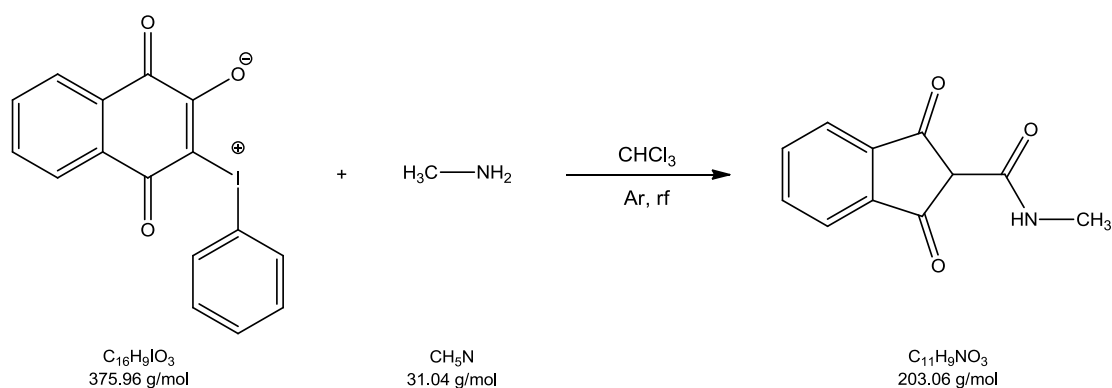
Solubility: 0.27 mg/mL  $\equiv$  1.43 mM

NMR-spectroscopy:



<sup>1</sup>H-NMR (500.10 MHz, DMSO-d<sub>6</sub>)  $\delta$ : 5.95 (br s, 2H, NH<sub>2</sub>), 7.63 – 7.86 (m, 4H, H4, H5, H6, H7, H8), 9.48 (br s, 1H, OH).

### 3.5.3 Synthesis of N-methyl-1,3-dioxo-2,3-dihydro-1H-indene-2-carboxamide (L1)



#### Synthesis:

The synthesis was performed according to the general procedure of 1,3-dioxo-2-indancarboxamides (see section 3.3.1), using 2-oxido-3-phenyliodonio-1,4-naphthoquinone (405 mg, 1.08 mmol) and methylamine (40 %, 93  $\mu$ L, 1.08 mmol) with a reaction time of 30 hours.

Yield: 217 mg (85 %), grey-green solid

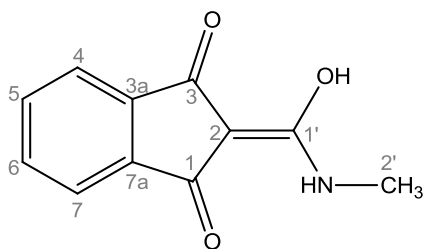
Melting point: 147 – 148 °C

Solubility: 0.43 mg/mL  $\equiv$  2.12 mM (Solubility is limited by DMSO-solubility)

#### Elemental analysis:

	L1	C[%]	H[%]	N[%]
C <sub>11</sub> H <sub>9</sub> NO <sub>3</sub> ·0.06C <sub>6</sub> H <sub>14</sub>	calculated	65.47	4.76	6.72
	found	65.61	4.43	6.43
	$\Delta$	0.14	0.33	0.29

NMR-spectroscopy:

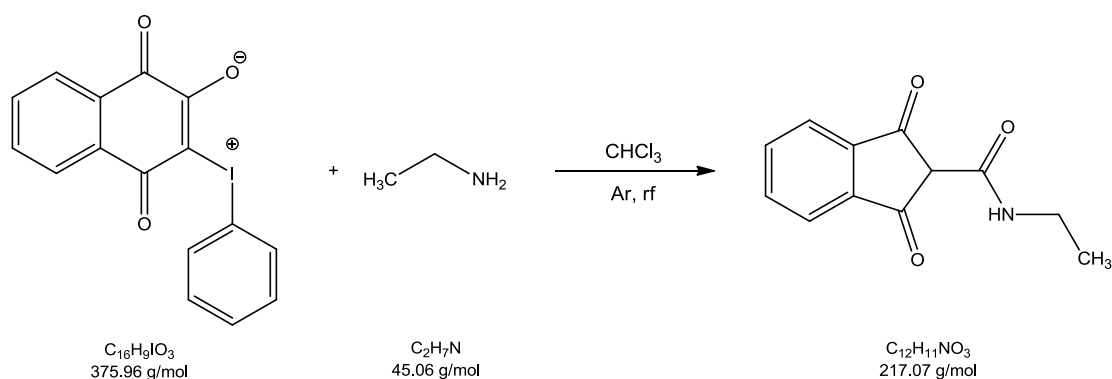


<sup>1</sup>H-NMR (500.10 MHz, DMSO-d<sub>6</sub>) δ: 2.92 (s, 3H, H<sub>2'</sub>), 7.55 – 7.66 (m, 4H, H<sub>4</sub>, H<sub>5</sub>, H<sub>6</sub>, H<sub>7</sub>), 8.69 (br s, 1H, NH).

<sup>13</sup>C-NMR (125.75 MHz, DMSO-d<sub>6</sub>) δ: 26.5 (C<sub>2'</sub>), 93.0 (C<sub>2</sub>), 120.8 (C<sub>4</sub>, C<sub>7</sub>), 133.1 (C<sub>5</sub>, C<sub>6</sub>), 137.8 (C<sub>3a</sub>, C<sub>7a</sub>), 166.0 (C<sub>1'</sub>), 190.7 (C<sub>1</sub>, C<sub>3</sub>).



### 3.5.4 Synthesis of N-ethyl-1,3-dioxo-2,3-dihydro-1H-indene-2-carboxamide (L2)



#### Synthesis:

The synthesis was performed according to the general procedure of 1,3-dioxo-2-indancarboxamides (see section 3.3.1), using 2-oxido-3-phenyliodonio-1,4-naphthoquinone (200 mg, 0.532 mmol) and ethylamine (70 %, 42  $\mu\text{L}$ , 0.532 mmol) with a reaction time of 30 hours.

Yield: 95 mg (83 %), orange solid

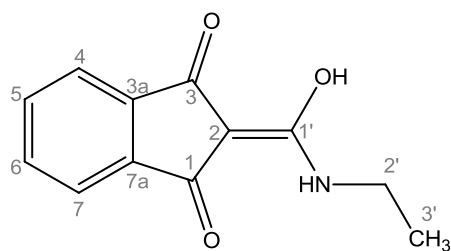
Melting point: 103 – 107 °C

Solubility: 0.30 mg/mL  $\equiv$  1.38 mM (Solubility is limited by DMSO-solubility)

#### Elemental analysis:

	<b>L2</b>	<b>C[%]</b>	<b>H[%]</b>	<b>N[%]</b>
$\text{C}_{12}\text{H}_{11}\text{NO}_3$	calculated	66.35	5.10	6.45
	found	66.41	5.01	6.01
	$\Delta$	0.06	0.09	0.44

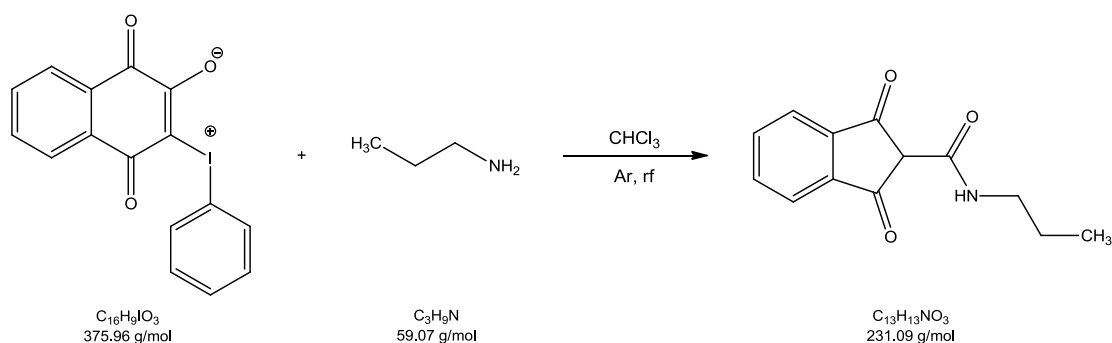
NMR-spectroscopy:



$^1\text{H-NMR}$  (500.10 MHz,  $\text{DMSO-d}_6$ )  $\delta$ : 1.17 (t,  $^3\text{J}(\text{H,H}) = 7$  Hz, 3H, H3'), 3.36 – 3.43 (m, 2H, H2'), 7.54 – 7.66 (m, 4H, H4, H5, H6, H7), 8.75 (br s, 1H, NH).

$^{13}\text{C-NMR}$  (125.75 MHz,  $\text{DMSO-d}_6$ )  $\delta$ : 14.6 (C3'), 34.7 (C2'), 92.8 (C2), 120.8 (C4, C7), 133.1 (C5, C6), 137.8 (C3a, C7a), 165.5 (C1'), 190.8 (C1, C3).

### 3.5.5 Synthesis of N-propyl-1,3-dioxo-2,3-dihydro-1H-indene-2-carboxamide (L3)



#### Synthesis:

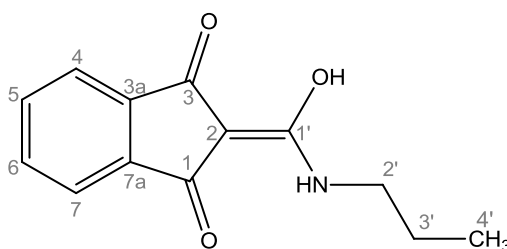
The synthesis was performed according to the general procedure of 1,3-dioxo-2-indancarboxamides (see section 3.3.1), using 2-oxido-3-phenyliodonio-1,4-naphthoquinone (751 mg, 1.99 mmol) and *n*-propylamine (137 $\mu$ L, 1.99 mmol) with a reaction time of 72 hours.

Yield: 341 mg (74 %), orange solid

Melting point: 78 – 80 °C

Solubility: 0.50 mg/mL  $\equiv$  2.16 mM

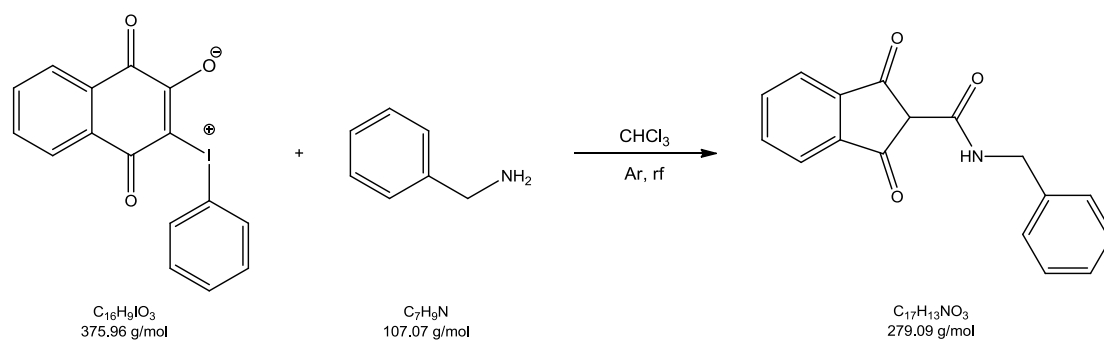
#### NMR-spectroscopy:



$^1H$ -NMR (500.10 MHz, DMSO- $d_6$ )  $\delta$ : 0,89 (t,  $^3J(H,H) = 7$  Hz, 3H, H4'), 1,55 – 1,62 (m, 2H, H3'), 3,28 – 3,37 (m, 2H, H2'), 7,55 – 7,67 (m, 4H, H4, H5, H6, H7), 8,73 (br s, 1H, NH).

$^{13}C$ -NMR (125.75 MHz, DMSO- $d_6$ )  $\delta$ : 11,0 (C4'), 22,2 (C3'), 45,1 (C2'), 92,9 (C2), 120,8 (C4, C7), 133,1 (C5, C6), 137,8 (C3a, C7a), 165,7 (C1'), 190,8 (C1, C3).

### 3.5.6 Synthesis of N-benzyl-1,3-dioxo-2,3-dihydro-1H-indene-2-carboxamide (L4)



#### Synthesis:

The synthesis was performed according to the general procedure of 1,3-dioxo-2-indancarboxamides (see section 3.3.1), using 2-oxido-3-phenyliodonio-1,4-naphthoquinone (100 mg, 0.266 mmol) of and benzylamine (29  $\mu$ L, 0.266 mmol) of with a reaction time of 8 hours.

Yield: 71 mg (96 %), orange solid

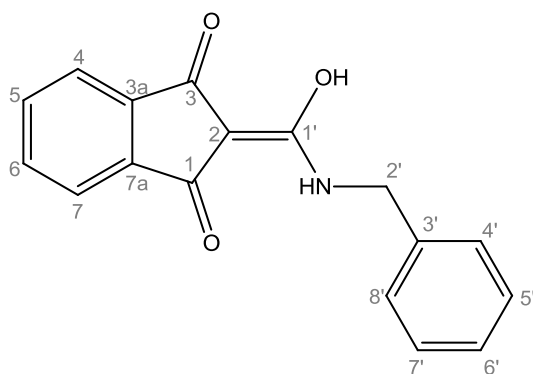
Melting point: 141 – 143 °C

Solubility: 0.20 mg/mL  $\equiv$  0.72 mM

#### Elemental analysis:

	<b>L4</b>	C [%]	H [%]	N [%]
$C_{17}H_{13}NO_3$	calculated	73.11	4.69	5.02
	found	72.81	4.43	4.69
	$\Delta$	0.30	0.26	0.33

NMR-spectroscopy:

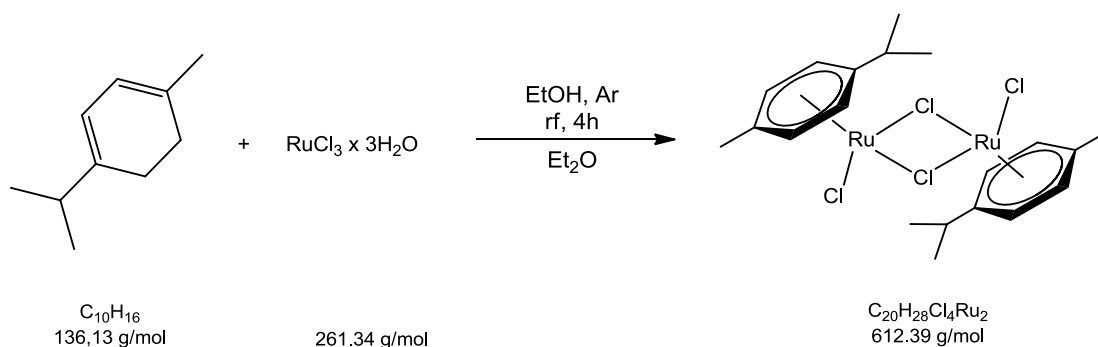


$^1\text{H-NMR}$  (500.10 MHz,  $\text{DMSO-d}_6$ )  $\delta$ : 4.57(s, 2H, H2'), 7.26- 7.30 (m, 1H, H6'), 7.32 – 7,39 (m, 4H, H4', H5', H7', H8'), 7.56 – 7.66 (m, 4H, H4, H5, H6, H7), 9.18 (br s, 1H, NH).

$^{13}\text{C-NMR}$  (125.75 MHz,  $\text{DMSO-d}_6$ )  $\delta$ : 42.9 (C2'), 93.4 (C2), 120.9 (C4,C7), 127.3 (C6'), 127.4 (C4'), 128.5 (C5'), 133.1 (C5, C6), 137.67 (C3a, C7a), 137.73 (C3'), 165.6 (C1'), 190.6 (C1, C3).

### 3.6 Syntheses of ( $\eta^6$ -cymene)-ruthenium(II) complexes

#### 3.6.1 Synthesis of the precursor metal complex *bis[dichlorido( $\eta^6$ -p-cymene)ruthenium(II)]*



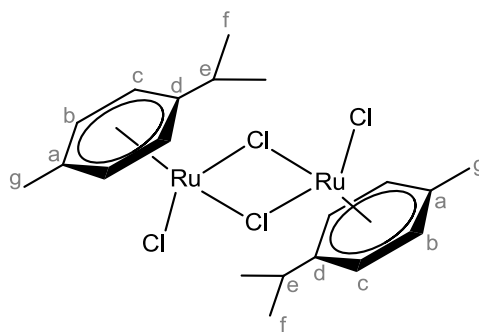
#### Synthesis:

$\alpha$ -Terpinene (12.5 mL, 76.9 mmol, 10 eq) was added to a solution of  $RuCl_3 \cdot 3H_2O$  (2.00 g, 7.65 mmol, 1 eq) in dry ethanol (75 mL). The reaction mixture was refluxed for 4 hours under argon atmosphere. Afterwards, the reaction mixture was allowed to cool to room temperature, the volume was reduced to ca. 35 mL and the product precipitated by addition of diethyl ether (40 mL). The complex was filtered off, washed with diethyl ether and dried *in vacuo*.

Yield: 2.14 g, (92 %), red powder

Melting point: >182 °C (decomposition)

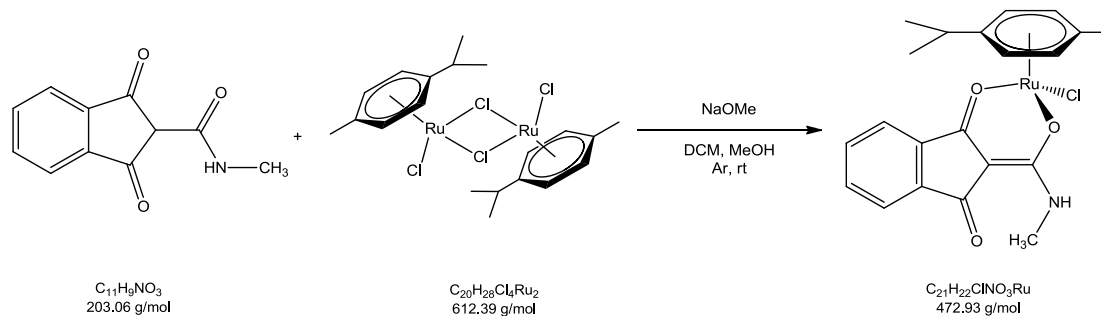
NMR-spectroscopy:



$^1\text{H-NMR}$  (500.10 MHz,  $\text{CDCl}_3$ )  $\delta$ : 1.28 (d,  $^3\text{J}(\text{H,H}) = 7$  Hz, 6H,  $2\text{CH}_3\text{-f}$ ), 2.16 (s, 3H,  $\text{CH}_3\text{-g}$ ), 2.88 – 2.96 (m, 1H, He), 5.34 (d,  $^3\text{J}(\text{H,H}) = 6$  Hz, 2H, Hb), 5.47 (d,  $^3\text{J}(\text{H,H}) = 6$  Hz, 2H, Hc).

$^{13}\text{C-NMR}$  (125.75 MHz,  $\text{CDCl}_3$ )  $\delta$ : 18.9 ( $\text{CH}_3\text{-g}$ ), 22.2 ( $2\text{CH}_3\text{-f}$ ), 30.6 (Ce), 80.5 (Cb), 81.3 (Cc), 96.7 (Ca), 101.2 (Cd).

### 3.6.2 Synthesis of [(chlorido)(1,3-dioxo-κO1-1H-inden-2(3H)-ylidene)(methylamino)methanolato-κO2]](η<sup>6</sup>-p-cymene)ruthenium(II) (1a)



#### Synthesis:

The synthesis was performed according to the general procedure of (η<sup>6</sup>-cym)-ruthenium(II) complexes (see section 3.3.2), using bis[dichlorido(η<sup>6</sup>-p-cymene)ruthenium(II)] (200 mg, 32 μmol), compound **L1** (146 mg, 717 μmol) and sodium methoxide (45 mg, 832 μmol).

Yield: 217 mg (70 %), brown crystals

Melting point: >159 °C (decomposition)

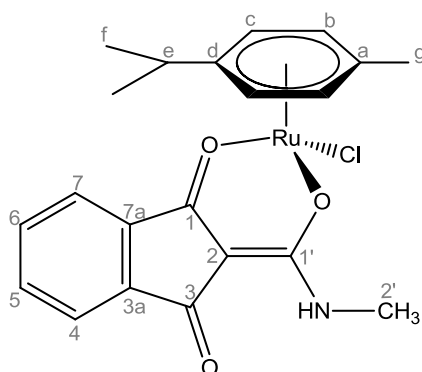
Solubility: 0.08 mg/mL ≡ 0.17 mM (Solubility is limited by DMSO-solubility)

#### Elemental analysis:

	<b>1a</b>	C [%]	H [%]	N [%]
$C_{21}H_{22}ClNO_3Ru \cdot 0.25CH_2Cl_2$	calculated	51.64	4.59	2.83
	found	51.72	4.25	2.77
	Δ	0.08	0.34	0.06



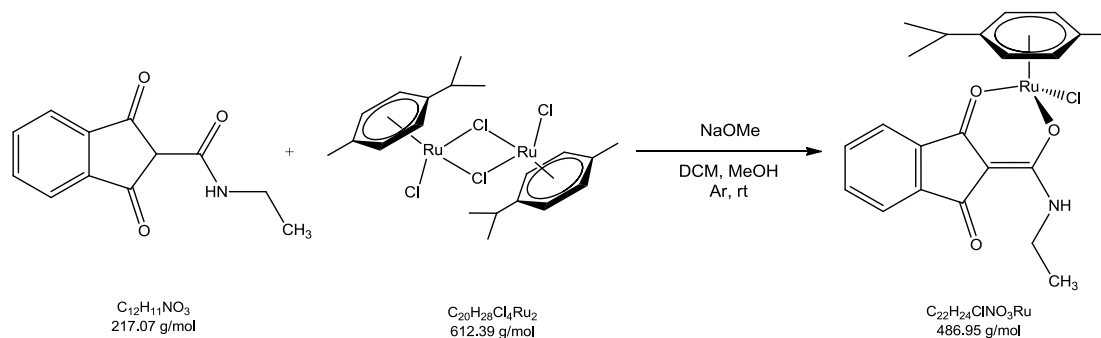
NMR-spectroscopy:



<sup>1</sup>H-NMR (500.10 MHz, CDCl<sub>3</sub>) δ: 1.39 – 1.45 (m, 6H, 2CH<sub>3</sub>-f), 2.30 (s, 3H, CH<sub>3</sub>-g), 2.96 – 3.04 (m, 4H, H2',He), 5.31 – 5.37 (m, 2H, Hb), 5.57 – 5.66 (m, 2H, Hc), 7.37 - 7.43 (m, 3H, H5, H6, H7), 7.50 – 7.54 (m, 1H, H4), 8.43 (q, <sup>3</sup>J(H,H) = 4.9 Hz, 1H, NH).

<sup>13</sup>C-NMR (125.75 MHz, CDCl<sub>3</sub>) δ: 17.9 (CH<sub>3</sub>-g), 22.40 & 22.43 (2CH<sub>3</sub>-f), 26.1 (C2'), 31.1 (Ce), 79.2 & 79.3 (Cb), 82.7 & 82.8 (Cc), 96.6 (Ca), 98.4 (C2), 99.4 (Cd), 120.6 (C7), 120.8 (C4), 132.0 (C5), 132.2 (C6), 136.4 (C7a), 137.8 (C3a), 166.6 (C1'), 190.7 (C3), 192.5 (C1).

### 3.6.3 Synthesis of [(chlorido)(1,3-dioxo-κO1-1H-inden-2(3H)-ylidene)(ethylamino)methanolato-κO2]](η<sup>6</sup>-p-cymene)ruthenium(II) (**2a**)



#### Synthesis:

The synthesis was performed according to the general procedure of (η<sup>6</sup>-cym)-ruthenium(II) complexes (see section 3.3.2), using bis[dichlorido(η<sup>6</sup>-p-cymene)ruthenium(II)] (250 mg, 0.408 mmol), compound **L2** (194 mg, 0.895 mmol) and sodium methoxide (54 mg, 1.01 mmol).

Yield: 317 mg (80 %), brown solid

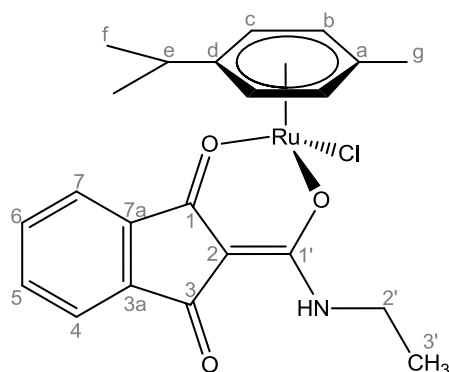
Melting point: >142 °C (decomposition)

Solubility: 0.10 mg/mL ≡ 0.21 mM

#### Elemental analysis:

	<b>2a</b>	C [%]	H [%]	N [%]
$C_{22}H_{24}ClNO_3Ru$	calculated	54.26	4.97	2.88
	found	53.98	5.05	2.83
	Δ	0.28	0.08	0.05

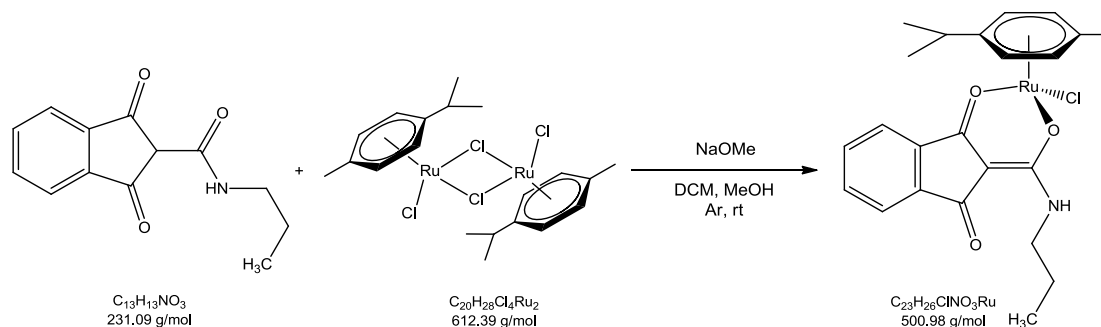
NMR-spectroscopy:



<sup>1</sup>H-NMR (500.10 MHz, CDCl<sub>3</sub>) δ: 1.23 (t, <sup>3</sup>J(H,H) = 7 Hz, 3H, H3'), 1.38 – 1.45 (m, 6H, 2CH<sub>3</sub>-f), 2.30 (s, 3H, CH<sub>3</sub>-g), 2.95 – 3.04 (m, 1H, He), 3.40 – 3.49 (m, 2H, H2'), 5.31 – 5.36 (m, 2H, Hb), 5.57 – 5.65 (m, 2H, Hc), 7.36 – 7.42 (m, 3H, H5, H6, H7), 7.50 – 7.54 (m, 1H, H4), 8.48 (t, <sup>3</sup>J(H,H) = 5 Hz, 1H, NH).

<sup>13</sup>C-NMR (125.75 MHz, CDCl<sub>3</sub>) δ: 15.1 (C3'), 17.9 (CH<sub>3</sub>-g), 22.39 & 22.42 (2CH<sub>3</sub>-f), 31.1 (Ce), 34.4 (C2'), 79.2 & 79.4 (Cb), 82.6 & 82.7 (Cc), 96.6 (Ca), 98.3 (C2), 99.4 (Cd), 120.6 (C7), 120.8 (C4), 132.0 (C5), 132.2 (C6), 136.4 (C7a), 137.8 (C3a), 166.0 (C1'), 190.7 (C3), 192.5 (C1).

### 3.6.4 Synthesis of [(chlorido)(1,3-dioxo- $\kappa$ O1-1H-inden-2(3H)-ylidene)(propylamino)methanolato- $\kappa$ O2)]( $\eta^6$ -p-cymene)ruthenium(II) (**3a**)



#### Synthesis:

The synthesis was performed according to the general procedure of ( $\eta^6$ -cym)-ruthenium(II) complexes (see section 3.3.2), using bis[dichlorido( $\eta^6$ -p-cymene)ruthenium(II)] (50 mg, 81  $\mu\text{mol}$ ), compound **L3** (39 mg, 168  $\mu\text{mol}$ ), and sodium methoxide (11 mg, 206  $\mu\text{mol}$ ).

Yield: 46 mg (56 %), red-brown crystals

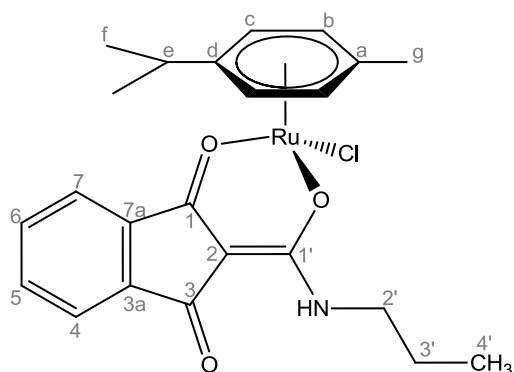
Melting point: >148  $^{\circ}\text{C}$  (decomposition)

Solubility: 0.15 mg/mL  $\equiv$  0.30 mM

#### Elemental analysis:

	<b>3a</b>	C [%]	H [%]	N [%]
$\text{C}_{23}\text{H}_{26}\text{O}_3\text{ClNRu} \cdot 0.25\text{H}_2\text{O}$	calculated	54.65	5.28	2.77
	found	54.46	5.36	2.65
	$\Delta$	0.19	0.08	0.12

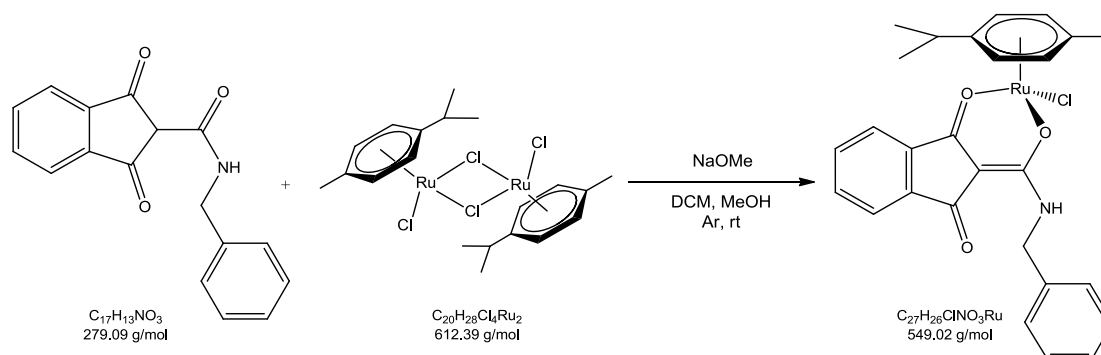
NMR-spectroscopy:



<sup>1</sup>H-NMR (500.10 MHz, CDCl<sub>3</sub>) δ: 0.98 (t, <sup>3</sup>J(H,H) = 7 Hz, 3H, H4'), 1.39 – 1.44 (m, 6H, 2CH<sub>3</sub>-f), 1.55 – 1.66 (m, 11H, H3' and res. water – see section 2.2.3), 2.30 (s, 3H, CH<sub>3</sub>-g), 2.95 – 3.04 (m, 1H, He), 3.32 – 3.43 (m, 2H, H2'), 5.31 – 5.36 (m, 2H, Hb), 5.57 – 5.64 (m, 2H, Hc), 7.38 – 7.42 (m, 3H, H5, H6, H7), 7.50 – 7.55 (m, 1H, H4), 8.56 (t, <sup>3</sup>J(H,H) = 6 Hz, 1H, NH).

<sup>13</sup>C-NMR (125.75 MHz, CDCl<sub>3</sub>) δ: 11.7 (C4'), 18.0 (CH<sub>3</sub>-g), 22.41 & 22.45 (2CH<sub>3</sub>-f), 23.1 (C3'), 31.1 (Ce), 41.2 (C2'), 79.1 & 79.4 (Cb), 82.6 & 82.8 (Cc), 96.6 (Ca), 98.3 (C2), 99.4 (Cd), 120.6 (C7), 120.8 (C4), 132.0 (C5), 132.2 (C6), 136.5 (C7a), 137.8 (C3a), 166.1 (C1'), 190.7 (C3), 192.5 (C1).

### 3.6.5 Synthesis of [(chlorido)(1,3-dioxo- $\kappa$ O1-1H-inden-2(3H)-ylidene)(benzylamino)methanolato- $\kappa$ O2)]( $\eta^6$ -p-cymene)ruthenium(II) (4a)



#### Synthesis:

The synthesis was performed according to the general procedure of ( $\eta^6$ -cym)-ruthenium(II) complexes (see section 3.3.2), using bis[dichlorido( $\eta^6$ -p-cymene)ruthenium(II)] (200 mg, 327  $\mu$ mol), compound **L4** (201 mg, 719  $\mu$ mol) and sodium methoxide (43 mg, 791  $\mu$ mol).

Yield: 302 mg (84 %), red crystals

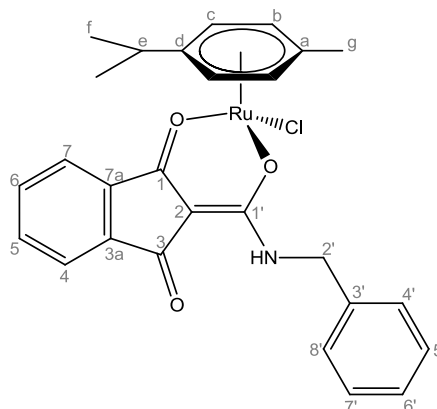
Melting point: >155 °C (decomposition)

Solubility: 0.02 mg/mL  $\equiv$  0.04 mM

#### Elemental analysis:

	4a	C [%]	H [%]	N [%]
C <sub>27</sub> H <sub>26</sub> ClNO <sub>3</sub> Ru	calculated	59.07	4.77	2.55
	found	58.93	4.60	2.42
	$\Delta$	0.16	0.17	0.13

NMR-spectroscopy:



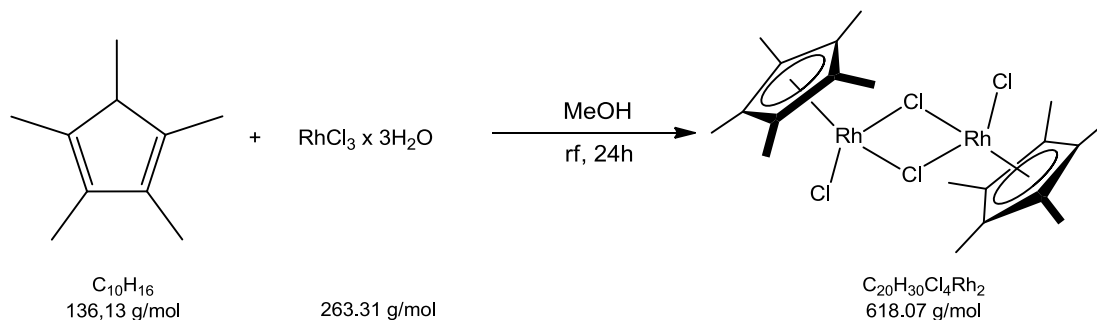
$^1\text{H-NMR}$  (500.10 MHz,  $\text{CDCl}_3$ )  $\delta$ : 1.28 – 1.35 (m, 6H,  $2\text{CH}_3$ -f), 2.21 (s, 3H,  $\text{CH}_3$ -g), 2.77 – 3.58 (m, 1H, He), 4.53 (dd,  $^2\text{J}(\text{H,H}) = 15$  Hz,  $^3\text{J}(\text{H,H}) = 6$  Hz, 1H, H2'), 4.72 (dd,  $^2\text{J}(\text{H,H}) = 15$  Hz,  $^3\text{J}(\text{H,H}) = 6$  Hz, 1H, H2'), 5.23 – 5.31 (m, 2H, Hb), 5.43 – 5.55 (m, 2H, Hc), 7.25 – 7.30 (m, 1H, H6'), 7.31 – 7.37 (m, 4H, H4', H5', H7', H8'), 7.39 – 7.45 (m, 3H, H5, H6, H7), 7.52 – 7.57 (m, 1H, H4), 8.94 (t,  $^3\text{J}(\text{H,H}) = 6$  Hz, 1H, NH).

$^{13}\text{C-NMR}$  (125.75 MHz,  $\text{CDCl}_3$ )  $\delta$ : 17.9 ( $\text{CH}_3$ -g), 22.3 & 22.4 ( $2\text{CH}_3$ -f), 30.9 (Ce), 43.4 (C2'), 78.9 & 79.3 (Cb), 82.4 & 82.7 (Cc), 96.7 (Ca), 98.2 (C2), 99.6 (Cd), 120.7 (C7), 120.9 (C4), 127.28 (C4', C8'), 127.30 (C6'), 128.7 (C5', C7'), 132.1 (C5), 132.3 (C6), 136.5 (C7a), 137.8 (C3a), 138.8 (C3'), 166.1 (C1'), 190.9 (C3), 192.5 (C1).

### 3.7 Syntheses of ( $\eta^5$ -Cp\*)-rhodium(III) complexes

#### 3.7.1 Synthesis of the precursor metal complex

##### *bis[dichlorido( $\eta^5$ -1,2,3,4,5-pentamethylcyclopentadiene)rhodium(III)]*



#### Synthesis:

1,2,3,4,5-Pentamethylcyclopentadiene (1.10 mL, 7.02 mmol, 1.09 eq) was added to a suspension of  $\text{RhCl}_3 \cdot \text{H}_2\text{O}$  (1.70 g, 6.46 mmol, 1 eq) in methanol (50 mL) and the mixture was refluxed for 24 hours. The red solid was filtered off, washed with diethyl ether, dried *in vacuo* and used without further purification.

Yield: 1.50 g, (75 %), red powder

Melting point: 152 – 154 °C

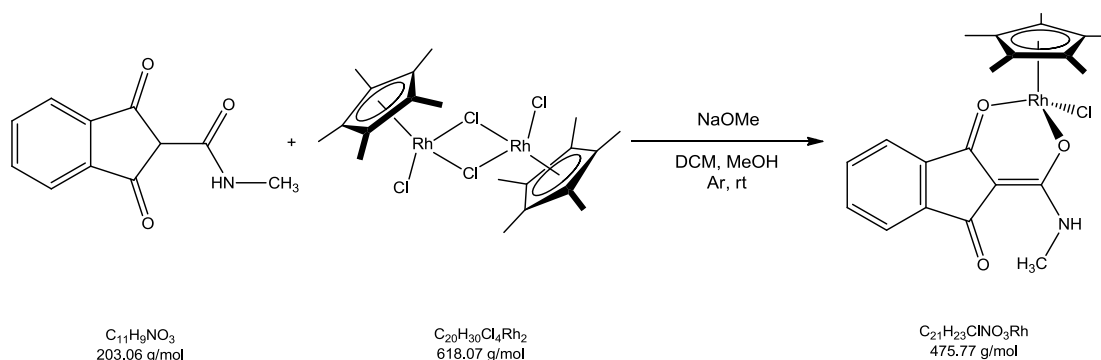
#### NMR-spectroscopy:

$^1\text{H-NMR}$  (500.10 MHz,  $\text{CDCl}_3$ )  $\delta$ : 1.62 (s, 30H, 10  $\text{C}_a$ ).

$^{13}\text{C-NMR}$  (125.75 MHz,  $\text{CDCl}_3$ )  $\delta$ : 9.5 (10  $\text{C}_a$ ), 94.3 (s,  $\text{C}_b$ ).



**3.7.2 Synthesis of [(chlorido)(1,3-dioxo- $\kappa$ O1-1H-inden-2(3H)-ylidene)(methylamino)methanolato- $\kappa$ O2)]( $\eta^5$ -1,2,3,4,5-pentamethylcyclopentadiene)rhodium(III) (**1b**)**



Synthesis:

The synthesis was performed according to the general procedure of ( $\eta^5$ -Cp\*)-rhodium(III) complexes (see section 3.3.2), using bis[dichlorido( $\eta^5$ -1,2,3,4,5-pentamethylcyclopentadiene)rhodium(III)] (50 mg, 81  $\mu$ mol) of, compound **L1** (37 mg, 181  $\mu$ mol), and sodium methoxide (11 mg, 209  $\mu$ mol).

Yield: 58 mg (76 %), yellow-orange solid

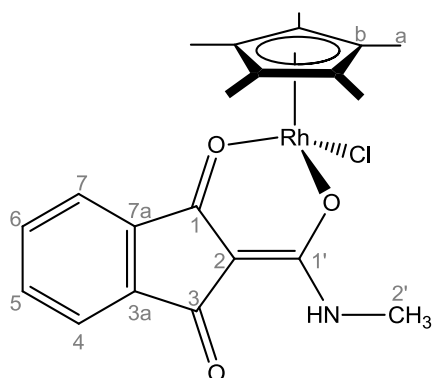
Melting point: >246 °C (decomposition)

Solubility: 0.10 mg/mL  $\equiv$  0.21 mM (Solubility is limited by DMSO-solubility)

Elemental analysis:

	<b>1b</b>	C [%]	H [%]	N [%]
$C_{21}H_{23}ClNO_3Rh$	calculated	53.01	4.87	2.94
	found	53.15	4.68	2.55
	$\Delta$	0.14	0.19	0.39

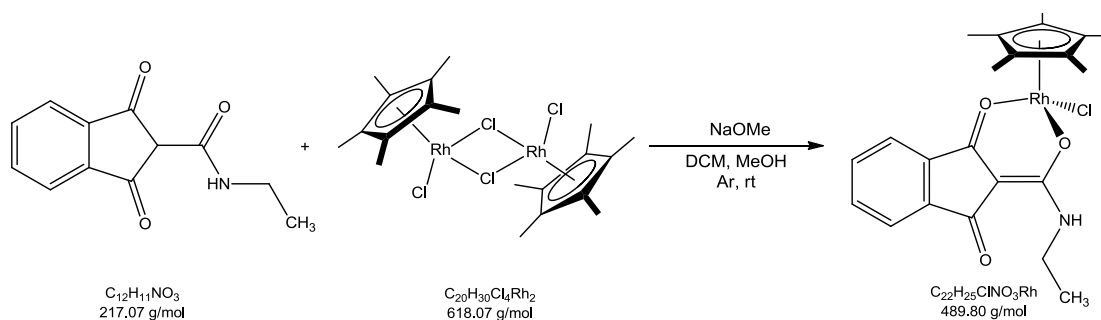
NMR-spectroscopy:



$^1\text{H-NMR}$  (500.10 MHz,  $\text{CDCl}_3$ )  $\delta$ : 1.69 (s, 15H,  $5\text{H}_a$ ), 2.99 (d,  $^3\text{J}(\text{H,H}) = 5$  Hz, 3H,  $\text{H}2'$ ), 7.37 – 7.46 (m, 3H,  $\text{H}5$ ,  $\text{H}6$ ,  $\text{H}7$ ), 7.53 – 7.59 (m, 1H,  $\text{H}4$ ), 8.58 (br q,  $^3\text{J}(\text{H,H}) = 4$  Hz, 1H, NH).

$^{13}\text{C-NMR}$  (125.75 MHz,  $\text{CDCl}_3$ )  $\delta$ : 8.8 ( $\text{C}_a$ ), 25.9 ( $\text{C}2'$ ), 92.4 ( $\text{C}_b$ ), 92.5 ( $\text{C}2$ ), 120.5 ( $\text{C}7$ ), 120.7 ( $\text{C}4$ ), 131.9 ( $\text{C}5$ ), 132.0 ( $\text{C}6$ ), 136.8 ( $\text{C}7a$ ), 138.6 ( $\text{C}3a$ ), 166.7 ( $\text{C}1'$ ), 190.7 ( $\text{C}3$ ), 192.9 ( $\text{C}1$ ).

**3.7.3 Synthesis of [(chlorido)(1,3-dioxo- $\kappa$ O1-1H-inden-2(3H)-ylidene)(ethylamino)methanolato- $\kappa$ O2)]( $\eta^5$ -1,2,3,4,5-pentamethylcyclopentadiene)rhodium(III) (**2b**)**



**Synthesis:**

The synthesis was performed according to the general procedure of ( $\eta^5$ -Cp\*)-rhodium(III) complexes (see section 3.3.2), using bis[dichlorido( $\eta^5$ -1,2,3,4,5-pentamethylcyclopentadiene)rhodium(III)] (250 mg, 0.405 mmol), compound **L2** (195 mg, 0.895 mmol), and sodium methoxide (54 mg, 1.01 mmol).

**Yield:** 324 mg (82 %), orange solid

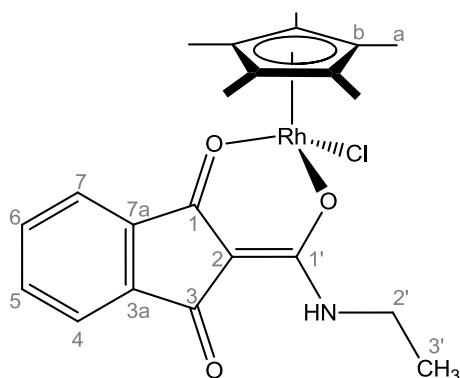
**Melting point:** >203 °C (decomposition)

**Solubility:** 0.09 mg/mL  $\equiv$  0.18 mM (Solubility is limited by DMSO-solubility)

**Elemental analysis:**

	<b>2b</b>	C [%]	H [%]	N [%]
$C_{22}H_{25}ClNO_3Rh \cdot 0.5H_2O$	calculated	53.01	5.26	2.81
	found	52.90	5.26	2.77
	$\Delta$	0.11	0.00	0.04

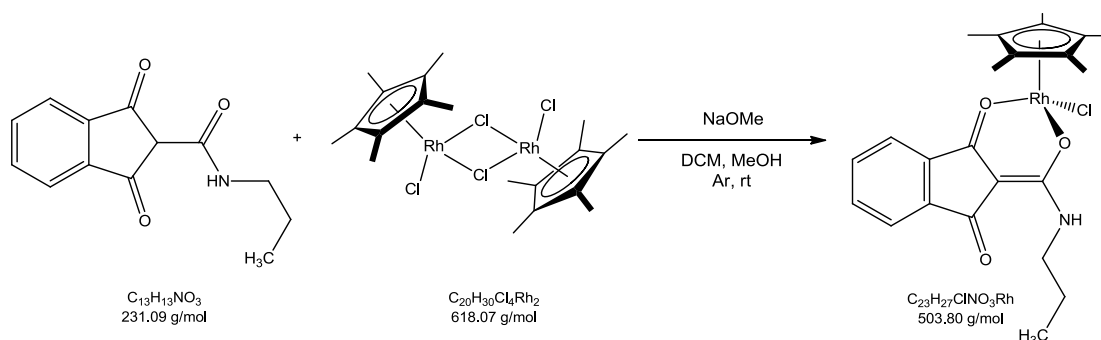
NMR-spectroscopy:



<sup>1</sup>H-NMR (500.10 MHz, CDCl<sub>3</sub>) δ: 1.23 (t, <sup>3</sup>J(H,H) = 7 Hz, 3H, H<sub>3'</sub>), 1.69 (s, 15H, H<sub>a</sub>), 3.41 – 3.53 (m, 2H, H<sub>2'</sub>), 7.38 – 7.44 (m, 3H, H<sub>5</sub>, H<sub>6</sub>, H<sub>7</sub>), 7.54 – 7.57 (m, 1H, H<sub>4</sub>), 8.63 (br t, <sup>3</sup>J(H,H) = 5 Hz, 1H, NH).

<sup>13</sup>C-NMR (125.75 MHz, CDCl<sub>3</sub>) δ: 8.8 (C<sub>a</sub>), 15.08 (C<sub>3'</sub>), 34.1 (C<sub>2'</sub>), 92.4 (C<sub>b</sub>), 92.5 (C<sub>2</sub>), 120.4 (C<sub>7</sub>), 120.7 (C<sub>4</sub>), 131.9 (C<sub>5</sub>), 132.0 (C<sub>6</sub>), 136.8 (C<sub>7a</sub>), 138.6 (C<sub>3a</sub>), 166.0 (C<sub>1'</sub>), 190.8 (C<sub>3</sub>), 192.9 (C<sub>1</sub>).

**3.7.4 Synthesis of [(chlorido)(1,3-dioxo- $\kappa$ O1-1H-inden-2(3H)-ylidene)(propylamino)methanolato- $\kappa$ O2)]( $\eta^5$ -1,2,3,4,5-pentamethylcyclopentadiene)rhodium(III) (**3b**)**



**Synthesis:**

The synthesis was performed according to the general procedure of ( $\eta^5$ -Cp\*)-rhodium(III) complexes, (see section 3.3.2), using bis[dichlorido( $\eta^5$ -1,2,3,4,5-pentamethylcyclopentadiene)rhodium(III)] (189 mg, 306  $\mu$ mol), compound **L3** (158 mg, 683  $\mu$ mol), and sodium methoxide (40 mg, 748  $\mu$ mol).

**Yield:** 262 mg (85 %), orange crystals

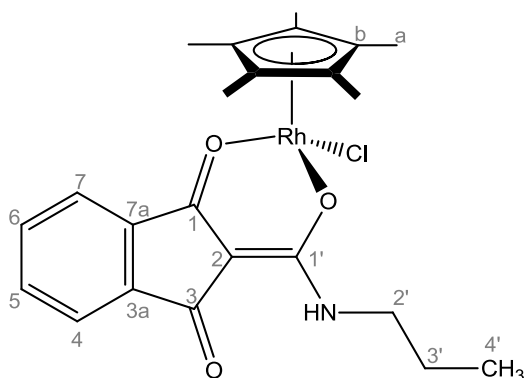
**Melting point:** >149 °C (decomposition)

**Solubility:** 0.20 mg/mL  $\equiv$  0.40 mM

**Elemental analysis:**

	<b>3b</b>	C [%]	H [%]	N [%]
C <sub>23</sub> H <sub>27</sub> ClNO <sub>3</sub> Rh·0.1H <sub>2</sub> O	calculated	54.67	5.43	2.77
	found	54.58	5.60	2.55
	$\Delta$	0.09	0.17	0.22

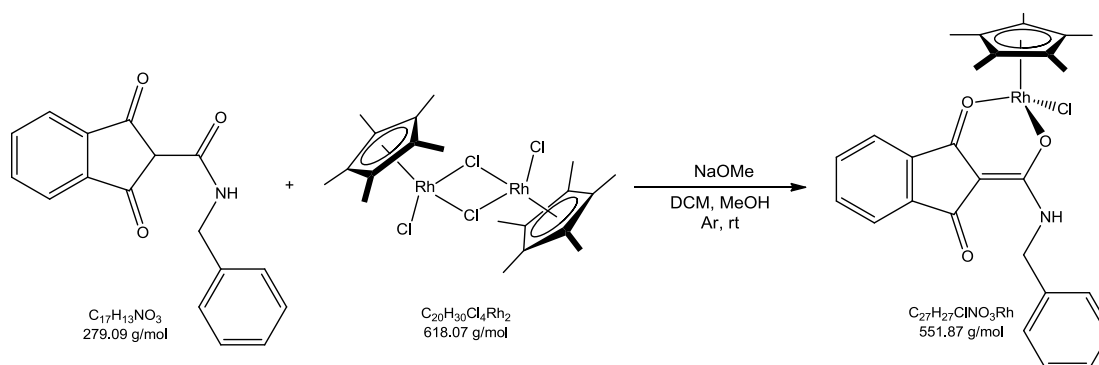
NMR-spectroscopy:



$^1\text{H-NMR}$  (500.10 MHz,  $\text{CDCl}_3$ )  $\delta$ : 0.98 (t,  $^3\text{J}(\text{H,H}) = 7$  Hz, 3H,  $\text{H}_{4'}$ ), 1.58 – 1.64 (m, 2H,  $\text{H}_{3'}$ ), 1.68 (s, 15H,  $\text{H}_a$ ), 3.30 – 3.49 (m, 2H,  $\text{H}_{2'}$ ), 7.37 – 7.44 (m, 3H,  $\text{H}_5$ ,  $\text{H}_6$ ,  $\text{H}_7$ ), 7.53 – 7.56 (m, 1H,  $\text{H}_4$ ), 8.71 (br t,  $^3\text{J}(\text{H,H}) = 6$  Hz, 1H, NH).

$^{13}\text{C-NMR}$  (125.75 MHz,  $\text{CDCl}_3$ )  $\delta$ : 8.8 ( $\text{C}_a$ ), 11.8 ( $\text{C}_{4'}$ ), 23.1 ( $\text{C}_{3'}$ ), 40.9 ( $\text{C}_{2'}$ ), 92.36 ( $\text{C}_b$ ), 92.44 ( $\text{C}_2$ ), 120.4 ( $\text{C}_7$ ), 120.7 ( $\text{C}_4$ ), 131.9 ( $\text{C}_5$ ), 132.0 ( $\text{C}_6$ ), 136.8 ( $\text{C}_{7a}$ ), 138.6 ( $\text{C}_{3a}$ ), 166.1 ( $\text{C}_{1'}$ ), 190.8 ( $\text{C}_3$ ), 192.9 ( $\text{C}_1$ ).

**3.7.5 Synthesis of [(chlorido)(1,3-dioxo- $\kappa$ O1-1H-inden-2(3H)-ylidene)(benzylamino)methanolato- $\kappa$ O2)]( $\eta^5$ -1,2,3,4,5-pentamethylcyclopentadiene)rhodium(III) (**4b**)**



**Synthesis:**

The synthesis was performed according to the general procedure of ( $\eta^5$ -Cp\*)-rhodium(III) complexes (see section 3.3.2), using bis[dichlorido( $\eta^5$ -1,2,3,4,5-pentamethylcyclopentadiene)rhodium(III)] (134 mg, 216  $\mu$ mol), compound **L4** (135 mg (483  $\mu$ mol), and sodium methoxide (43 mg (791  $\mu$ mol).

**Yield:** 203 mg (85 %), orange solid

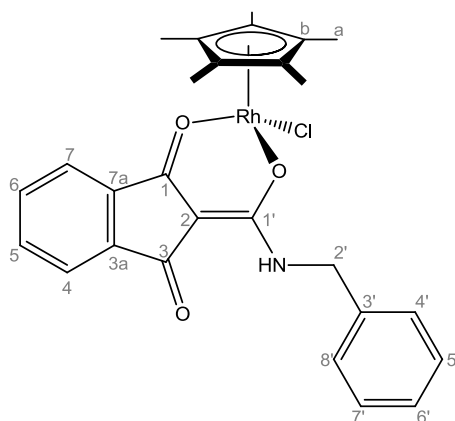
**Melting point:** >132 °C (decomposition)

**Solubility:** 0.10 mg/mL  $\equiv$  0.18 mM

**Elemental analysis:**

	<b>4b</b>	C [%]	H [%]	N [%]
$C_{27}H_{27}ClNO_3Rh \cdot 0.6CH_2Cl_2$	calculated	55.07	4.73	2.33
	found	55.00	4.55	2.28
	$\Delta$	0.07	0.18	0.05

NMR-spectroscopy:



$^1\text{H-NMR}$  (500.10 MHz,  $\text{CDCl}_3$ )  $\delta$ : 1.58 (s, 15H,  $\text{H}_a$ ), 4.48 (dd,  $^2\text{J}(\text{H,H}) = 16$  Hz,  $^3\text{J}(\text{H,H}) = 6$  Hz, 1H,  $\text{H}_{2'}$ ), 4.83 (dd,  $^2\text{J}(\text{H,H}) = 16$  Hz,  $^3\text{J}(\text{H,H}) = 6$  Hz, 1H,  $\text{H}_{2'}$ ), 7.22 – 7.28 (m, 1H,  $\text{H}_{6'}$ ), 7.31 – 7.34 (m, 4H,  $\text{H}_{4'}$ ,  $\text{H}_{5'}$ ,  $\text{H}_{7'}$ ,  $\text{H}_{8'}$ ), 7.40 – 7.47 (m, 3H,  $\text{H}_5$ ,  $\text{H}_6$ ,  $\text{H}_7$ ), 7.56 – 7.59 (m, 1H,  $\text{H}_4$ ), 9.13 (br t,  $^3\text{J}(\text{H,H}) = 6$  Hz, 1H, NH).

$^{13}\text{C-NMR}$  (125.75 MHz,  $\text{CDCl}_3$ )  $\delta$ : 8.7 ( $\text{C}_a$ ), 43.1 ( $\text{C}_{2'}$ ), 92.5 ( $\text{C}_b$ ), 92.6 ( $\text{C}_2$ ), 120.6 ( $\text{C}_7$ ), 120.8 ( $\text{C}_4$ ), 127.1 ( $\text{C}_{6'}$ ), 127.2 ( $\text{C}_{4'}$ ,  $\text{C}_{8'}$ ), 128.7 ( $\text{C}_{5'}$ ,  $\text{C}_{7'}$ ), 132.0 ( $\text{C}_5$ ), 132.2 ( $\text{C}_6$ ), 136.9 ( $\text{C}_{7a}$ ), 138.6 ( $\text{C}_{3a}$ ), 139.1 ( $\text{C}_{3'}$ ), 166.3 ( $\text{C}_{1'}$ ), 191.0 ( $\text{C}_3$ ), 192.9 ( $\text{C}_1$ ).



## 4 Conclusion

Due to the fact that cancer is still the second leading cause of death, the research for chemotherapeutics is a matter of great importance. Apart from investigation of analogues of the platinum complexes which are currently in clinical use, other coordination compounds of other transition metals are being researched. Since NAMI-A and KP 1019 entered and passed phase I of clinical trials, the interest in ruthenium anticancer compounds increases constantly and in addition, many rhodium compounds have shown promising efficacy against cancer cells, as well.

Within this work, four 1,3-indandione derivatives were synthesized in good to excellent yield (74 – 96 %). These compounds were reported in literature to exhibit promising anticancer. However, no method was found to synthesize *N*-alkylated 2-amino-3-hydroxy-naphtho-1,4-quinones in satisfying yields and with sufficient purity.

The prepared ligands were reacted with organometallic precursors, yielding four Ru<sup>II</sup>( $\eta^6$ -cym) and four Rh<sup>III</sup>( $\eta^5$ -Cp\*) ‘piano-stool’ configured half-sandwich complexes. The Ru<sup>II</sup>( $\eta^6$ -cym) organometallics were obtained with 57 – 84 % yield, and the Rh<sup>III</sup>( $\eta^5$ -Cp\*) analogues with 76 – 85 %. All compounds were characterized *via* elemental analysis, <sup>1</sup>H-NMR, <sup>13</sup>C-NMR, and 2D NMR-methods, the latter employing <sup>1</sup>H-<sup>1</sup>H-COSY, <sup>1</sup>H-<sup>13</sup>C-HMBC, and <sup>1</sup>H-<sup>13</sup>C-HSQC. Their decomposition points and solubilities were determined. Two ruthenium complexes yielded single crystals, suitable for x-ray diffraction analysis. Moreover, ESI-ion trap mass spectrometry was employed to determine the stabilities of the complexes, as well as their reactivity towards biomolecules. These investigations showed that the rhodium complex exhibits higher stability in aqueous media. Both compounds showed a higher affinity towards amino acids, compared to nucleoside triphosphates. Amongst amino acids both complexes reacted favorably with cysteine, as expected.

In the case of one ligand (*N*-propargyl substituted) it was not possible to synthesize pure Ru<sup>II</sup>( $\eta^6$ -cym) or Rh<sup>III</sup>( $\eta^5$ -Cp\*) complexes due to the ligand’s capability to react *via*  $\eta^2$ -coordination. However, this propargyl group is an excellent starting point for click-chemical derivatization and other modifications, in order to yield complexes with higher solubility or even dinuclear complexes by linking a second coordination site.

Furthermore, different synthetic conditions could facilitate the synthesis more complexly *N*-substituted 1,3-indandione scaffolds or even the synthesis of the desired *N*-alkylated 2-amino-3-hydroxy-naphtho-1,4-quinones.



---

## Curriculum Vitae

### Personal information

First name / Surname **Stephan Mokesch, B.Sc.**  
Address Robert-Lachgasse 1-3/21/6, 1210 Wien, Austria  
Mobilephone Austria: +43 699 10 80 16 71  
E-mail stephan.mokesch@gmx.at  
Nationality Austria  
Date of birth 07.10.1988

### Desired Occupational field

Bioinorganic Chemistry, Analytical Chemistry, Organic Chemistry,...

### Work experience

Dates	September 2006 – May 2007
Status of employment	A-Level Teamproject – Designing Methods for obtaining Active Pharmaceutical Ingredients from Uhudler-Marc (Austrian vine marc)
Main activities and responsibilities	Optimization of extraction methods, employing numerous chemical technological processes; Characterization of the extracts by employing numerous analytical and spectroscopical methods
Name and address of employer	AV RR DI Dr. Hans Andres College of Chemistry, Rosensteigasse79 Vienna
Working field	Chemical Technology, Analytical Chemistry, Spectroscopy, ...
Dates	July 2004
Status of employment	Internship – Microbiological Quality Control Laboratory / Food Testing institute Vienna 19
Main activities and responsibilities	Petri-dish testing for harmful bacteria; generating and autoclaving nutrient solutions
Name and address of employer	Dr. Perko Lebensmittel Versuchsanstalt LVA Blaasstraße 29 1190 Wien
Working field	Microbiology
Dates	July 2003
Status of employment	Internship – Analytical Quality Control Laboratory / Food Testing Institute Vienna 19
Main activities and responsibilities	Performing analytical standard techniques to test for the content of the following in foods: different fats, theobromine, caffeine, preservatives, ...
Name and address of employer	Dr. Perko Lebensmittel Versuchsanstalt LVA Blaasstraße 29 1190 Wien
Working field	Analytical and environmental chemistry

---

---

**School and University Education**

Dates	October 2009 – January 2013
Name of the Institute	University of Vienna Währinger Straße 40-42, 1090 Wien, Austria
Main Subjects	Inorganic Chemistry, Organic Chemistry, Food Chemistry In theory and laboratory
Dates	September 2007 – June 2008
Name of the Institute	Dublin Institute of Technology DIT Kevin Street, Dublin 8, Ireland
Main Subjects	Analytical Chemistry, Inorganic Chemistry, Organic Chemistry, Spectroscopy, Physical Chemistry, Chemical Technology, Environmental Chemistry, Pharmaceutical Chemistry. In theory and laboratory
Qualification	Bachelor of Science Projected Results: Distinction
Dates	September 2005 – June 2007
Name of the Institute	College of Chemistry Specialising in the Technology of Leather and Natural Materials Rosensteingasse 79, 1170 Wien, Austria
Main Subjects	Chemical Technology of Leather, Chemical Technology of Natural Materials, Organic Chemistry, Physical Chemistry, Process Engineering; All of the above in Theory and Laboratory
Qualification	School leaving certificate / A-level Results: Distinction
Dates	September 2002 – June 2005
Name of the Institute	College of Chemistry Rosensteingasse 79, 1170 Wien, Austria
Main Subjects	Analytical Chemistry, Inorganic Chemistry, Microbiology, Organic Chemistry, Physics, Process Engineering, Quality Management, Analytical & Microbiological Laboratories; All of the above in Theory and Laboratory
Dates	September 1998 – June 2002
Name of the Institute	Gymnasium Franklinstraße 26, BRG21 Franklinstraße 26, 1210 Wien, Austria
Dates	September 1994 – June 1998
Name of the Institute	Volkschule Pastorstraße Pastorstraße 19, 1210 Wien, Austria

---

---

**Personal skills and competences**

Mother tongue(s) **German**

Other language(s) **English**

Reading Very good

Writing Very good

Talking Very good

Certificate Level 1 Certificate in English (ESOL)  
Grade A

Social skills and competences Easy-going and calm sociable person  
Attendance to a martial art (Jiu Jitsu) dojo (VKS Pastorstraße)  
Trainer of said martial art, training children for 3 years  
professional ballroom dancing  
certified paramedic (December 2009)  
Chemistry tutor

Technical skills and competences Experience in Servicing and Handling of Chemical Instruments and devices

Computer skills and competences Excellent knowledge of Microsoft Office

Organisational competences Team and Project leading Character  
Ability to direct team members, to organise and share the work.  
Leading to very good team project results.

**Referees**

**DI Maria Weber**, Organic Chemistry Lecturer  
College of Chemistry, Rosensteigasse79 Vienna  
T: +43 1 486 14 89 225

**AV RR DI Dr. Hans Andres**, Chemical Technology of  
Leather/Natural Material lecturer and private supervisor for  
A-Level team-project.  
College of Chemistry, Rosensteigasse 79; 1017 Vienna  
T: +43 1 486 14 89 151 E: [h.andres@schule.at](mailto:h.andres@schule.at)

**Mag Michaela Schmee**, English and Presentation Skills Teacher  
College of Chemistry, Rosensteigasse 79; 1017 Vienna  
T: +43 1 4861489 135

**Dr. Barry Foley**, Assistant Head of School of Chemical and  
Pharmaceutical Sciences  
DIT Kevin Street, Dublin 8.  
T: +353 1 402 4645 E: [barry.foley@dit.ie](mailto:barry.foley@dit.ie)

**DI Dr. Wolfgang Kandioller**  
University of Vienna, Währinger Straße 40-42; 1090 Vienna  
T: +43-1-4277-52609 E: [wolfgang.kandioller@univie.ac.at](mailto:wolfgang.kandioller@univie.ac.at)

---